Fundamental Aspects of Netted Radar Performance

Yu Teng

A thesis submitted to UCL

for the Degree of

Doctor of Philosophy

Department of Electronic & Electrical Engineering

UCL

January, 2010

I, Yu Teng, confirm that the work presented in this thesis is my own. Where information has been derived from other sources, I confirm that this has been indicated in the thesis.

Abstract

Netted radar employs several spatially distributed transmitters and receivers for information retrieval. This system topology offers many advantages over traditional monostatic and bistatic systems which use a single transmitter and a single receiver. For example, it provides better utilization of reflected energy, more flexible system arrangement and enhanced information retrieval capability. Therefore, the netted radar system is of emerging interests among radar researchers.

This work investigates several fundamental aspects that determine netted radar performance. This includes netted radar sensitivity, the netted radar ambiguity function and the netted radar ground plane effect. Mathematical models are developed to provide a mean to examine different aspects of netted radar performance. Software simulations examine netted radar performance over a range of parameter variations. Simulation results show that netted radar can offer better performance over traditional monnostatic and bistatic radar in many cases.

Some elementary field trials have been conducted using a prototype netted radar system developed within the UCL radar group to examine aspects of netted radar performance in practice. The field trials are focused on netted radar range and sensitivity which are fundamental. The field trial results show that the theoretical benefits that netted radar can offer are generally realizable in practice.

Acknowledgements

First and foremost, I would like to sincerely thank my supervisors Professor Chris Baker and Dr Karl Woodbridge for their unwavering support and advice over the entire period of my studies at UCL. They graciously provided me with the opportunity to pursue the research study and offered incredible insight, enthusiasm and direction. It has been a privilege to work under their supervision and I am deeply grateful to them both.

I also owe thanks to many without whom this thesis would not have been in your hands. First, my colleagues Dr Graeme Smith and Dr Shaun Doughty in the Department of Electronic and Electrical Engineering at UCL, who engaged in insightful discussions with me and helped me in the netted radar field trials. I would also like to acknowledge Dr Dai Jiang for his encouragement and support throughout my time at UCL.

On a personal note, the past few years at UCL have been a transformational experience for me. My family has always been there and gave me incredible strength and support every step of the way. I would like to thank my parents and my sister for believing in me and encouraging me to challenge myself in many ways.

The work reported in this thesis was funded by the Electro-Magnetic Remote Sensing (EMRS) Defence Technology Centre (DTC). I would like to thank the members on the EMRS DTC supervisory board for their interests in this work and valuable feedback and suggestions they provided during meetings and technical conferences. Finally, as a recipient of the Dorothy Hodgkin Postgraduate Awards (DHPA) I would like to thank the committee for supporting my studies.

Publications

Parts of the research work presented here have been published:

- Y. Teng, H. D. Griffiths, C. J. Baker and K. Woodbridge, Netted Radar Sensitivity and Ambiguity, *IET Radar, Sonar & Navigation special issue on DTC projects*, December 2007

- Y. Teng, C. J. Baker and K. Woodbridge, Netted Radar Sensitivity and the Ambiguity Function, *2006 CIE International Conference on Radar*, Shanghai, China, October 2006

- Y. Teng, K. Woodbridge and C. J. Baker, Comparison of the 2D and 3D Netted Radar Ambiguity Function, *European Radar Conference 2006*, Manchester, U. K., September 2006

- Y. Teng, C. J. Baker, and K. Woodbridge, Evaluation of Netted Radar Performance. *EMRS DTC 3rd Annual Technical Conference*, Edinburgh, U. K., July 2006

- Y. Teng, H. D. Griffiths and C. J. Baker, Fundamental Aspects of Netted Radar Systems, *RTO SET-095 Specialist Meeting on Bistatic-Multistatic Radar and Sonar Systems*, La Spezia, Italy, June 2006

- Y. Teng, S. Doughty, K. Woodbridge, H. D. Griffiths and C. J. Baker, Netted Radar Theory and Experiments, *IDC (Information, Decision and Control) 2007 Conference*, Adelaide, Australia, February 2007

Original Contributions

A framework for investigating fundamental aspects of netted radar performance has been built:

- A three-dimensional netted radar sensitivity simulation model has been developed. It has been shown that, compared with monostatic radar, netted radar can offer sensitivity gains and a new degree of freedom in radar system design to deploy a real radar system in a specific surveillance area. In this way, netted radar can better utilize the overall emitted power. (Chapter 4)

- A three-dimensional netted radar ambiguity function simulation model has been developed. It has been shown that the netted radar ambiguity function has a strong dependency on the system geometry. Compared with monostatic radar, netted radar can offer a more flexible way to control the ambiguity properties. The complexity and variability of netted radar ambiguity function has been learnt. This is important to help design a netted radar system. (Chapter 5)

- A bistatic radar ground plane effect model has first been developed. A netted radar ground plane effect model has then been developed based on the bistatic radar ground plane effect model. It has been shown that, compared with monostatic radar, a netted radar can offer a more stable sensitivity map when the ground plane effect is involved. This is very useful in determining the system geometry for a real netted radar system. (Chapter 6)

- A set of netted radar field trial results has been presented to examine netted radar sensitivity performance experimentally. It has been shown that the theoretical sensitivity

gains a netted radar can offer is realizable in a real world situation. It has also been revealed that it is complex and difficult to perform outdoor netted radar experiment. The experience gained will be valuable for future netted radar studies. (Chapter 7)

Contents

List of Figures

List of Tables

Acronyms

ATC Air Traffic Control

CEC Cooperative Engagement Capability

COTS Commercial off the Shelf

CW Continuous Wave

DC Direct Current

DFR Direct Fourier Reconstruction

DSP Digital Signal Processing

FM Frequency Modulation

FPGA Field-Programmable Gate Array

GDOP Geometric Dilution of Precision

GNSS Global Navigation Satellite Systems

GPS Global Positioning System

GUI Graphical User Interface

ISAR Inverse Synthetic Aperture Radar

MIMO Multiple Input Multiple Output

MISO Multiple Input Single Output

MoD Ministry of Defence

NEC Network Enabled Capability

PRF Pulse Repetition Frequency

RCS Radar Cross Section

SAR Synthetic Aperture Radar

SNR Signal to Noise Ratio

SPWVD Smoothed Pseudo Wigner-Ville Distribution

WMEKF Weighted Modified Extended Kalman Filter

WLS Weighted Least Square

Chapter 1

Introduction

1.1 Overview

Research in radar engineering over the last few decades has been mainly focused on improving target detection, parameter estimation accuracy, and reliable target classification in monostatic radar. Despite recent advancement in radar component technology such as antennas, transmitters, receivers and processors, modern high requirements cannot always be met by traditional monostatic radars in many cases. An emerging concept termed here "netted radar" has gained more and more attentions in recent years. Compared with traditional monostatic radar and bistatic radar where only a single transmitter and a single receiver is used, netted radar employs several spatially distributed transmitting and receiving nodes to form a radar network. Therefore, advantages are expected to be gained through application of this different system topology and through new data processing methods.

It is well known that when an object is illuminated by electronic-magnetic waves, the radiation is scattered in all directions. Monostatic receivers can only extract information from one small portion of the reflected energy and most of the energy will be lost. Netted radar, however, offers the possibility to retrieve information from many different directions by employing several spatially separated, cooperative transmitting and receiving stations. This allows more efficient utilization of reflected energy, so as to improve target detection and information gathering. One promising application area for netted radar systems would be to confront stealth technology. A stealth target would generally have a very small RCS (Radar Cross Section) to

dramatically reduce the energy reflected back to the radar and therefore hard to be detected. To detect such a target, increased sensitivity will be required for the radar system. It is difficult to either increase transmit power or antenna size for a monostatic or bistatic radar. Netted radar might be a good solution as with the same transmit power level and antenna gain, netted radar will be shown (Chapter 4) to have increased sensitivity compared with monostatic or bistatic radar.

Recent development in relevant technologies such as multichannel antennas with electronic beam steering, high speed digital processors and computers, high capacity communication links, and precise synchronization systems, e.g. GPS (Global Positioning System), give rise to the possible implementation of low cost and stable netted radar systems [1].

This research work is focused on developing and examining theoretical models for netted radar. The developed theoretical models are tested within the simulation environment which allows the performance of example systems to be assessed. The performance of netted radar system is also examined with experimental data captured using a prototype netted radar system, being developed in the UCL radar group [2] [3] [4]. In this way the research is aimed at understanding the fundamental aspects of netted radar performance and help to identify the most promising application areas for netted radar systems.

1.2 Aims of the research

The main objectives of this research project are as follows:

- To understand fundamental aspects of performance and performance limitations of netted radar systems. This includes building a framework for investigating and answering basic questions regarding netted radar systems. The following aspects are examined: sensitivity and coverage capability of netted radar system, resolution and ambiguity of netted radar systems in terms of range and velocity, and the influence of ground plane on netted radar systems. This will help enable the advantages and disadvantages of netted radar systems over traditional simple monostatic radar systems to be evaluated. A set of Matlab tools will be developed to assess the performance of such systems quantitatively and graphically.

- To examine netted radar performance using real netted radar hardware. It is important to perform field trials to examine real netted radar performance. This helps confirm the theory of netted radar systems, indicate inadequacy of current hardware and theoretical models and identify possible directions for future research.

- To begin to identify the most realizable and promising application areas for netted radar systems. This will link the theoretical research with practical usage together.

1.3 Thesis outline

This thesis is composed of eight chapters. Chapter 2 gives a comprehensive literature review in order to build up the research territory that this research work is based on, and to identify where this research will fit in. Then the need to look at fundamental aspects of netted radar performance including sensitivity, the ambiguity function and the ground plane effect is justified. Chapter 3 discusses the theoretical background knowledge related to this work, including radar fundamentals, monostatic and bistatic radar fundamentals and finally an introduction into netted radar concept and the general netted radar theory.

Chapter 4, 5, and 6 are dedicated to the main mathematical models and software development work that are assembled to describe netted radar performance. Chapter 4 deals with netted radar sensitivity. Chapter 5 concentrates on the netted radar ambiguity and Chapter 6 introduces the netted radar ground plane effect. Each of these three chapters begins with a general description of basic concepts. This is followed by a review of theory and presentation of simulation examples for monostatic or bistatic systems. Subsequently, mathematical models and software simulations are developed. Finally, a series of simulation results are presented and analysed to examine netted radar performance, compare it with monostatic and bistatic radar systems and draw important conclusions regarding performance differences.

Chapter 7 presents the field trial results that have been performed to examine netted radar performance experimentally. This includes an introduction to the UCL netted radar hardware as well as the experimental methodology. Field trial results for netted radar range and sensitivity performance are presented and analysed.

Chapter 8 summarizes the conclusions achieved in the scope of this research work. Then

main achievements and novel contributions of this work are addressed. Finally, possible directions for future work in this research field are identified.

Chapter 2

Literature Review

This chapter introduces the history of radar, bistatic radar and netted radar systems. The previous work carried on in netted radar research world is then reviewed to give the background of this research work.

2.1 Historical overview

Radar was initially invented for military purposes. Christian Hulsmeyer, a German engineer, is usually credited as the inventor of the first radar, which was used for ship detection, documented by a patent in 1904 [5] [6]. However, the idea of using radio waves to detect objects did not generate much interest until a few years prior to the Second World War. After that, early radar systems were developed in parallel in many countries, such as the US, the UK, Germany and the Soviet Union. In the UK, interest in radar development began from early 1935. Robert Watson-Watt showed the detection of an aircraft by observing the beats between the echo signal and the directly received signal. The equipment employed would now known as passive continuous wave (CW) bistatic radar, using the short-range BBC broadcast signal as the transmitter and a non-collocated receiver. UK researchers had demonstrated the technique of using pulses to measure range of an aircraft target by June 1935. However, bistatic continuous wave radars were still dominant due to technical limitations. From 1936, after the duplexer was invented by the US Naval Research Laboratory as a means of using a common antenna for both transmitting and receiving, pulsed monostatic systems became popular. Later on, bistatic systems revived in the 1950s and a second resurgence of such systems occurred in

the 1970s and 1980s.

2.2 Literature review

2.2.1 Early installations

The United States and the USSR (Russia) made the most contributions to the earliest development in distributed or netted radar [1]. In the USSR the earliest netted radar, Vega, comprised one transmitting and five receiving stations and was constructed in 1936 to detect aircraft. However, this system did not go into general use later on. In 1957 a netted radar system with several spatially separated monostatic radars was used to track the first Soviet *Sputnik*. After modifications, such a system is still in use today. Later, considerable development in both passive and active-passive netted radars was made in the USSR [1]. In the US, early netted radar systems played an important role in precision measurement of missile trajectories. All these systems were composed of a ground based transmitting station and several spatially separated, precisely located receiving stations. One example is the CW interferometric netted radar, Azuza, which was put into operation from 1950s, containing one transmitter and nine receivers. Navspasur (Navy Space Surveillance System) is one of the first netted radars in the US. It is a CW netted radar and has been in operation since 1960. It is capable of detecting orbiting objects as they pass through an electronic fence located over continental United States. This system is composed of three groups of stations. Each group contains one transmitting station and two receiving stations [1]. In 1977 Lincoln Laboratory (MIT) began working on a netted radar programme aiming at improving battlefield surveillance, target acquisition and battle management capabilities. The experimental system developed under this scheme showed high effectiveness of netted radar. The same laboratory has developed Multistatic Measurement System (MMS) in 1978-1980 at the Kwajalein Missile Test Range in Marshall Islands to collect bistatic signature data and track re-entry targets highly accurately [1].

2.2.2 Modern development

Further development and implementation of netted radar have been carried out in many different countries. The Jindalee over-the-horizon Operational Radar Network was implemented in Australia (JORN), as shown in Figure 2.1. This system is designed to provide long range

detection and tracking of aircraft and ships. It comprises two cooperative but spatially incoherent HF bistatic radars with a centralised control centre, known as JORN Coordination Centre (JCC). An extensive network of beacons and sounders is also built up as part of the frequency management system, at widely separated sites around the Australia northern coast line, islands and national offshore territories [7]. The Norwegian Defence Research Establishment has developed a prototype of netted radar, which is composed of several bistatic pairs to detect and extract parameters for classification. Testing measurements of a helicopter were made with experimental CW radar [8].

Figure 2.1: Jindalee over-the-horizon operational radar network

Netted radar is also developed for civilian applications. A few works are dedicated to applications in Surface Movement Guidance and Control System (SMGCS) at airports. A short range radar network module has been designed at the Institute for Radio Frequency

Technology of the German Aerospace research Establishment. Depending on the topology of the specific airport, several modules are employed to provide a satisfactory surveillance area, with each single module having at least three monostatic radar stations installed at separated sites [9]. Netted radar systems with similar functions has been proposed by the University of Rome. The concept has a detailed subsystem architecture where a network of short range radars known as miniradars for their small dimensions and weight are employed. The number of radars also depends on the actual airport situation, with a typical number of two to four. This system boasted high resolution, elimination of shadowing, and the inclusion of image processing techniques in the track while scan function [10]. An evaluation of the applicability of netted radar to airport surface surveillance has been performed via proof of concept experiments at Baltimore-Washington International Airport [11], with emphasis on mitigation of detection of false multipath targets. Other than airport applications, netted radar with closely spaced sensors has also been developed for adaptive automotive cruise control and collision avoidance [12].

There are several long term initiatives, mainly developed by national military sectors, which are dedicated to integrating multiple sensors. The Cooperative Engagement Capability (CEC) is a US Navy project, managed within the Navy Programme Executive Office for Theater Air Defense. Functions include composite tracking, precision cueing and coordinated cooperative engagements. Advanced features, such as cruise missile defence, tactical ballistic missile defence are exhibited [13]. Network Enabled Capability (NEC) is a UK Ministry of Defence (MoD) vision comprising a series of projects to research the integration of sensors to achieve enhanced information sharing, improved situation awareness, collaborative decision-making and synchronisation of actions [14]. Also, the Royal Australian Air Force has launched similar UC^2 (Ubiquitous Command and Control) plan, which emphasizes devolution of decision making, command and control capability on each platform, automation, and integration of automated and human decision making [15]. TechSat 21 is the acronym for Technology Satellite of the 21st Century. Figure 2.2 shows a schematic of TechSat 21 satellite clusters. This is a US research programme initially began as an approach to explore the technical challenges and the benefits of replacing large single satellites with formations of microsatellites to

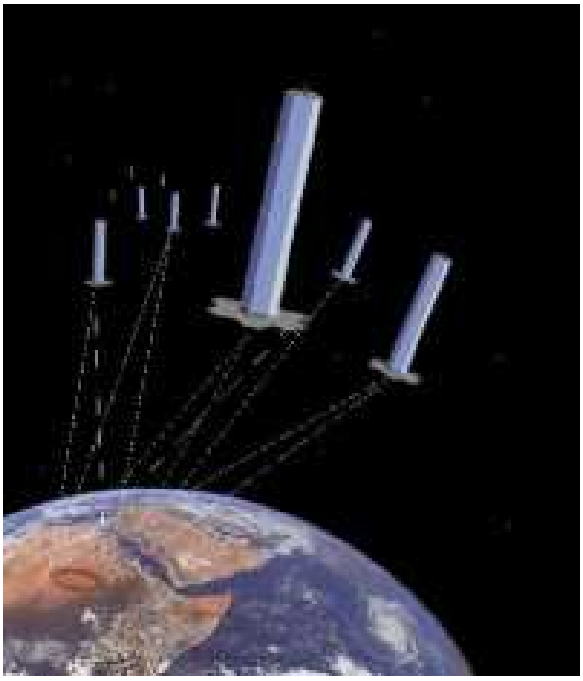

Figure 2.2: TechSat 21 satellite clusters

perform the same mission [16]. The TechSat21 space-based radar concept employed a cluster of free-floating satellites, with each transmitting its own orthogonal signal and receiving all reflected signals. The satellites operate coherently at X band and the cluster forms a multi-element interferometer with large number of grating lobes and significant ground clutters. A novel technique for pattern synthesis in angle-frequency space with thinned arrays is proposed in [17], and a full evaluation of this technique and its effectiveness in clutter suppression is given in [18]. Regretfully, this project was not funded and had to stop.

2.3 Netted radar research

2.3.1 Netted radar

The book authored by Chernyak [1] is probably the most comprehensive on netted radar theory so far. This book is composed of three main parts. General netted radar definitions and characteristics are discussed in the first part. Netted radar detection theory is developed in the second part, considering a variety of signal and interference models and different types of radar networks. Finally, netted radar target coordinate estimation and tracking issues are

specified in part three.

There are many papers analysing netted radar performance from different perspectives.

Target detection issues are discussed in the following papers. In [19] a procedure for deriving the detection statistics of multistatic radar binomial detectors is presented, which is similar to the monostatic "M-out-of-N" detector, but being able to cope with false alarms generated by both noise threshold crossings and target ghosting. Optimized receiver structures for a netted radar system composed of one transmitter and multiple receivers is presented in [20] to show the improved probability of detection compared with uniform weighting receiver structures. In [21] and [22] the likelihood ratio test method for multistatic radar detection is developed for a multiple airborne radar system where each sensor platform is a coherent space-time radar. In this research, simulation results showed the improved signal-to-interference-plus-noise ratio (SINR) of multistatic radar over single platform radar. The statistical detection performance of the optimum and decentralized detectors developed in this research is also evaluated to show the improvement obtained through both geometry and diversity gains in a multistatic radar system. A specific kind of use of multistatic radar in detecting breast cancer is discussed in [23] and [24]. The successful detection of a small tumour is shown in [23] using model they developed. [24] is mainly focused on developing calibration methods for the multistatic radar systems and choosing appropriate calibration methods depending on the practical cases.

The following papers are dedicated to target location issues. A research group has done a series of investigations of multistatic radar target location [25] [26] [27] [28]. A very important parameter that they used to evaluate multistatic radar location performance is GDOP (Geometric Dilution of Precision). In [25] a location estimation method based on ranging information is presented and shows a receiver geometry scheme providing better location performance based on this method. In [26] a target location method based on range-difference information is presented, which gives flexibility of locating a short range target without knowing each single transmitter position. In [27] an analytical method to determine the location of the geometric centre and the length of a cylindrical target is presented. In [28] target location and speed estimation using a maximum likelihood based iteration approach is presented. In

[29] algorithm to estimate target position with emphasis on examining the influence of sensor position uncertainty is developed. [30] presents a Finite-Difference Time-Domain and optical geometry combined method to accurately estimate the location of an intruder inside the residence from outside using multistatic radar operating with ultra-wideband pulses.

Netted radar tracking is also discussed in several research papers. Location and tracking technique for netted radar comprising one transmitter and multiple receivers are introduced in [31] ,where each bistatic pair performs the tracking functions using WMEKF (Weighted Modified Extended Kalman Filter) algorithm and then the data from multiple bistatic pairs are fused with Weighted Least Square (WLS) algorithm in a command centre. A radar netting optimization algorithm is developed in [32] to achieve a satisfactory surveillance area. The same research group has developed a data fusion algorithm which is applicable to netted radar stealth target tracking [33].

Several papers are specifically dedicated to netted radar passive coherent location issues, where the electromagnetic signals are from external wireless transmitting sources, such as TV signals, GPS signals and radio broadcasts (so-called illuminators of opportunity) [34]. Direct Fourier Reconstruction (DFR) and Smoothed Pseudo Wigner-Ville Distribution (SPWVD) based SAR (Synthetic Aperture Radar) imaging algorithms for multistatic passive radar imaging are applied in [35] and [36], respectively. Simulation results demonstrated that the latter produces images with better quality than the former. An approach of using the latest technology in Global Navigation Satellite Systems (GNSS) as a silent multistatic for air defence is discussed in [37].

2.3.2 MIMO radar

Another emerging concept MIMO stands for Multiple-Input-Multiple-Output. This concept originated from the communication research area, where the MIMO systems have been shown to have the potential to apply diversity techniques to significantly improve the system performance over single antenna systems. Inspired by the success in MIMO communication systems, the MIMO radar concept has been emerged in recent years. MIMO radar employs multiple antennas for transmitting and receiving. It can be implemented in monostatic or multistatic

modes [38]. When it is implemented in multistatic mode, which means it employs multiple radar nodes for transmitting and receiving, it is a kind of so-called netted radar systems. There are several different forms of MIMO radar concepts, which may cause confusion. One of those is spatial MIMO radar systems [39]. This kind of MIMO radar systems takes advantage of the spatial diversity provided by radar nodes to improve radar detection and localization capability. Another form is the one which has closer liaison with the one used in MIMO communication systems, where it emphasises the beamforming aspect of using multiple transmitting and receiving elements [40] [41] [42] [43] [44] [45]. There is a third kind of MIMO radar system called frequency MIMO which is introduced in [39], where multiple independent frequency signals are transmitted from each element of an array antenna to enjoy the advantage of being able to implement the MIMO technique in a compact single radar site mode. A review of the first above-mentioned kind of MIMO radar research will be given below, because it is most relevant to our netted radar research. The rest of MIMO radar research will not be reviewed in details.

A research group in the US has developed a series theory and models for spatial MIMO radar system [38] [46] [47]. [46] is the starting point for them to begin this investigation, where they defined a general approach to the problem with a signal model in an additional white Gaussian noise environment. Here they emphasis the spatial separation of radar nodes to exploit the independence between signals at the array elements and evaluated the system performance in terms of Cramer-Rao bound. They further investigated the MIMO concept for radar systems in [38] and [47], where [47] is a more complete presentation. Here the MIMO radar exploits the target angular spread to overcome target fading and improve the system detection performance. The MIMO radar performance is also compared with MISO (Multiple Input Single Output) system, which sometimes could also be a kind of netted radar when multiple nodes are implemented. Apart from the above-mentioned research, another research group has developed the MIMO radar detection models in a general coloured noise environment [48]. A first study of MIMO radar performance in clutter is also presented in this research work. UCL radar group has also developed a series of models to discuss MIMO radar detection issues under different conditions and compared the performance between different

system schemes [39] [49] [50]. Two research groups has investigated MINO radar ambiguity function almost in parallel. The first group has developed a MIMO radar ambiguity model and examined MIMO radar ambiguity function properties with a few different transmit signal types [51]. The second group has developed their MIMO radar ambiguity function model and further developed mathematical expressions for some of the ambiguity function properties [52] [53].

2.4 The context of this work

Although a lot of work has been done to address various aspects of radar system performance, it has been mainly focused on monostatic or bistatic radar systems. Netted radar is still an emerging concept. There are many gaps in netted radar research area that need to be filled in.

Netted radar sensitivity is initially discussed in [54], but a three-dimensional radar sensitivity simulation model has not been discussed in any literature even for monostatic and bistatic radar systems. This is one of the topics that will be discussed for netted radar sensitivity in this thesis. Also, a netted radar sensitivity model will be further developed to account for influence of various influencing factors. Monostatic radar ambiguity function has been well developed and discussed in literature. Bistatic radar ambiguity function model is developed in [55]. This is the starting point for the investigation of netted radar ambiguity function. This work will develop a novel netted radar ambiguity function model to account for ambiguity performance of a three-dimensional netted radar system where the radar nodes and the target are distributed in three-dimensional space. Monostatic radar ground plane effect was briefly discussed in [56]. Bistatic radar and netted radar ground plane models have not appeared in literature. This work will then develop models for bistatic radar and netted radar to examine netted radar ground plane effect. Also, it is lack of netted radar experimental results achieved using real netted system in literature. This work will cover examining fundamental aspects of netted radar performance using real netted radar hardware.

Chapter 3

Introduction to Radar and Netted Radar

The theoretical background of netted radar is presented in this chapter. This includes radar basics, monostatic and bistatic radar fundamentals and finally netted radar concepts. The introduction to monostatic and bistatic radar will be focused on the calculation of range, Doppler as well as the radar equation, because these are the most fundamental and essential aspects of a radar system and constitute the theoretical basis for further investigation of netted radar properties in the following chapters. The introduction to netted radar will be focused on establishment and critique of netted radar concepts. Further theoretical and experimental analysis of fundamental netted radar properties will be presented in later chapters.

3.1 Radar fundamentals

3.1.1 Fundamental aspects of radar functions

The word Radar is basically an acronym derived from RAdio Detection And Ranging. It tells us the original function of a radar system, which is to detect the presence of objects and to measure their positions by using radio waves [57]. Radar can detect objects by sending out and receiving radio waves. It can determine the range by measuring the transmission time of radio waves. It can measure the target velocity and differentiate between moving target and stationary ground returns by employing the Doppler effect. It can retrieve angular information by concentrating the radiated waves into a narrow beam [58]. Modern radar has developed more powerful capabilities, such as target tracking, target classification and high resolution imaging. An introduction to the above mentioned basic aspects of radar functions will be

given in this section.

First of all, the most basic task of a radar system is to determine whether or not a target is present. This function is considered as radar detection. Radar systems perform this function by sending out signals and analysing the returned signals. The presence of noise and clutter in the radar operating environment sometimes makes this difficult. For example, the returned signal power might be comparable to receiver noise power and this quite often is the case. Therefore, signal processing techniques such as matched filtering are usually applied before the decision as to whether or not a target is present is made in order to compare the signal strength with respect to noise. Once the presence of an object is confirmed, further parameters can be estimated. Therefore, radar detection becomes the foundation of other aspects of radar functions.

Closely associated with target detection, a radar system has to discriminate whether it is detecting one single target or multiple targets and if multiple targets how many they are. This is called radar resolution. Radar resolution is normally used to refer to the minimum separation between two targets whilst still being recognized as two separate targets rather than one. In a pulsed radar system, this separation can be either in time delay associated with the target range or in frequency associated with Doppler shift. Multiple targets being treated as one single target will present difficulties in further radar functions such as parameter estimation, tracking and target identification. Thus, radar resolution is a very important aspect of radar.

After the decision of the presence of a target is made, it is naturally desirable to measure basic target parameters such as the range and velocity in two or three dimensions. This is radar parameter estimation. Target range is normally retrieved from the echo signals. Sometimes the information of orientation and beamwidth of the radar antenna is also used. How accurate the parameter estimation can be made depends on many factors. Signal and noise power are two influential parameters. Higher signal to noise ratio will result in better parameter estimation accuracy. The signal processing method being used by a radar system, i.e. how the raw signals are combined to retrieve target parameters, will also be an important factor that affects parameter estimation accuracy. Some other factors will also determine the accuracy of parameter estimation. For example, the uncertainty of radar position will deteriorate the

accuracy of target position estimation. In this case, even if the accuracy of range measurement by the radar system is known to be very high, the overall accuracy of target position estimation will still be limited.

Tracking is another aspect of radar functions. When a radar system performs this function, it continuously monitors the location and velocity of a moving target in order to determine its historical path and predict its future path. A tracking radar is focused on observing one target continuously with great precision. When performing a tracking function, the antenna of the radar may be facing the target at all time. In this way, the target is kept in the centre of the radar main beam to achieve the maximum signal to noise ratio assisting accuracy. As soon as the target moves away from the centre of radar main beam, an error voltage will be produced and fed back to direct the antenna back to the target.

Once a target is detected and target information is retrieved by the radar, all relevant information can be used to identify targets. This is another aspect of radar functions called target identification or classification. Target identification could be based on the radar signal level. For example, by examining the polarisation of the return signal or analysing subtle differences in micro-Doppler signature, a radar system can identify targets.

Further processing of radar signals can be used to generate images of targets, so called radar imaging. The well known SAR (Synthetic Aperture Radar) and ISAR (Inverse Synthetic Aperture Radar) perform this kind of radar function. A SAR radar system uses the movement of a radar over a stationary target, e.g. the ground to synthesis an aperture with a larger dimension than that of the physical antenna. This processing method allows the radar to generate target images with very high resolution. In contrast, an ISAR radar system uses a stationary radar and a moving target to generate high resolution images of targets.

From the above analysis, it is not hard to see that fundamental radar functions are interlinked. Most radar systems will perform a combination of basic radar functions rather than one single function.

3.1.2 Fundamental radar applications

Based on the fundamental radar functions, radar systems are widely employed in many practical application areas, both military and civilian. It is well known that radar plays an important role in air defence systems and the operation of weapons such as missiles. Surveillance radar performs various basic radar functions such as target detection, target recognition and target tracking. Weapon-control radars mainly perform target tracking and guidance roles. High resolution imaging radar systems can be used to detect stationary and moving targets in battlefields.

Radar is also used in remote sensing. Weather observation radar is one of the examples of radar remote sensing. It is widely used in weather reporting and weather prediction. Another example of radar remote sensing is observation of the earth from space for a range of applications such as ocean monitoring, crop monitoring etc..

Radar systems have also been widely used to guarantee the safety of air traffic around airport areas, known as air traffic control (ATC). There are also radar systems specifically designed to observe weather around airport areas, known as Terminal Doppler Weather Radar.

Radar systems are used for aircraft safety and navigation. For example, airborne weather-avoidance radar finds out regions of precipitation so that the pilot can avoid dangerous weather conditions. Terrain avoidance and terrain following radars allow pilots of low-flying military aircrafts to avoid collisions with obstructions and high terrain.

Radar systems are used for civilian vehicles in highway safety application. The well known radar speed meter is used by police to enforce speed limits. It is also used to detect intruders or warn of obstructions or people in the driver's blind zone.

Radar systems are employed by ships and boats to avoid collisions and to observed navigation buoys. This is especially useful when the visibility is poor. Similar radars are used for harbours and river traffic surveillance.

Radar systems have also gained wide applications in industry for application such as non-contact measurement of speed and distance and oil and gas exploration. Entomologists use radars to observe the movement of insects and other animals. This is hardly achievable by

other means.

It can be concluded that radar systems found a variety of applications in both military and civilian areas.

3.2 Monostatic and bistatic radar

Radar can be classified by the topology of transmitting and receiving stations (i.e. by their locations). Both monostatic radar and bistatic radar employ a single transmitter and a single receiver. In the monostatic case, the transmitter and receiver are co-located and may share one common antenna, whereas in the bistatic case, the transmitter and receiver are spatially separated. Netted (or Multistatic) radar comprises several transmitting and receiving stations, where the transmitters and receivers can be co-located or spatially separated. Regardless of the way these transmitters and receivers work, monostatic and bistatic radar are always the elementary components in a netted radar system, so that it is necessary to have a good understanding of both of them.

Radar systems in their early days used continuous wave (CW) signals to detect the presence of targets, where the transmitter and receiver were located on two widely separated sites. These were known as bistatic CW radar [6] [57]. After the invention of the duplexer, which allows one antenna to be used for both transmission and receiving, monostatic radar became more popular and bistatic radar was less used until the 1950s. Experiencing several resurgences, bistatic radar is still very useful in certain areas and will potentially be useful in some new applications. This is due to the advantage that the receivers are passive, and therefore less possible to be detected [5] [59].

The most fundamental aspects of monostatic and bistatic radar will be presented in this sections to give a general background, such as the calculation of monostatic and bistatic range and Doppler shift as well as the well-established monostatic and bistatic radar equations. The introduction to netted radar system will be mainly focused on the establishment and critique of the netted radar concept while the corresponding analysis of netted radar fundamentals will be presented in the following chapters.

3.2.1 Monostatic radar fundamentals

Figure 3.1 shows a typical topology of a monostatic radar, where the transmitter and receiver are collocated. It calculates the range to a point target R, i.e. the distance from the radar to a target, by measuring the time delay τ between transmitting the pulse and receiving the return:

$$R = \frac{1}{2}c\tau \tag{3.1}$$

where c is the speed of radio wave propagation (i.e. light).

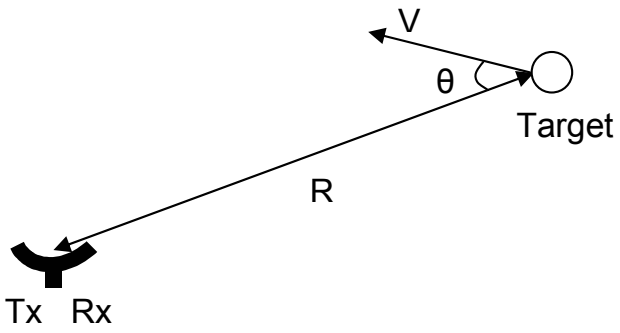

Figure 3.1: Monostatic radar topology

Another important parameter measured by radar is Doppler shift, which is the change in the frequency of the transmitted signal caused by the relative motion of the target to the radar and therefore commonly used for accurate target speed estimation. In a monostatic radar system the Doppler shift f_d and target speed V are related by:

$$f_d = -\frac{2V\cos\theta}{\lambda} \tag{3.2}$$

where λ is the wavelength of transmitted signal and θ is the angle between the target velocity direction and the line connecting target and monostatic radar node. It reveals that monostatic Doppler shift is proportional to the radial speed of the moving target and a decreasing path length generates a positive Doppler shift.

The radar equation is probably the most useful fundamental mathematical tool to analyse radar performance. It relates the radar range to many other radar characteristics of the system such as transmitter, receiver, target and the environment. It not only is used to determine the

maximum detectable range for a particular radar, but also serves as a mean of analysing the factors which affect radar performance. In this case, it plays an important role in radar system design.

The radar equation can be expressed in different forms according to the parameters to be analysed. The generally used monostatic radar range equation is given by:

$$R^2 = [\frac{P_t G_t G_r \sigma \lambda^2}{(4\pi)^3 k T_s B(SNR) L}]^{\frac{1}{2}} \tag{3.3}$$

where R is the range between the target and the monostatic radar station, P_t is the transmitted power, G_t is the transmitter gain, G_r is the receiver gain, σ is the radar cross section (RCS) of the target, λ is the wavelength, SNR is the signal to noise ratio, k is the Boltzmann's constant, T_s is the receiving system noise temperature, B is the noise bandwidth and L is the system loss ($L > 1$).

Figure 3.2 shows a comparison of monostatic constant range and SNR contours. The unit for the lines on the range coutour is km and the unit for the lines on the SNR contour is dB. As the simulation results in this chapter are aiming at giving a general image of the fundamental aspects of radar systems, no specific parameters will be mentioned and analysed. Detailed discussion will be given in the following chapters as necessary. Monostatic radar range contours are defined by the curves with the points on each curve having the same distance to the monostatic radar. This is by nature a series of concentric circles, with a centre at the monostatic radar station. From Equation 3.3 it is seen that the same value of R results in the same SNR if other parameters are fixed. This tells us that monostatic radar SNR contours coincide with constant range contours.

3.2.2 Bistatic radar fundamentals

Bistatic radar uses separate antennas at different locations for transmission and reception. Figure 3.3 shows a typical geometry of a bistatic radar, where a transmitter and a receiver are placed at two sites, separated by a distance L, normally comparable with the target distance, known as the baseline. The angle between the transmitter and receiver with the vertex at the target is known as bistatic angle. In a bistatic radar system, the transmitter, receiver and target form the bistatic triangle, and furthermore the bistatic plane.

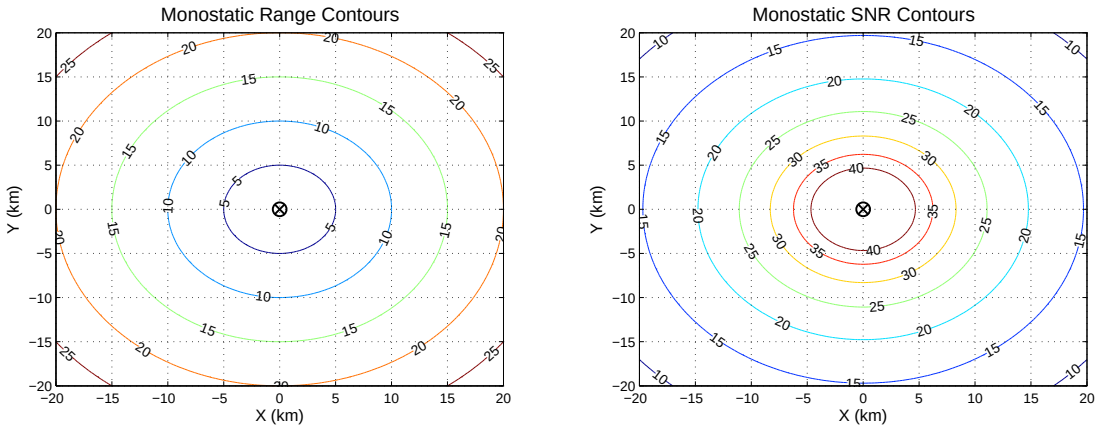

Figure 3.2: Monostatic radar range and SNR contours

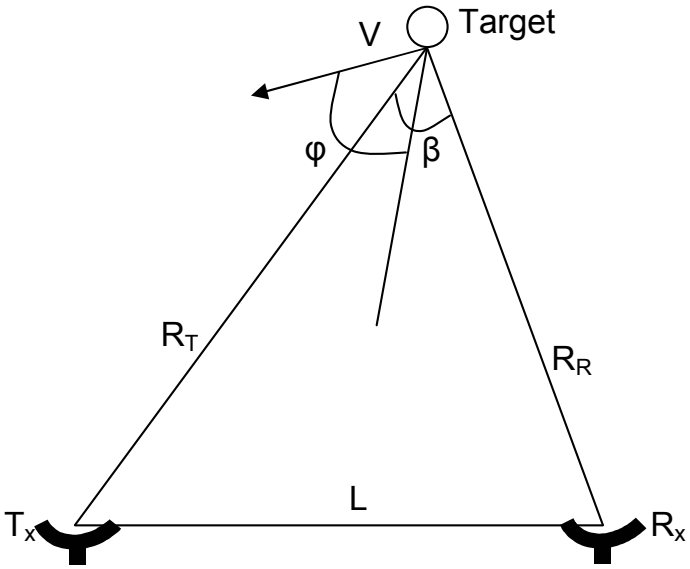

Figure 3.3: Bistatic radar topology

Unlike monostatic radar, bistatic radar usually measures the range sum, which equals to the total path length of the transmitter to target range R_t and the target to receiver range R_r, calculated by:

$$R_t + R_r = \frac{1}{2} c\tau \tag{3.4}$$

where τ is the total delay from transmission to reception, and c is the speed of radio wave

propagation.

In a bistatic radar system, when the transmitter and receiver positions are fixed, the bistatic Doppler f_b at the receiver site generated by the moving target is calculated by the time rate of change of the total path length of the transmitted signal, normalized by wavelength λ:

$$f_b = \frac{\frac{dR}{dt}}{\lambda} = \frac{\frac{d(R_t+R_r)}{dt}}{\lambda} \tag{3.5}$$

where $\frac{dR_t}{dt}$ is the projection of target velocity onto the transmitter-to-target line-of-sight, given by:

$$\frac{dR_t}{dt} = V\cos(\phi - \beta/2) \tag{3.6}$$

and $\frac{dR_r}{dt}$ is the projection of target velocity onto the receiver-to-target line-of-sight, given by:

$$\frac{dR_r}{dt} = V\cos(\phi + \beta/2) \tag{3.7}$$

then the total Doppler shift is given by:

$$f_b = \frac{2V\cos\phi\cos(\beta/2)}{\lambda} \tag{3.8}$$

where ϕ is the angle between target velocity and bistatic bisector, positive clockwise.

Figure 3.4 shows the normalized bistatic Doppler as a function of angle ϕ. Three representative target positions are chosen, forming different bistatic angle β. This is shown in Figure 3.5. β = 120° represents a normal target position. β = 0° and β = 180° represent two extreme target positions, where when β = 0° the target locates on the extension of transmitter-receiver baseline and when β = 180° the target locates on the transmitter-receiver baseline. It should be noted that when β = 0° the bistatic Doppler equation reduces to

$$f_b = \frac{2V\cos\phi}{\lambda} \tag{3.9}$$

This conforms with the monostatic Doppler Equation 3.2, which means the corresponding curve in Figure 3.4 can represent both monostatic Doppler and bistatic Doppler with β = 0°.

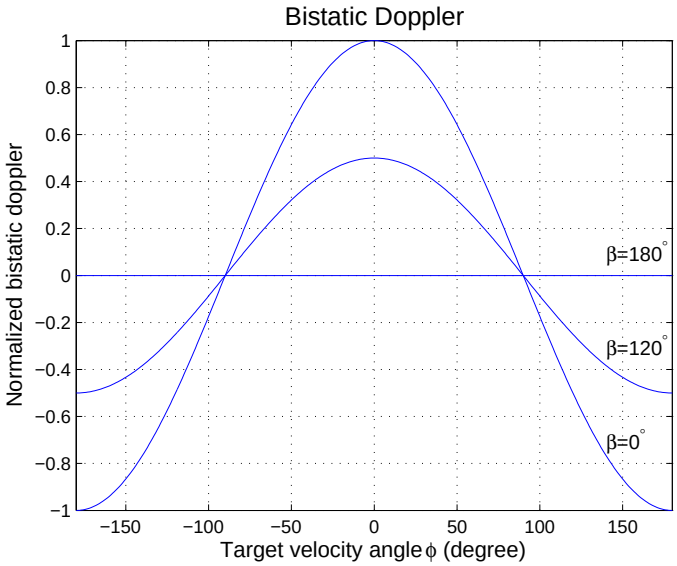

Figure 3.4: Normalized bistatic radar Doppler

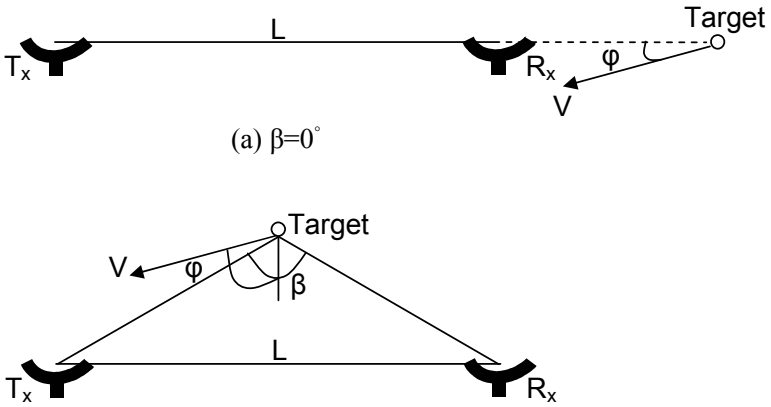

(a) β=0°

(b) β=120°

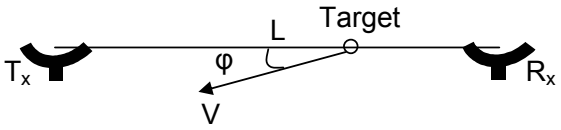

(c) β=180°

Figure 3.5: Bistatic radar system geometry

From Figure 3.4 it is observed that the maximum Doppler shift is generated when a target lies on the extension of transmitter-receiver baseline and moves towards the receiver ($\phi = 0°$

and β = 0°). When the target is at any point on the baseline, the bistatic Doppler is zero (β = 180°). For all values of β, as long as the angle ϕ is in the range of -90° to 90° the bistatic Doppler remains positive, which means with respect to the bistatic bisector an approaching target generates a positive Doppler. Finally, for any given ϕ, the magnitude, i.e. the absolute value, of bistatic Doppler is never greater than that of a corresponding monostatic Doppler.

In the bistatic case, the transmitter and receiver are not collocated as in the monostatic case. The transmitter to target range and target to receiver range are R_t and R_r, respectively. The bistatic RCS σ_b depends on many factors such as look angle. It is not equal to monostatic RCS, and is often found to be close to the monostatic value measured along the bistatic bisector [57]. Similar to the derivation of the monostatic radar equation, the bistatic radar range equation is given by:

$$R_t R_r = [\frac{P_t G_t G_r \sigma_b \lambda^2}{(4\pi)^3 k T_s B (SNR) L}]^{\frac{1}{2}} \tag{3.10}$$

Compared with monostatic radar range equation, a major difference here is that the range product $R_t R_r$ replaces the range square R^2 in Equation 3.4. This results in a change of shape of both the constant range and the constant signal to noise ratio contours. In this case, they are not simple concentric circles surrounding the radar stations. This is shown in Figure 3.6 where the unit for the lines on the range coutour is km and the unit for the lines on the SNR contour is dB.

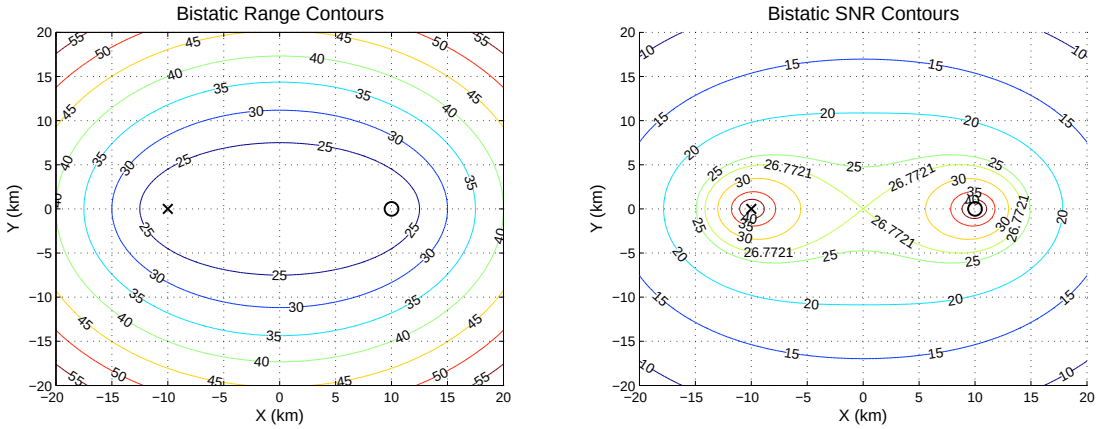

Figure 3.6: Bistatic radar range and SNR contours

It is shown that the bistatic radar constant range contours, defined by constant $R_t + R_r$, take the shape of ellipses with two foci at the transmitting and receiving antenna respectively. They are no longer coincident with the constant signal to noise ratio contours, as in monostatic systems, while bistatic radar constant signal to noise ratio contours are defined by the well-known ovals of Cassini. It is seen that the bistatic ovals of Cassini comprise three different operating regions: the receiver centred region, which is the small oval around the receiver; the transmitter centred region, which is the small oval around the transmitter; and the receiver-transmitter centred region, namely cosite region, which is any of the ovals surrounding both transmitter and receiver. This causes the received SNR to be a function of the position of the target on a constant range sum contour, whereas in monostatic cases, the constant SNR contours are constant range contours as well. It is noticed that the spatial separation of radar stations causes the changes in basic radar properties and system performance.

Via these glimpse comparison of bistatic operation, it is seen that there are fundamental differences between monostatic and bistatic radars. These differences will be inherent in netted radar operation which can be thought as collection of bistatic and/or monostatic radars and hence provides motivation for investigating netted radar concept further.

3.3 Netted radar

3.3.1 Concept

The idea of using several spatially separated, cooperative transmitting and receiving stations for effective energy use and better information retrieval has long been in the mind of radar engineers. However, there is no uniform terminology describing radar systems designed with this concept in mind. A couple of terms appear in the literature with slightly different definitions, such as multistatic radar [57] [60] [61], multisite radar [1], radar network [9] [62], distributed radar [63] and netted radar [54] [64]. Netted radar is used in this thesis.

A typical arrangement of a netted radar is showed in Figure 3.7. It is composed of three elements: radar stations, data processing units and the communication links between radar nodes.

The basic components of netted radar are the traditional monostatic and bistatic radars.

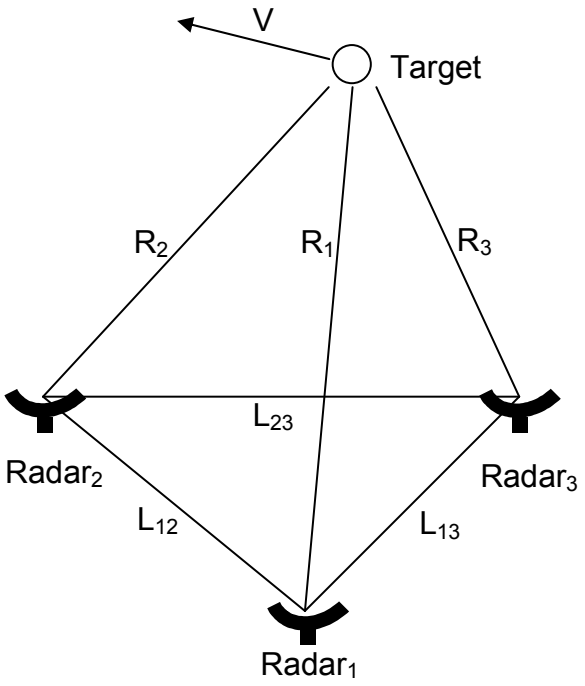

Figure 3.7: Netted radar topology

Each station can be transmitting, receiving or both transmitting and receiving, giving rise to three operational modes: multiple monostatic operation, multiple bistatic operation and a combination of monostatic and bistatic operation. Most of the data received in radar stations are sent to the central unit for final processing. The inherent complexity of radar networks results in a higher requirement for communications, including bandwidths, paths, traffic, concealment, etc. [60] [65].

3.3.2 Categorization of netted radar types

Netted radar can be categorized in a number of different ways [1]. The most useful categorizations are discussed here with a brief introduction to some other methods.

Two characteristics are of essential importance in determining netted radar performance. These are (1) the degree of spatial coherence and (2) the data fusion level.

Netted radar is divided into three classes in terms of coherency: spatially coherent network, short-term spatially coherent network and spatially incoherent network. In a spatially coherent netted radar, the RF signal frequency and interstation phase offsets are determinis-

tic and are maintained over a long period, usually much greater than the duration of signals, so that the information contained in the scattered signals can be better utilized. This implies increased system complexity and cost. In a short term coherent netted radar, the interstation phase differences are maintained over a short period of time which is no less than the signal duration. This allows, for example, velocity estimation by Doppler. In a spatially incoherent netted radar, the interstation phase information is completely eliminated. It should be noted that spatial incoherent netted radar may maintain temporal coherency in each single radar, where the Doppler shift and therefore target velocity can still be measured at each receiver.

Netted radar can be classified into four categories, according to the data fusion level. The lowest is track data. In this case, the signal processing accomplished in each station results in target trajectory information. These tracks can then be combined in the central processing centre. The next level is plot data, where threshold and parameter estimation is carried out at each station, and a final decision is made in the data fusion centre, where the combined plots can be used for tracking. The third level is detection, where detection information from each station is sent to a central processing unit to jointly form one plot. Finally, the highest level is raw data. At this level the original received coherent signals, noises and interferences from all stations are jointly processed. In general, the higher is the level that data fusion applied, the higher is the requirement for the communication links ability and the complexity of system increases rapidly.

Netted radar coherency and data fusion level are interrelated. In the spatially coherent and short-term coherent cases, raw data fusion can be in combination with plot fusion. In incoherent netted radar, where only detection, plot or track fusion are possible, plot or track fusion is more likely to be used. In a practical netted radar, data may be fused at several different levels simultaneously.

As mentioned in Section 3.3.1, netted radar can be categorized as a multiple monostatic network, a multiple bistatic network, and a mixture of the two. In the multiple monostatic case, each radar can transmit a specific signal and receive the return originated from this unique transmitted signal only. An example of the multiple bistatic case is a radar network comprising one common transmitter and N spatially separated receivers where each transmitter-receiver

pair forms a bistatic radar. Finally, when each station in the network can transmit and receive signals originated from any stations in the network, the system is fully netted. This is a netted radar example, which is composed of both monostatic and bistatic radars. Figure 3.8 illustrates examples of the above three different operation modes of netted radar.

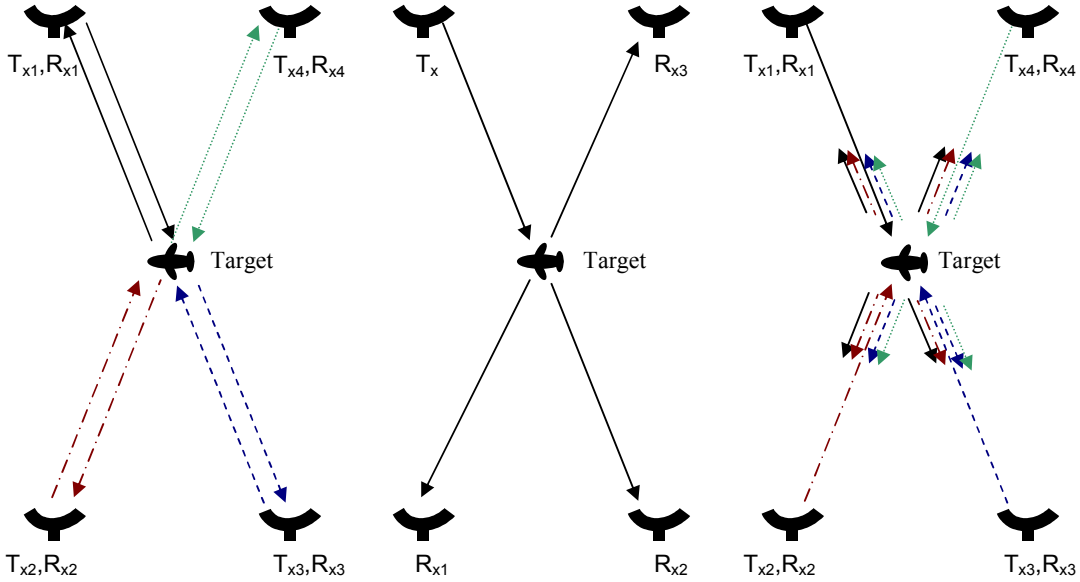

(a) Multiple Monostatic (b) Multiple Bistatic (c) Fully Netted

Figure 3.8: Netted radar operation modes

Netted radar can also be classified by many other features. It can be categorized as active where at least one transmitting station is included, or passive, where only receiving stations are used to detect radiating targets, and a combination of the above two. It can also be categorized according to station locations. Ground based, airborne, spaceborne and shipborne netted radars are examples of this classification. Netted radar can be categorized as centralized and decentralized systems. Also, netted radar can be classified as long baseline and short baseline systems.

Figure 3.9 attempts to summarize the categorization and complexity of different types radar networks, where green means that the system is relatively easy to implement, amber is more difficult and red represents the most difficult and complex system. This is used as a guide only to illustrate some examples of possible network types.

	Case 1	Case 2	Case 3	Case 4	Case 5	Case 6
Location	Fixed	Fixed	Fixed	Fixed	Fixed and moving platforms	Nodes on moving platforms
Data level	Tracks	Tracks	Detections	Detections	Raw	Raw
Coherency	Incoherent	Incoherent	Incoherent	Coherent	Coherent	Coherent
Operation mode	N Tx, N Rx monostatic	1 Tx, N Rx multi-static	1 Tx, N Rx multi-static	M Tx, 1 Rx multi-static	M Tx, 1 Rx multi-static	M Tx, N Rx multi-static
Distribution	De-centralised	De-centralised	Semi De-centralised	Centralised	Centralised	Centralised
Assessment	Straight-forward	Multiple bistatics	Challenging	Complex	Very complex	Extremely complex

Figure 3.9: Netted radar category

In Case 1, the netted radar is composed of fixed position monostatic radars. This is a decentralised netted radar system as most of the processing is done at the individual monostatic radar receivers and only tracks are sent to a central processing unit. In this kind of system, the communication requirement can be categorised as low. In Case 2, bistatic configuration is introduced. This kind of netted radar is composed of multiple bistatic radars. Similar to the system in Case 1, this is again a decentralised netted radar system which transmits tracks, but in this case these are produced by the multiple bistatic radars rather than the multiple monostatic radars introduced in Case 1. The netted radar in Case 3 keeps the bistatic radar as the basic element, but this time the amount of useful data being transmitted to the central processing unit is increased. Thus detections are used to form the plots instead of combining tracks. This is considered as a semi-decentralised network. In Case 4 and Case 5, the proposed system topologies introduce significant problems to the operation of the system, in terms of bandwidth and processing algorithms. Coherency refers to the knowledge of phase of the signals at each radar station. The coherent operation demands precise synchronisation of the

signals from each radar station. In both cases the netted radar is strongly centralised, as most of the processing is done in the central processing unit. The system in Case 5 is even more complicated as the higher is the level of data to be combined, the higher is the level of system complexity. Finally, in Case 6, the radar stations are mounted on mobile platforms and the raw data will be coherently combined and processed. It is easy to see that this kind of netted radar is extremely complex, less cost effective but with more system capabilities.

3.3.3 Advantages and disadvantages

Compared with monostatic and bistatic radar, where only a single transmitter and a single receiver are employed, netted radar provides more flexible choice of system geometry and radar parameters, such as multiple baseline length, transmitted signal form and pulse repetition frequency (PRF), giving rise to a series of advantages over monostatic and bistatic radar.

The most evident advantage is the flexibility to form a more tailored coverage area. Thanks to the use of multiple transmitting and receiving stations, the geometry of the netted radar can be tailored to meet the needs of specific requirements. Combined with suitable data fusion algorithms the extension of the coverage area in a given directions is clearly achievable.

Another obvious advantage is the increase of system sensitivity. Due to the additional use of radar receivers alone, the total received signal power will be clearly augmented, leading to an increase in overall signal to noise ratio (SNR), and consequently higher system sensitivity. This issue will be explored in more details in the next chapter.

In a netted radar system, the accuracy of position estimation of a target will be improved. This is achieved by integration of range measurements from several spatially separated monostatic or bistatic components. The tracking accuracy may be improved as well, due to the higher track updating rate compared to monostatic and bistatic radar.

In a netted radar system, the target is observed from multiple perspectives rather than a single direction. Not only does this make better use of the scattered energy, it also permits additional information retrieval. Therefore, it might be possible to get improved target classification, recognition, or even three-dimensional imaging [66] [67] [68] [69].

Also, the survivability and reliability are improved significantly in a netted radar. The loss

of one or even several stations may not be completely fatal, and leads to the concept of graceful degradation, because there are still some other stations working properly. Additionally, passive operation of the receiving stations makes them less vulnerable to physical attacks.

Although netted radar provides valuable advantages, there are still some unavoidable disadvantages, which present the most challenging problems to radar designers. In a netted radar system, data fusion is far more complicated than in a single monostatic or bistatic radar. This implies the requirement for reliable communication links, powerful data processors and computer systems. It is necessary to achieve highly accurate location information for each station, because the sensor position uncertainty greatly influences system performance [29]. Finally, precise synchronization method is required in a spatially coherent netted radar system to achieve the common awareness of frequency and phase. A possible way to keep the satisfactory coherency of radar network is to use Global Positioning System (GPS) as reference signals [70] [71]. GPS disciplined oscillators receive the atomic clocks contained in the GPS satellites as a reference. Therefore, they provide a stable frequency standard. However, due to large amounts of clock jitter at the output of the GPS receiver, this long term stability does not correspond to short term stability or low phase noise. In this case, when an oscillator with a better short term stability, such as an Over Controlled Crystal Oscillator or rubidium oscillator, is disciplined by the GPS receiver over a long period of time, optimal short and long term stability can be achieved.

Chapter 4

Netted Radar Sensitivity

In this chapter the most fundamental and important aspect of netted radar performance is examined. We introduce, develop and analyse a new form of the radar equation which indicates netted radar performance in target detection. To give a background, the well established monostatic radar equation is briefly cited. Then, based on the monostatic and bistatic sensitivity models, the netted radar sensitivity model is developed and analysed.

4.1 Introduction

In simple terms, radar sensitivity may be defined as the received signal to noise ratio (SNR). It is the starting point to evaluate the overall performance of any radar system, as it provides a measure of the ability of a radar to determine the presence or absence of a target. Although its use is limited to being largely a performance indicator only, it makes an instructive reference point with which to compare the potential performance of netted radar. In a radar system, detection is a statistical concept. Normally, a certain signal to noise ratio is required to achieve a designated probability of detection (P_d) for a chosen probability of false alarm (P_{fa}). According to the conventionally used monostatic radar equation, when a minimally acceptable SNR is given, the maximum achievable range can subsequently be derived. In a noise-limited monostatic radar system, the maximum range is defined as the maximum distance from the radar where a given target can just be detected above receiver thermal noise. It is then most typically used to describe the coverage capability of the system [5] [6] [72]. However, in a netted radar system matters are not quite so straightforward. There are some fundamental differences

when such a system has a spatial distribution of transmitters and receivers as this immediately implies that the coverage volume (which in the monostatic system is always spherical in shape with a radius given by the maximum range) will have a shape that depends on and varies with system geometry. This has some further implications that require careful treatment. For example, the potentially irregular shaping of the coverage resulting from the distribution of radar nodes results in a lack of a clear choice of reference point that may be used to define the maximum range of the whole system. Indeed the concept of a maximum range becomes a dubious one if more transmitters or receivers are added to the network. Thus, for simplicity, in this thesis this problem has been circumvented by depicting coverage as a volumetric coverage map whose boundaries represent system sensitivity. Typically the contour of maximum detection range is used rather than a potentially misleading single figure for a maximum detection range. This basic example illustrates just how monostatic and netted radar systems are fundamentally quite different. Hence there is a need to establish new expressions allowing computation of performance of netted radar that have an equivalence to those long used in monostatic radar.

In this chapter, a framework for evaluating the sensitivity of a scenario radar network is developed. Radar performance is subsequently investigated in terms of sensitivity for monostatic, bistatic, and netted radar cases. This includes a formulation of mathematical models, a description of the simulation method and an analysis of simulation results.

4.2 Monostatic radar sensitivity

4.2.1 Monostatic radar equation

As mentioned in Section 4.1, monostatic radar sensitivity is the received signal to noise ratio, which can be defined by one form of the commonly used radar equations. Since radar equation is the foundation of the following analysis in this chapter, it is worth deriving rather than simply quoting.

By definition, signal to noise ratio, or SNR, is the ratio of received signal power to noise power. If the received signal and noise power can be calculated separately, then the SNR can be consequently derived. Now let us consider the received signal power first.

If the power transmitted by radar is P_t, and it is radiated evenly over all solid angles, the

power density at distance R, where the target is, can be calculated by:

$$PowerDensity = \frac{P_t}{4\pi R^2} \tag{4.1}$$

When a directional antenna is used, which is normally the case, the radiated energy is concentrated in a particular direction via formulation of a beam. In this case the power density at target distance R will be:

$$PowerDensity(DirectionalAntenna) = \frac{P_t G}{4\pi R^2} \tag{4.2}$$

where G is the monostatic radar antenna gain.

A certain amount of this radiated power will be intercepted and scattered by the target at distance R. The power reflected back by the target towards the radar direction is calculated by:

$$PowerBack = \frac{P_t G \sigma}{4\pi R^2} \tag{4.3}$$

where σ is known as Radar Cross Section (RCS), which reflects the scattering properties of a target. Assuming that this amount of power is radiated back isotropically, the power density received at radar antenna will be:

$$PowerDensityBack = \frac{P_t G \sigma}{(4\pi R^2)(4\pi R^2)} \tag{4.4}$$

Part of this re-radiated power will be captured by the radar antenna. This received power at the radar antenna (P_r) can be calculated by the following equation after introducing the term of effective area of the antenna A_e.

$$P_r = \frac{P_t G \sigma A_e}{(4\pi R^2)(4\pi R^2)} \tag{4.5}$$

Considering that the effective area of an antenna is related to the antenna gain, and generally monostatic radar will use the same antenna for transmitting and receiving, the relationship between radar antenna gain G and effective area of the antenna is given by:

$$G = \frac{4\pi A_e}{\lambda^2} \tag{4.6}$$

the received power will be:

$$P_r = \frac{P_t G^2 \sigma \lambda^2}{(4\pi)^3 R^4} \tag{4.7}$$

And finally a factor L, known as system loss, is normally introduced to account for various losses that may occur in a radar system. Then the received power can be written as:

$$P_r = \frac{P_t G^2 \sigma \lambda^2}{(4\pi)^3 R^4 L} \tag{4.8}$$

where $L > 1$.

As the received power is derived, the next step is to calculated noise power. A major part of the receiver noise to be considered is the so-called thermal noise. For most practical radars, thermal noise N_0 can be considered as white noise having a flat power spectral density and calculated by [57]:

$$N_0 = kT_0B \tag{4.9}$$

where k = Boltzmann's constant = 1.38 $\times$ 10^{-23} JK^{-1} and T_0 = system temperature, which is generally assumed to be 290 K. The product kT_0 gives a noise density of -204 $dBWHz^{-1}$, a figure very useful in radar design. It should be noted that, although the noise spectrum spans much wider than the bandwidths of the radar system, the noise to be considered here is restricted by the passband of the radar receiver, known as band-limited white noise. This thermal noise is independent of the radar frequency. Whether a radar operates at 2.4 GHz (S-band) or 1.5 GHz (L-band), as long as the radar bandwidth is the same, for example 1 MHz, the thermal noise would be the same, i.e. -144 dBW.

In practice, a noise figure F_n is normally introduced to account for additional system noise as the noise condition in a practical radar system is generally worse than the ideal radar system having only thermal noise. Then the total system noise is calculated by:

$$N = kT_0BF_n \tag{4.10}$$

Considering the received signal power calculated by Equation 4.8 and the receiver noise power calculated by Equation 4.10, we can calculate the monostatic radar signal to noise ratio, i.e. sensitivity, by:

$$SNR = \frac{P_t G^2 \sigma \lambda^2}{(4\pi)^3 k T_0 B R^4 L F_n} \tag{4.11}$$

where

P_t = transmitted power

G = antenna gain

σ = radar cross section (RCS)

λ = wavelength

k = Boltzmann's constant

T_0 = receiving system noise temperature

B = noise bandwidth

R = target range

L = system loss

F_n = noise figure

This gives the general form of the monostatic radar equation. It should be noted that in Equation 4.11 the transmitted power P_t is peak power. The radar equation can take different forms depending on the specific type of transmitted signal and operational mode. For example, with a pulse radar, it might be more convenient to use the average power P_{av} rather than peak power P_t. They are related by:

$$P_t = \frac{P_{av}}{(PRF)\tau} \tag{4.12}$$

where PRF is the pulse repetition frequency of the pulse radar and τ is the pulse length. In a pulse radar system a factor of nL_n needs to be included on the top of the basic radar Equation 4.11 to account for the gain from the integration of multiple pulses where n is the number of pulses and L_n is the efficiency factor for adding n pulses together and L_n is less than unity for non-ideal integration. Then the radar equation for a pulse radar can be written as:

$$SNR = \frac{P_{av} G^2 \sigma \lambda^2 n L_n}{(4\pi)^3 k T_0 L F_n (B\tau)(PRF) R^4} \tag{4.13}$$

In a radar system the product $B\tau$ is normally approximately equal to unity. Therefore, the

pulse radar equation can be simplified as:

$$SNR = \frac{P_{av} G^2 \sigma \lambda^2 n L_n}{(4\pi)^3 k T_0 L F_n (PRF) R^4} \tag{4.14}$$

Equation 4.14 will apply to a radar which observes a target continuously to receive n pulses such as tracking radar. As for surveillance radar which observes an angular volume Ω in a given time t_s, this is not the case, the radar equation need to be modified correspondingly, which can be given by [73]:

$$SNR = \frac{P_{av} G \sigma \lambda^2 L_n t_s}{(4\pi)^2 k T_0 L F_n R^4 \Omega} \tag{4.15}$$

From the above analysis, it is seen that each particular radar system will need to employ the form of radar equation that suits its particular needs. Since the main objective in this chapter is to compare and understand the performance difference between monostatic, bistatic and netted radar in terms of sensitivity, standard radar equation will be used for analysis. Also, once the analysis based on one form of radar equation is done, it is not hard to extend it to analysis based on other forms of radar equations. Therefore, the basic form of radar equation given by Equation 4.11 is chosen for the analysis that follows in this chapter for generality and convenience. Although it is simplified, it still good to evaluate possible trade-offs among the parameters that will affect radar performance. From this equation, it is not hard to see that radar sensitivity is affected by a number of key parameters, such as transmitted power, antenna gain, wavelength, which can be chosen by radar designers, and other parameters, such as target cross section, target distance from radar receivers, etc., which are a function of application and use.

4.2.2 Monostatic radar sensitivity analysis

In this section, a set of computer simulation will be presented to examine simple monostatic radar sensitivity. This is to provide a benchmark for evaluation of the properties of more complicated bistatic and netted radar sensitivities that will be presented in the following sections. The analysis of monostatic radar sensitivity will be all based on Equation 4.11. This will begin with examining the sensitivity of monostatic radar in two dimensions. A set of arbitrary radar parameters are selected and listed in Table 4.1 for illustration purpose.

Parameter	Description	Value
Pt (W)	Transmitter power output	6
G (dB)	Antenna gain	30
λ (m)	Wavelength	0.1
k (JK^{-1})	Boltzmann's constant	1.38×10^{-23}
T_0 (K)	receiving system noise temperature	290
B (MHz)	Bandwidth	2
L (dB)	System loss	5
F_n (dB)	Noise Figure	4
σ (m^2)	Radar cross section	1
SNR_{min} (dB)	Signal to noise ratio	13

Table 4.1: Parameters used for monostatic radar sensitivity simulation

A few points need to be mentioned about the chosen radar parameters. According to equation $\lambda = \frac{c}{f}$, 0.1 m wavelength will represent a frequency of 3 GHz. This falls into the S-band. The detection threshold is set to 13 dB, which means when the signal is 20 times greater than the noise power, the target is just detectable, i.e. if the signal is more than 20 times greater than the noise power, the target will be detectable while if the signal is less than 20 times greater than the noise power, the target is undetectable. In the traditional monostatic radar systems this signal to noise ratio provides a detection probability of 0.85 for a false alarm probability of 10^{-6} assuming a non-fluctuating signal [57].

Assuming a constant target cross section in a Gaussian noise background, one example of a two-dimensional monostatic sensitivity map for the above chosen radar parameters is shown in Figure 4.1. In this example, the sensitivity map on the ground plane is plotted with the different colours representing different signal to noise ratios, and the single radar system is located at the coordinate origin. The sensitivity is shown in two dimensions where the position of a specific spot can be defined by x and y coordinates. The surveillance region is taken as a 12×12 km^2 square area with the coordinate origin at the geometrical centre. Those areas,

where the signal to noise ratio is below the detection threshold, are left blank, i.e. coloured white. It is shown that in this two-dimensional representation, the monostatic radar sensitivity map takes the shape of concentric circles with decreasing intensity form the centre outwards as expected. With the range getting closer to radar node, the sensitivity increases rapidly, this is due to the R^4 term in the radar equation. For example, when the range is reduced from 1 km to 0.5 km, the SNR will be increased by $40lg2$ = 12 dB.

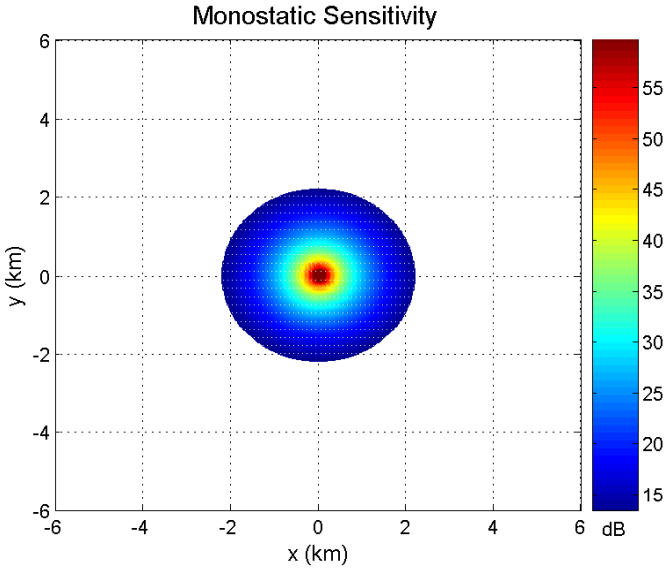

Figure 4.1: Monostatic radar sensitivity map

The following simulations are made to assess monostatic radar sensitivity in three-dimensional space in order to make a comparison with two-dimensional cases. This is for the first time to analysis radar sensitivity in three dimensions which is never shown in literature before. This is a very useful extension for radar performance estimation and will become significant when netted or distributed geometries are considered.

In Figure 4.2 the coverage plots for the exemplar system are shown in both two dimensions and in three dimensions. The two-dimensional coverage plot is shown on the left hand side. As in Figure 4.1, it depicts the intersection of the detection envelope at the maximum range with the ground plane where the radar system is located. In other words it represents the 13 dB contour. For the given system parameters, targets located outside this boundary will

result in a signal to noise ratio which is lower than the designated threshold and are assumed not to be detected. Three dimensional coverage plot is shown on the right hand side and hence represents the total volumetric detection envelope of the system including that above the ground plane. The radar transmitter and receiver are represented by a cross and a circle respectively. In this monostatic example they are coincident. This form of representation is used in preparation for presenting the netted configurations that follow later.

Thus using this simple example, it has been shown that, as expected, monostatic radar gives a spherical sensitivity iso-surface in three-dimensional space hence a circular contour in two dimensions as is well-known.

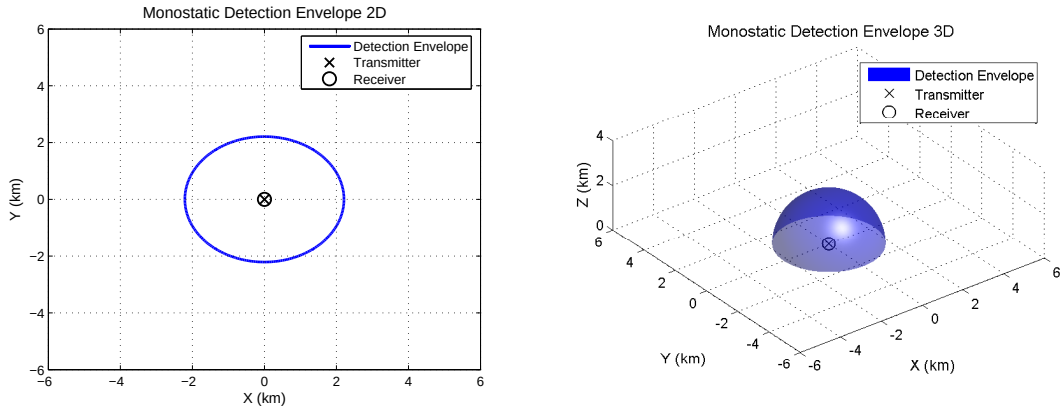

Figure 4.2: 2D and 3D monostatic radar sensitivity

4.3 Bistatic radar sensitivity

4.3.1 Bistatic radar equation

In this section a more complicated bistatic radar configuration is considered that also employs a single transmitter and a single receiver. Compared with simple monostatic radar, the major difference for bistatic radar is that the transmitter and receiver are not collocated any more. They are geographically separated by a baseline length. In this case the monostatic radar Equation 4.11 needs to be extended to account for this bistatic configuration. Basically two factors need to be modified. One is the antenna gain G. As a bistatic radar uses different antennae for transmitting and receiving, it is suitable to use G_t and G_r to represent transmitting

antenna gain and receiving antenna gain separately. The other one is the target range R. Due to the geographical separation of the transmitter and the receiver, the transmitter to target range and target to receiver range need to be separated as R_t and R_r. This results in complex dependence of radar performance on system geometry.

$$SNR = \frac{P_t G_t G_r \sigma \lambda^2}{(4\pi)^3 k T_0 B R_t^2 R_r^2 L F_n} \tag{4.16}$$

where

P_t = transmitted power

G_t = transmitter gain

G_r = receiver gain

σ = radar cross section (RCS)

λ = wavelength

k = Boltzmann's constant

T_0 = receiving system noise temperature

B = noise bandwidth

L = system loss ($L > 1$)

F_n = noise figure

R_t = transmitter to target range

R_r = target to receiver range

The simple changes made to extend the monostatic radar equation to suit bistatic systems will cause major changes in the radar sensitivity map due to interactions between the system configuration and radar performance parameters which will be discussed in the following section.

4.3.2 Bistatic radar sensitivity analysis

As for the monostatic case, bistatic radar sensitivity simulations are developed based on bistatic radar Equation 4.16. To make a fair comparison with the monostatic counterpart, all the used parameters and assumptions remain the same as in Section 4.2. The transmitter gain and receiver gain are assumed to have the same value as monostatic antenna gain 30 dB.

An exemplar bistatic radar sensitivity map on the ground plane is shown in Figure 4.3, where the transmitter and receiver are separated by a baseline of 4km. This figure shows that in this bistatic case, the separation of the transmitter and receiver sites results in a more complex sensitivity map compared with the one shown by the monostatic counterpart. Three regions can be identified: (i) the receiver centred region, (ii) the transmitter centred region and (iii) the receive-transmitter centred region, namely the cosite region.

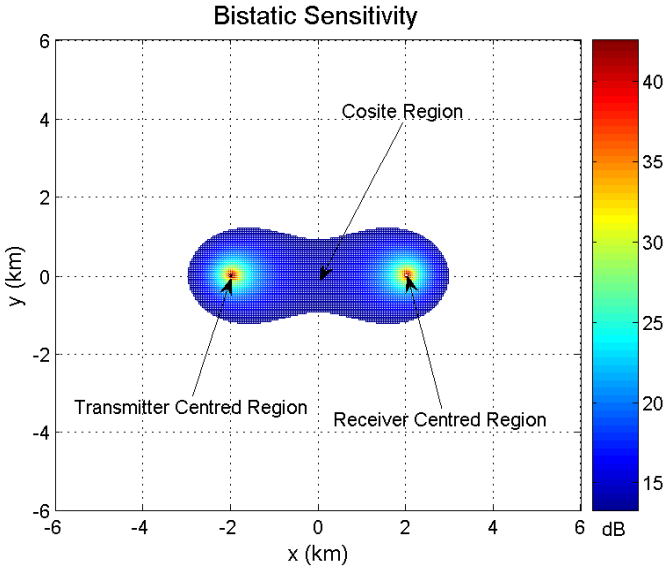

Figure 4.3: Bistatic radar sensitivity map

Again, the following simulations are made to assess bistatic radar sensitivity in three dimensions. Two and three-dimensional coverage plots of this exemplar bistatic radar system are shown in Figure 4.4. It is shown that the shape of bistatic radar three-dimensional coverage is elongated compared with its monostatic counterpart. The coverage volume approximately takes the shape of two adjacent spheres with smaller radius while the monstatic radar coverage volume has a spherical shape. Coverage in the third dimension of height is reduced. This reduction in height is typical if one wants to keep the coverage volume unchanged. This can be mimicked by splitting a spherical water drop into two water drops that connect to each other. When one splits a bigger water drop into two adjacent ones, the radius of the two adjacent water drops will be smaller than the original one. Since the total water amount

contained in the water drops is unchanged, the volume will remain the same. The radius of the split water drop is comparable to the radius of the smaller sphere in the three-dimensional bistatic coverage map which corresponds to the third dimension of height. In this particular example, it is seen that the coverage area of this bistatic radar in the first two dimensions, i.e. the projection of the volumetric coverage map on the ground plane is similar to the monostatic counterpart, although they take different shapes. Therefore, the coverage volume, which can be calculated by integrating the coverage area in the first two dimensions against 360° angle, will also be similar for monostatic and bistatic radar.

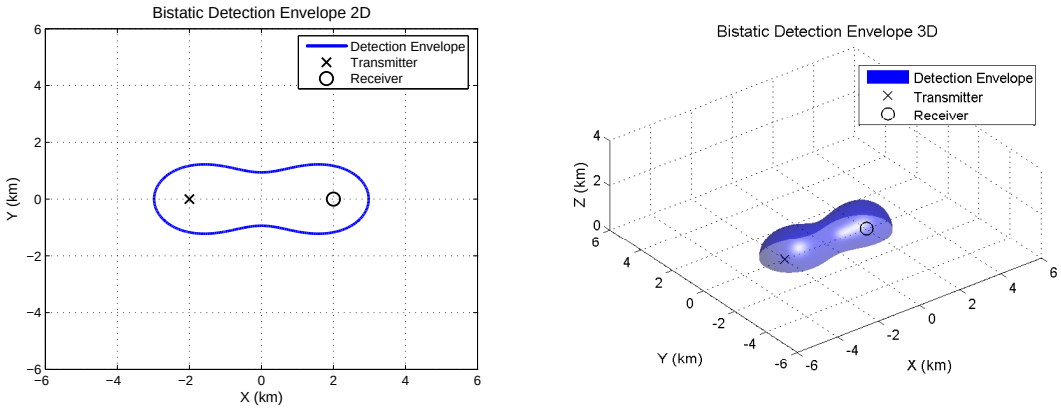

Figure 4.4: 2D and 3D bistatic radar sensitivity

Thus even this very simple case begins to show very significant differences between monostatic and bistatic radar, especially highlighting the need to examine volumetric coverage. This analysis of bistatic radar sensitivity will also constitute the foundation of formulation of netted radar sensitivity which will be the main topic of the following section.

4.4 Netted radar sensitivity

4.4.1 Netted radar equation

In this section we develop the radar equation further to represent the netted radar cases. Using this formulation, we then analyse the sensitivity space for various netted radar geometries. The netted radar equation can be generated by generalising the familiar form of the monostatic and bistatic radar equations to cater for the case of multiple transmitters and/or receivers. Firstly, a

fully coherent radar network is considered, which means that the radars comprising the whole network are assumed to have a common and perfect knowledge of time and space. The whole network is composed of arbitrary number of m transmitters and n receivers. It follows that the whole network is perfectly synchronized and works cooperatively such that each receiver is capable of receiving echoes of the signals from any of the transmitters in the network. The whole radar network can be broken down into a set of $m \times n$ transmitter-receiver pairs, each with a bistatic component contributing to the entirety of the netted radar sensitivity. When the transmitter and receiver constituting the bistatic pair are collocated, it reverts back to the monostatic case, which could also be treated as a special bistatic radar with zero baseline. Thus the network is considered as a connected series of bistatic radar systems. Thermal noise at each receiver is assumed to be statistically independent. For these conditions, the overall netted radar sensitivity can be calculated by summing up the partial signal to noise ratio of each transmitter-receiver pair, which leads to the following equation:

$$SNR_{total} = \sum_{i=1}^{m} \sum_{j=1}^{n} \frac{P_{ti} G_{ti} G_{rj} \sigma_{ij} \lambda_i^2}{(4\pi)^3 k T_0 B_i R_{ti}^2 R_{rj}^2 L_{ij} F_{nij}} \tag{4.17}$$

where

P_{ti} = ith transmitted power

G_{ti} = ith transmitter gain

G_{rj} = jth receiver gain

σ_{ij} = radar cross section (RCS) of the target as seen by the ith transmitter jth receiver

λ_i = ith transmitted wavelength

k = Boltzmann's constant

T_0 = receiving system noise temperature

B_{ij} = bandwidth for the ith transmitter and jth receiver

L_{ij} = system loss for ith transmitter jth receiver, $L_{ij} > 1$

F_{nij} = noise figure for ith transmitter jth receiver, $F_{ij} > 1$

R_{ti} = distance from ith transmitter to target

R_{rj} = distance from target to jth receiver

For $i = j = 1$, when $R_t = R_r$, this equation reverts to the monostatic situation; when $R_t \neq R_r$ it reverts to the bistatic situation.

A simple netted case maybe considered where the radar parameters for every transmitter-receiver combination are the same, then the netted radar equation can be written as:

$$SNR_{total} = \frac{P_t G_t G_r \sigma \lambda^2}{(4\pi)^3 k T_0 B L F_n} \sum_{i=1}^{m} \sum_{j=1}^{n} \frac{1}{R_{ti}^2 R_{rj}^2} \tag{4.18}$$

Now if we compare the netted radar Equation 4.18 with the monostatic radar Equation 4.11 and assume the power transmitted by each transmitter composing the netted radar is the same as the monostatic transmitted power, the transmitter gain and receiver gain for netted radar are the same as monostatic radar gain, all the other parameters are the same for netted radar and monostatic radar, for this particular type of netted radar, the sensitivity gain over corresponding monostatic radar would be:

$$\frac{SNR_{netted}}{SNR_{monostatic}} = R^4 \sum_{i=1}^{m} \sum_{j=1}^{n} \frac{1}{R_{ti}^2 R_{rj}^2} \tag{4.19}$$

If we make a further assumption that $m = n = N$ and $R_{ti} = R_{rj}$ then we will have:

$$\frac{SNR_{netted}}{SNR_{monostatic}} \propto N^2 \tag{4.20}$$

Then the ratio of netted radar sensitivity to monostatic sensitivity will be proportional to the square of the number of transmitters or receivers composing this particular type of radar network. Although this is an approximation, it is still sufficient to give a good estimation of the sensitivity gain achieved by netted radar over monostatic radar.

If the netted radar is non-coherent, the total sensitivity is given by the ratio of total received power over total noise. Therefore, for a non-coherent netted radar composed of m transmitters and n receivers, the radar equation is given by:

$$SNR_{total} = \frac{\sum_{i=1}^{m} \sum_{j=1}^{n} \frac{P_{ti} G_{ti} G_{rj} \sigma_{ij} \lambda_i^2}{(4\pi)^3 R_{ti}^2 R_{rj}^2 L_{ij} F_{nij}}}{\sum_{q=1}^{n} k T_0 B_q} \tag{4.21}$$

As with the coherent netted radar case, if a simple netted radar case is considered where the radar parameters for every transmitter-receiver combination are the same, then the netted radar equation for a non-coherent netted radar can be written as:

$$SNR_{total} = \frac{\frac{P_t G_t G_r \sigma \lambda^2}{(4\pi)^3 L F_n} \sum_{i=1}^{m} \sum_{j=1}^{n} \frac{1}{R_{ti}^2 R_{rj}^2}}{\sum_{q=1}^{n} kT_0 B} \tag{4.22}$$

If $m = n = N$, the above equation can be simplified as:

$$SNR_{total} = \frac{P_t G_t G_r \sigma \lambda^2}{N(4\pi)^3 k T_0 B L F_n} \sum_{i=1}^{N} \sum_{j=1}^{N} \frac{1}{R_{ti}^2 R_{rj}^2} \tag{4.23}$$

The sensitivity gain over monostatic radar will be:

$$\frac{SNR_{netted}}{SNR_{monostatic}} = \frac{R^4}{N} \sum_{i=1}^{N} \sum_{j=1}^{N} \frac{1}{R_{ti}^2 R_{rj}^2} \tag{4.24}$$

Therefore, the sensitivity gain for a non-coherent netted radar over corresponding monostatic radar will be N.

If we consider a netted radar composed of three identical transmitters and three identical receivers, when the processing is coherent, the expected sensitivity gain over corresponding monostatic radar would be 9, while when the processing is non-coherent, the expected sensitivity gain over corresponding monostatic radar would be 3.

In the netted radar Equation 4.18, it is clear that the netted radar geometry (i.e. the positions of target and radar nodes in the network) will be dominant in determining the overall netted radar sensitivity and hence coverage. Thus the relationship between system geometry and performance is beginning to be established. Computer simulations and graphical representation of this geographical dependency for netted radar sensitivity constitute the main topic of the next section. Since the focus is to examine the influence of netted radar geometry on netted radar sensitivity, only examples of coherent netted radar will be shown. Non-coherent netted radar examples can be derived in a similar way.

4.4.2 Netted radar sensitivity analysis

An exemplar coherent netted radar sensitivity map is shown in Figure 4.5. This netted radar system is composed of three identical transmitters and three identical receivers. In order to make a fair comparison between the monostatic and netted cases, the total transmitted power over the whole network is kept the same as for the previous monostatic and bistatic examples. This means that for each of the three transmitters in the network, the transmitted power will

be one third of the transmitted power in previous monostatic and bistatic radar, i.e. 2 W. All the other parameters remain the same as those used for the previous monostatic and bistatic examples. This is the case for all of the following examples, unless stated otherwise. It is further assumed that transmitting and receiving beams are synchronised to look at the same point in space at the same time. Figure 4.5 shows that the netted radar sensitivity map on the ground plane also shows radar-station-centred regions and a decreasing intensity of SNR from the centre outwards with the form of coverage map more complicated than both monostatic and bistatic cases.

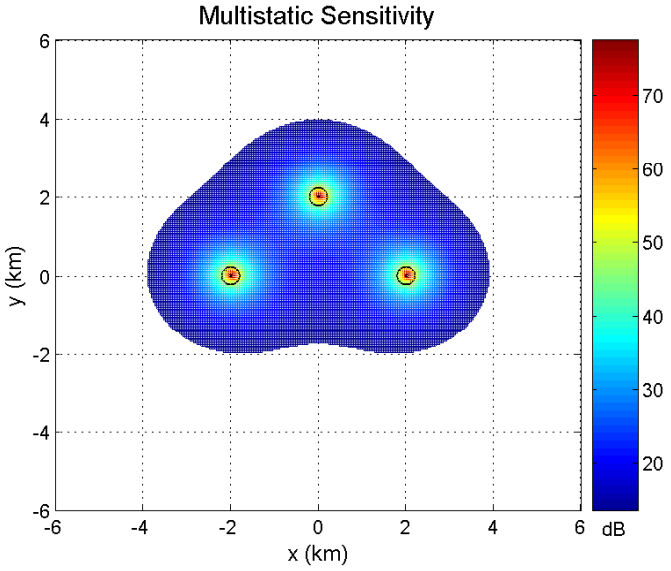

Figure 4.5: Netted radar sensitivity map

As with monostatic and bistatic radars, the next step is to examine netted radar sensitivity in three dimensions. Examples in Figure 4.6 to 4.11 show the range of performance now possible when a network of transmitters and receivers are employed, as compared to the much more familiar concept of monostatic and bistatic systems. Two dimensional and three-dimensional netted radar coverage maps with various system configurations to give a comprehensive understanding of netted radar sensitivity performance. Emphasis will be put on examining the influence of netted radar system geometry, as from netted radar Equation 4.18 it is seen that the geometry will become dominant in determining netted radar sensitivity. This will begin

with examining sensitivity of the simplest netted configuration that mimics simple monostatic radar. In Figure 4.6 the three transmitters and three receivers are all collocated. This arrangement is used to imitate the monostatic system. It is seen that the shape of the coverage map is as expected and is equivalent to the monostatic case. However, the coverage volume is now increased, despite the total transmitted power being the same as in the previous monostatic case. This is because each receiver accepts echoes from all the transmitters, giving a rise in the total received power and therefore resulting in the enlarged coverage volume. In this somewhat extreme example of a netted radar geometry, the radius of the maximum detectable sphere for the netted configuration is 1.3 times greater than the monostatic configuration. It corresponds to 1.7 times increase in the coverage area in two dimensions and 2.2 times increase in the coverage volume in three dimensions. This begins to illustrate the potential sensitivity advantage of a netted configuration.

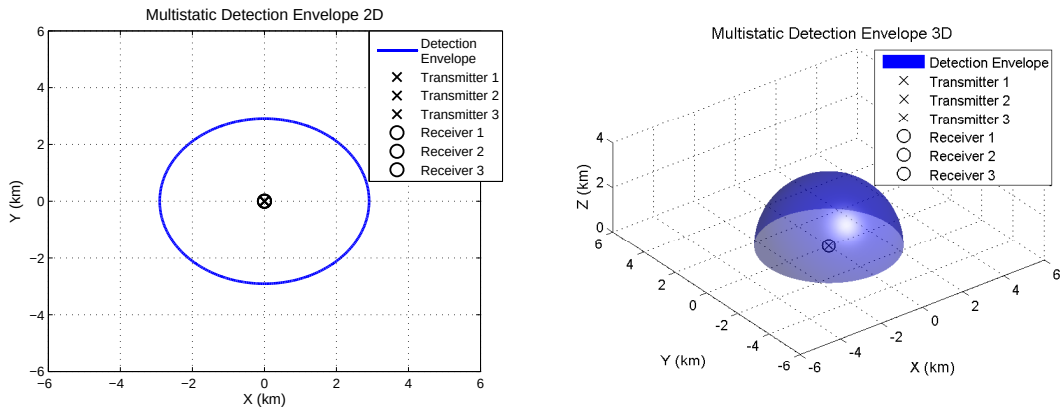

Figure 4.6: 2D and 3D netted radar sensitivity - collocated

The next example is to separate the radar nodes to represent a more realistic configuration, compared with the extreme example shown in Figure 4.6. In this example the netted radar system is composed of three coherently connected monostatic radars, where each single transmitter is collocated with a single receiver. Sensitivity plots of a netted radar system with separated transmitter and receiver nodes are shown in Figure 4.7. In this case the two-dimensional coverage is increased, whereas the average coverage in the third dimension of height is now reduced compared to the one shown in Figure 4.6. This can be explained in a

similar way as in Section 4.3.2 for bistatic cases as the coverage volume remains unchanged. It is noted that with this netted radar configuration the shape of the coverage map in three dimensions becomes more irregular compared with the regular spherical shape provided by simple monostatic radar. This provides a kind of freedom in radar system design.

Another aspect of design freedom of this dispersed coherent netted radar system is clearer to see when compared with the independent monostatic radars, shown in Figure 4.8. It is seen that, when the three monostatic radars work independently, which means each station only receives the signal sent by that station, the area around the coordinate origin is not covered by any of the three radars. When the three radars work coherently, this area is within the system coverage envelope, which means that some targets not detectable (i.e. with SNR $<$ 13 dB) by the independent multiple monostatic radars become detectable by coherent netted radar system with the same geographical configuration. In this way the flexibility of coverage and the improved offering of energy collection are combined to provide greater flexibility in system performance.

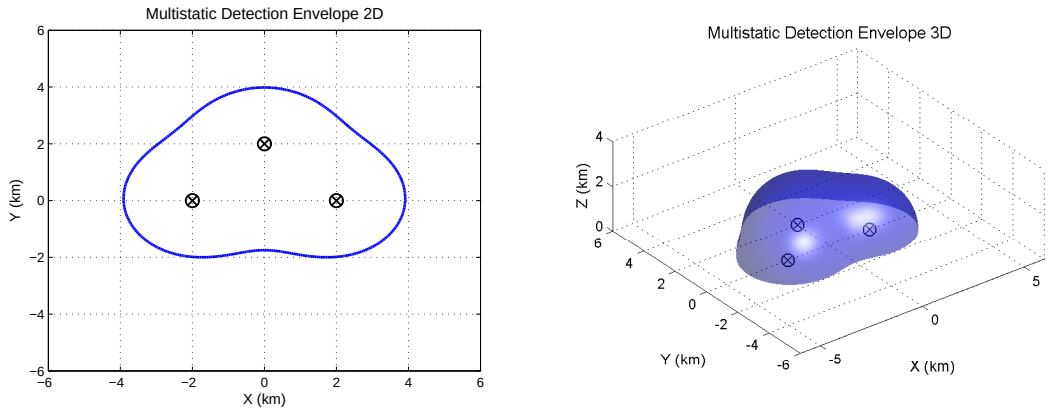

Figure 4.7: 2D and 3D netted radar sensitivity - dispersed

In the third example the transmitters and receivers are further dispersed. This represents a netted radar configuration which is not similar to any combination of monostatic configuration in any ways as no transmitter and/or receiver are collocated. This is shown in Figure 4.9. It is shown that, in this case, the coverage area in the first two dimensions is further increased, while the coverage in the third dimension of height is again reduced. This again illustrates that

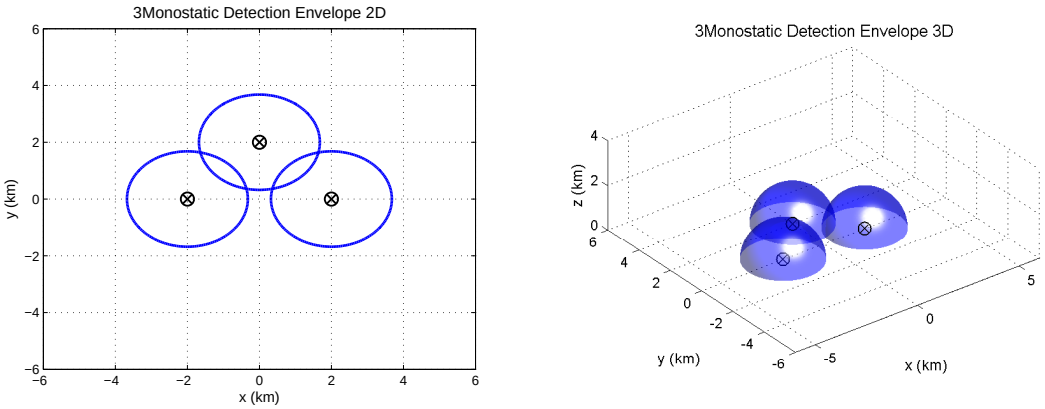

Figure 4.8: 2D and 3D netted radar sensitivity - 3 monostatic

coverage with a netted radar concept can be tailored to a particular requirement.

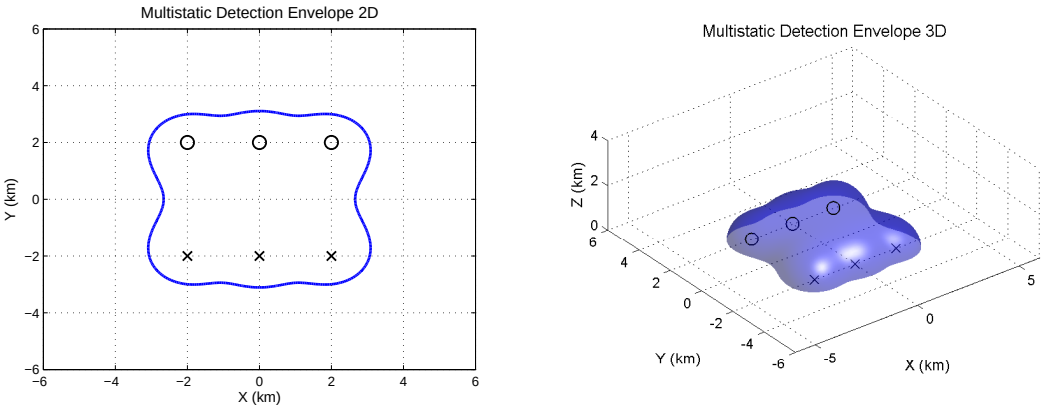

Figure 4.9: 2D and 3D netted radar sensitivity - fully dispersed

In the last example which shows the dependency of netted radar sensitivity on system geometry, a more flexible radar configuration is considered. This represents a type of asymmetrically distributed netted radar system. Here, two monostatic radars are positioned at the bottom part of the surveillance region, while a single transmitter and a single receiver are positioned separately at the top left and right parts of the region respectively, as shown in Figure 4.10. It is shown that coverage maps in three-dimensional space also have asymmetrical shape due to the asymmetrical distribution of the transmitted energy. This occurs in both the ground plane and in height. This offers the possibility to tailor the radar coverage map to a specific

area of interest while still not lose coverage in less interested areas. Therefore the transmitted power can be better utilized.

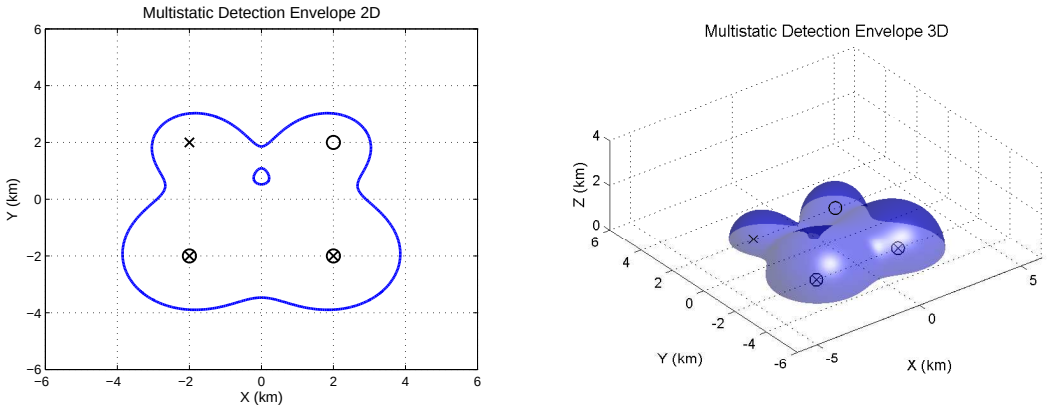

Figure 4.10: 2D and 3D netted radar sensitivity - asymmetrically distributed

A final example is made to examine the influence of other factors apart from geographical configuration in radar equation. This is represented by changing the transmitted power. In Figure 4.11 the total transmitted power is reduced to half of the previous examples, whilst other parameters remain the same. It is shown that the effect is evident. When the transmitted power is reduced, the coverage is reduced in three dimensions as expected.

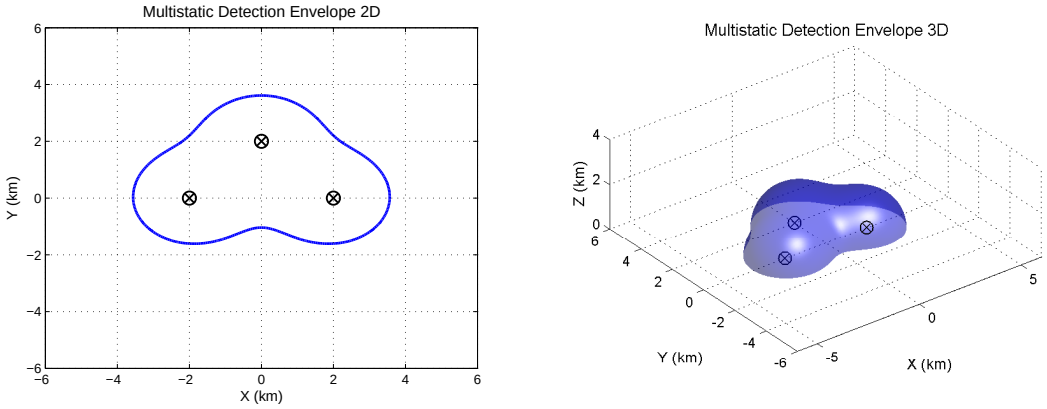

Figure 4.11: 2D and 3D netted radar sensitivity - reduced power

4.5 Practical radar sensitivity influencing factors

The theoretical radar sensitivity model developed and discussed so far is to some extent idealistic. In practical radar applications, one may have to consider other influencing factors to get the most practical radar sensitivity. In this section, some possible influencing factors will be discussed.

The first factor to be considered is the RCS of a target that describes the apparent area of the target perceived by the radar, because in practice its value is not really constant even for simple monostatic radar. Typically the RCS of a monostatic radar partially depends on the radar wavelength. In more complicated bistatic case, the RCS also depends on aspect angle and bistatic angle.

Another factor to consider is whether or not the target is within the line of sight. In the above theoretical models we all assumed that the target is within the line of sight. However, in real radar environment, the line of sight is very likely to be obstructed by other unwanted objects. For example, in a urban area it is possible to be obstructed by tall buildings while in rural area it is more often to be obstructed by hills. Even if the target is within the line of sight, quite often, we still can not simply calculate the noise term as in the equations in the above session. Figure 4.12 is used to show some influencing elements in radar operational environment.

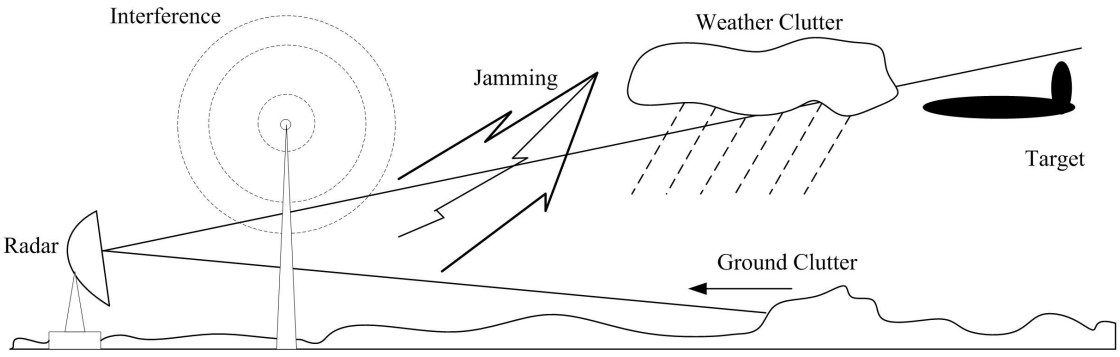

Figure 4.12: Radar and the environment

There is also a good chance to have various factors that will contribute to the system loss term in the radar equation. Depending on the operational situation, the radar signal might be

affected by the return from the ground. It might be influenced by special weather conditions such as rain, hail or snow. The return signal may also be interfered by the transmission of other signals, such as the transmission of other radar signals, intentional jamming signals or other electromagnetic interference.

All the above mentioned elements may be considered as contributing to the noise term in the radar equations and need to be analysed depending on specific implemental situations. Basically for each specific radar system, all factors that may impact the sensitivity of this system need to be examined and included in order to calculate fairly accurate radar sensitivity value.

Finally, it is worth mentioning that, although the sensitivity model developed in this research is simplified, it still provides a useful method to roughly estimate netted radar sensitivity performance, especially when the focus is to compare the netted configuration with other configurations, for example, monostatic or bistatic radar.

4.6 Conclusions

In this chapter, a form of the netted radar equation has been developed and used to analyse netted radar sensitivity as a function of network parameters especially geometry. Three dimensional radar sensitivity simulation method has been developed. This provides a useful way to examine radar sensitivity more comprehensively. Two and three-dimensional simulation examples of monostatic, bistatic and netted radar cases have been presented and compared to demonstrate a range of aspects of radar performance in terms of sensitivity. It has been shown that netted radar system geometry, i.e. the positions of radar transmitters and receivers comprising a radar network has strong impact on netted radar sensitivity. For a ground based netted radar system, the dispersion of radar nodes provides enlarged coverage area in the first two dimensions, but reduced coverage in the third dimension of height. This is in part a function of maintaining transmit power at the same level. Therefore power is conserved and is traded between the horizontal and vertical dimensions of coverage.

Netted radar can also offer a more flexible arrangement of the geometry of the whole system, compared with monostatic and bistatic radar, so that it is possible to configure radar

nodes properly to form desired coverage area. This provides a new degree of freedom in radar system design. This might be extremely valuable in, for example, deployment of a ground based netted radar system in hilly terrain where the probability of achieving a line of sight to a particular zone of interest can be maximized. In other words, netted radar topology can provide a more efficient way to use the available transmitted and reflected power. In addition, the shape of coverage as well as the overall system coverage capability are dependent on the specific geometrical arrangement of the radar nodes, which constitute the netted radar system. Therefore, a specific coverage map can be achieved by carefully arranging the positions of radar nodes in the surveillance area.

Chapter 5

Netted Radar Ambiguity Function

In this chapter we introduce, develop and examine a new form of the ambiguity function that describes range and Doppler resolution and range and Doppler ambiguity, fundamental to the performance of any radar system. To set the scene, the well known monostatic ambiguity function is briefly reviewed. This is followed by an introduction to a bistatic form of ambiguity function. We then develop the bistatic concept by linking pairs of bistatic ambiguity function to create description for the netted cases. This is then used to highlight differing ambiguity conditions in netted radar.

5.1 Introduction

5.1.1 Background

The ambiguity function arose from detection and parameter estimation problems concerning a slowly fluctuating point target being observed in an additive white Gaussian noise. It is widely recognized that the ambiguity function is an important tool to qualitatively assess radar performance in terms of resolution and clutter rejection. It should be noted that for a radar system the concept of resolution is different from accuracy. Resolution refers to the radar ability to distinguish different targets which are close to each other in terms of range and Doppler. It is obvious that the further separated in range and Doppler the two targets, the easier they will be distinguished one from the other [57]. Figure 5.1 can be used to illustrate the concept of range resolution. It is shown in Figure 5.1 (a) that, when the separation of the returns from two targets in the time domain is greater than one pulse duration, two echoes can be observed

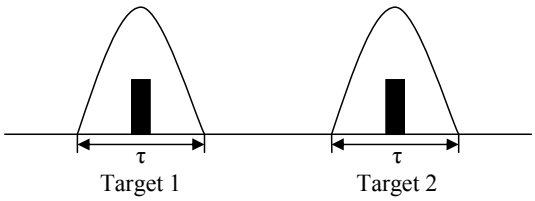

(a) Two targets separated by more than one pulse duration

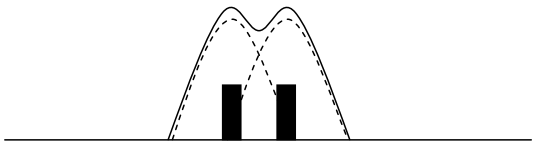

Target 1 Target 2

(b) Two targets separated by less than one pulse duration

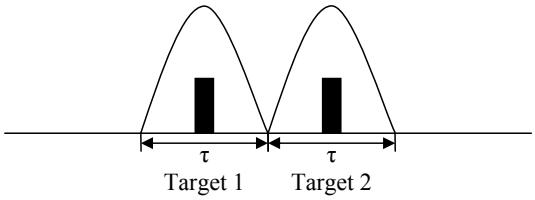

(c) Two targets separated by one pulse duration

Figure 5.1: Radar range resolution

leading to two separate targets. When the separation of the two returns from different targets in the time domain is smaller than the duration of the pulse, the returns will merge. In this case, the two targets might be determined as one big target, as shown in Figure 5.1 (b). When the separation of the two returns is similar to the duration of the pulse, they become just recognizable as two separate targets, as in Figure 5.1 (c). Considering the relation between range and delay defined by Equation 3.1, the range resolution in this simple illustrative example is given by:

$$\Delta R = \frac{1}{2} c\tau \tag{5.1}$$

where ΔR is the range resolution, τ is the pulse duration, c is the speed of radio wave propagation.

Measurement accuracy is the ability of a radar to determine the real location and absolute velocity of a target. It is more complicated than resolution. Intuition tells us that the accuracy

will be affected by the sharpness of the pulse, which is related to the bandwidth of radar. Typically, the wider the bandwidth the more likely for the system to have higher accuracy. Another factor influencing the accuracy of a radar system is the signal to noise ratio, due to the fact that the noise can corrupt the shape of the pulse.

Resolution and accuracy are both related to another term called ambiguity, which is just another word for uncertainty. The following example explains the ambiguity in radar applications. In Figure 5.2 a pulse train is used as the transmitting signal. If the target is at a short range from the radar, it is necessary to ensure that the return of the echo from target is in between the transmission of the first and the second pulse, i.e. the echo returns before the second pulse is transmitted, as the echo from target A (Figure 5.2), the target range can be decided as 40 km with no ambiguity. However, if the target is at a relatively long range from the radar, (target B shown in Figure 5.2), the echo from it comes back after the second pulse is transmitted. It is impossible to decided whether it is echo from the second pulse, which corresponds to a short range of 40 km or from the first pulse, which corresponds to the longer range of 140 km. We can assume a maximum unambiguous range of 100 km, R_u. Now this is an example where the echo comes back after the second pulse has been transmitted. If the echo comes back after a few pulses have been transmitted, a decision has to be made among several R_u. And the ambiguity is even more complex. From this relative simple example, it is easy to see that the maximum unambiguous range for such a radar system relates to the time duration of the pulse transmitting interval. Considering the relation of range and time defined by Equation 3.1, the maximum unambiguous range is given by:

$$R_u = \frac{1}{2}cT \tag{5.2}$$

where T is the pulse transmitting interval which is inversely proportional to Pulse Repetition Frequency (PRF), i.e. $T = \frac{1}{PRF}$.

5.1.2 Definition of ambiguity function

The ambiguity function was first defined by Woodward [74]. It can be seen as the absolute value of the envelope of the output of a matched filter when the input to the filter is a Doppler

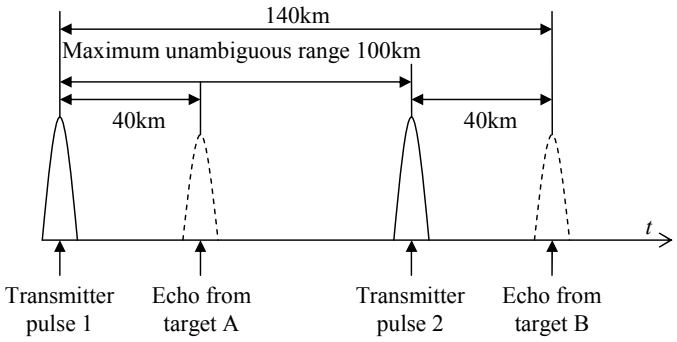

Figure 5.2: Radar range ambiguity

shifted version of the original transmitted signal, to which the filter is matched. If $u(t)$ is the complex envelope of the transmitted signal, the transmitted signal can be expressed as:

$$S_T(t) = Re\{u(t)\exp(j\omega_c t)\} \tag{5.3}$$

where ω_c is the carrier frequency.

At reception, the signal will be delayed by the travel path and the Doppler affected by target movement. Ignoring the propagation losses, the received signal reflected from a slowly moving point target is given by:

$$S_R(t) = Re\{u(t-\tau)\exp[j(\omega_c+\omega_d)t]\} \tag{5.4}$$

where ω_d is the Doppler shift resulted from target moving given by:

$$\omega_d = 2\pi\nu \tag{5.5}$$

where τ is the time delay, and ν is the Doppler frequency. In monostatic radar systems they will have the following relations with range R and target velocity V, respectively.

$$\tau = \frac{2R}{c} \tag{5.6}$$

where c is the speed of radio wave propagation.

$$\nu = -\frac{V\omega_c\cos\theta}{\pi c} \tag{5.7}$$

where θ is the angle between target velocity and the line connecting monostatic radar node and the target.

By passing through the received signal to a matched filter, the output is defined as ambiguity function, which is given by[75]:

$$|\chi(\tau,\nu)| = \left| \int_{-\infty}^{\infty} u(t)u^*(t-\tau)\exp(j2\pi\nu t)dt \right| \tag{5.8}$$

The practical importance of the ambiguity function is that it describes the output signal from a matched filter when the input signal is time delayed by τ and Doppler shifted by ν with respect to the nominal signal with which the matched signal is supposed to give the maximum output. The two key parameters for ambiguity function calculation are the time delay τ, and the frequency shift ν. Special attention should be taken when applying this equation, as the time delay and Doppler frequency defined relative to a nominal point in the delay-Doppler plane. When the nominal point is not at the coordinate origin, appropriate substitutions should be made to reflect the shift. For example, in a monostatic case, if the matched filter is matched to a point with 600 s delay and 5000 Hz Doppler frequency, τ should be substituted by $\tau_a - 600$, and ν should be substituted by $\nu_a - 5000$, where τ_a and ν_a are the actual delay and Doppler of the signal in the delay-Doppler plane of interest.

From this definition it is seen that the ambiguity function associates two system parameters determining the radar performance, range and velocity, with two signal parameters, delay and Doppler. Therefore, it provides a tool to evaluate how well one can find the range and velocity of targets and how the design of signal can help. The definition of ambiguity function may vary slightly in literature. Sometimes the name of ambiguity function is used for $\chi(\tau,\nu)$ or $|\chi(\tau,\nu)|$, and sometimes for $|\chi(\tau,\nu)|^2$. This is not going to affect the core concept of ambiguity function so as to the function of this tool.

Since the ambiguity function is two-dimensional, i.e. each function value is defined by two independent variables, it is helpful to analyse the ambiguity properties by looking at the cuts along two separate axes representing different independent variables, which by definition are delay and Doppler. The first interesting cut is the ambiguity function cut along the delay axis. Setting $\nu = 0$ in Equation 5.8, it is given by:

$$|\chi(\tau,0)| = \left| \int_{-\infty}^{\infty} u(t)u^*(t-\tau)dt \right| \tag{5.9}$$

This cut of ambiguity function along the delay axis represents the shape of "Range Window" at zero Doppler. It tells us how the shape of the matched filter output will change with time.

Naturally, the other cut of interest will be the cut along the frequency axis. This is derived by setting $\tau = 0$ in Equation 5.8, given by:

$$|\chi(0,\nu)| = \left| \int_{-\infty}^{\infty} |u(t)|^2 \exp(j2\pi\nu t) dt \right| \tag{5.10}$$

And this cut of ambiguity function along the frequency axis tells us how the shape of the matched filter output will change with Doppler frequency.

As a useful tool, the ambiguity function is normally represented by graphical plots. Typically it is plotted in three dimensions with respect to the delay-Doppler plane. However, it is more meaningful to plot it on a range-velocity plane, because these two are the useful parameters for measurement, and extremely useful to show the influence of system geometry on the shape of ambiguity function. From Equation 5.6 and 5.7, it is seen that in monostatic radar cases, the transformation from delay to range and Doppler to velocity are both linear. Therefore, the transformation from the delay-Doppler plane to the range-velocity plane should not affect the shape of the monostatic ambiguity function.

Examples of ambiguity function for monostatic, bistatic and netted radar cases will be presented in the following sections. Emphasis is put on the development of netted radar ambiguity models, and comparison of netted radar with monostatic and bistatic radar performance in terms of ambiguity properties.

5.2 Monostatic radar ambiguity

This section provides examples of the monostatic radar ambiguity function, i.e. where the transmitter and receiver are collocated. From the definition in Equation 5.8, the following basic properties of the monostatic ambiguity function can be proven for a normalized transmitting signal, where the complex envelope of the signal $u(t)$ has a unit energy, i.e. $E = 1$:

1.

$$|\chi(\tau,\nu)| \leq |\chi(0,0)| = 1 \tag{5.11}$$

2.

$$\int_{-\infty}^{\infty}\int_{-\infty}^{\infty}|\chi(\tau,\nu)|^2\,d\tau d\nu = 1 \tag{5.12}$$

3.

$$|\chi(-\tau,-\nu)| = |\chi(\tau,\nu)| \tag{5.13}$$

4. if $u(t) \leftrightarrow |\chi(\tau,\nu)|$, then

$$u(t)\exp(j\pi kt^2) \leftrightarrow |\chi(\tau,\nu+k\tau)| \tag{5.14}$$

Property 1 says that the maximum value of the ambiguity function for a normalized signal is one, which is achieved at the origin point defined by nominal delay and Doppler. Property 2 says that the volume underneath the ambiguity function is a constant equal to one. The combination of these two tells us an important thing that, if we try to squeeze the ambiguity function into a very sharp spike at the origin point, the volume must appear somewhere else, implying the ideal form of ambiguity diagram is unachievable. Property 3 indicates the symmetry of the ambiguity function with respect to the nominal origin. Property 4 says when the complex envelope of a signal is multiplied by a linear frequency, the relation between this new signal and the original signal. This is very useful when analysing the ambiguity function of a pulse compressed signal, e.g. linear FM (Frequency Modulation) signal. The proof of these properties can be found in [76].

Three basic transmitted signals are used to show the influence of signal type on the shape of the monostatic ambiguity function, including a single frequency pulse, a linear FM pulse and a train of three coherent pulses. Each example contains an ambiguity function 3D mesh plot, a contour plot, and cuts along range and velocity axes, where the x, y, z axes represent the magnitude of range, velocity and ambiguity function respectively. It should be noted that the ambiguity function is plotted with respect to the range-velocity plane, rather than the more typically used delay-Doppler plane, because range and velocity are the parameters of interest in practice. According to the relations between range-delay and velocity-Doppler defined by Equation 3.1 and 3.2, in monostatic cases the transformation from delay to range and Doppler

to velocity are both linear. In this case, the shape of monostatic ambiguity function should not be affected by this change of axes.

Figure 5.3 shows the ambiguity diagram of a single pulse. The envelope of a single pulse is a real function given by:

$$u(t) = \frac{1}{\sqrt{t_p}} \text{rect} \frac{t}{t_p} \tag{5.15}$$

where t_p is the pulse length, and the "rect" function is defined as:

$$\text{rect}(x) = \begin{cases} 1, & |x| < 1/2 \\ 0, & |x| > 1/2 \end{cases} \tag{5.16}$$

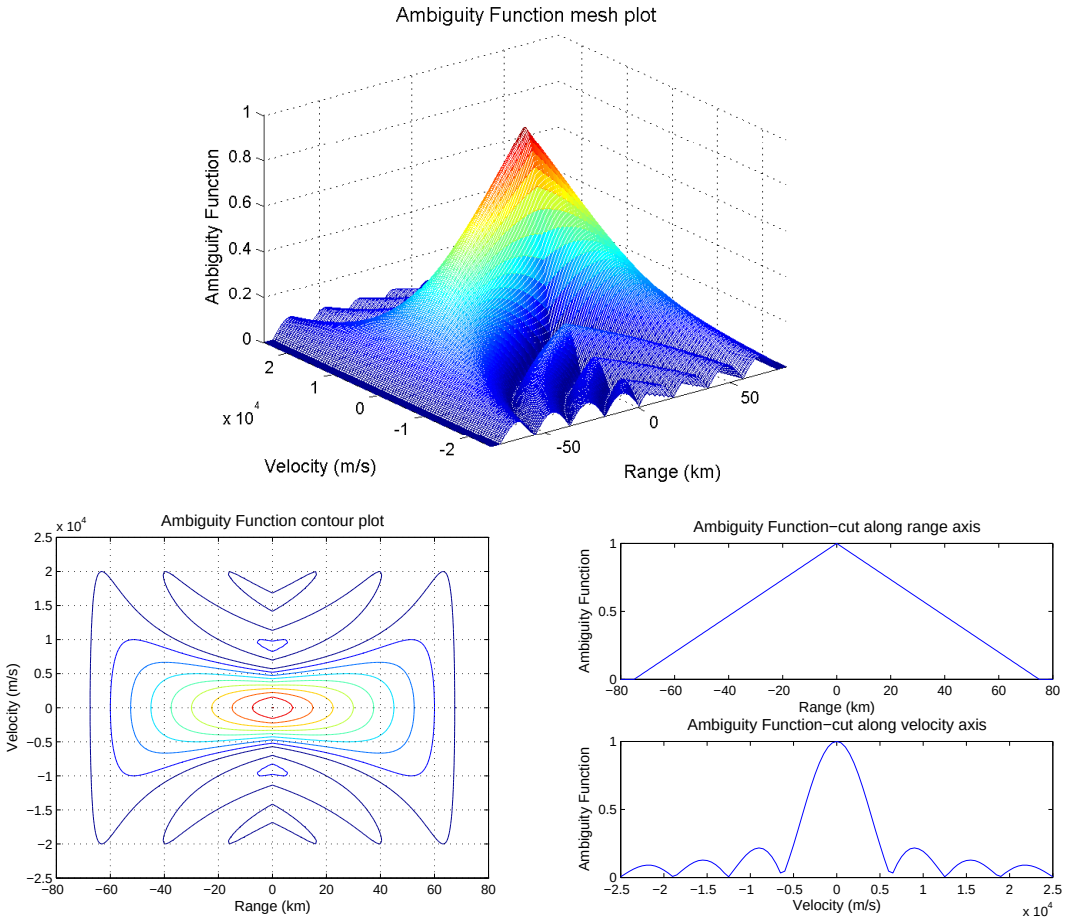

Figure 5.3: Ambiguity function of a single pulse

In this illustrative example, the filter is matched to a stationary target, V_a = 0, at R_a = 0. The pulse length is 500 μs, choosing an arbitrary pulse length. The cut along range and velocity axes are obtained by setting $V = 0$ and $R = 0$ respectively. The resolution is given by the width of the main peak. This first simple example shows that the shape of ambiguity function of an actual signal is different from the ideal radar ambiguity diagram (a spike of infinitesimally small width appears at the origin and everywhere else is zero).

The next example shows the ambiguity diagram of a linear FM pulse in Figure 5.4. This is a typical waveform employed in modern radar systems. The complex envelope of such a signal is given by:

$$u(t) = \frac{1}{\sqrt{t_p}}\text{rect}\left(\frac{t}{t_p}\right)\exp(j\pi kt^2) \tag{5.17}$$

The instantaneous frequency $f(t)$ of this signal is given by differentiating the argument of the exponential and then dividing by 2π:

$$f(t) = \frac{1}{2\pi}\frac{d(\pi kt^2)}{dt} = kt \tag{5.18}$$

It is clear that $f(t)$ is a linear function.

In this example, the filter is again matched to a stationary target, V_a = 0, at R_a = 0. The pulse length is 100 μs. Looking at cuts along range and velocity axes gives us clear understanding of resolution property of this signal. From Figure 5.4, we can see that the cut along the velocity axis does not change because we did not add amplitude modulation. However, the change in the cut along the range axis is significant, because of the frequency modulation. It is found that in a linear FM signal, a Doppler shift is coupled to a delay, making it potentially difficult to distinguish between them.

The final example shows the ambiguity diagram of a coherent pulse train, the general form of the complex envelope of such a signal is given by:

$$u(t) = \frac{1}{\sqrt{N}}\sum_{n=0}^{N-1} u_n(t - nT_R) \tag{5.19}$$

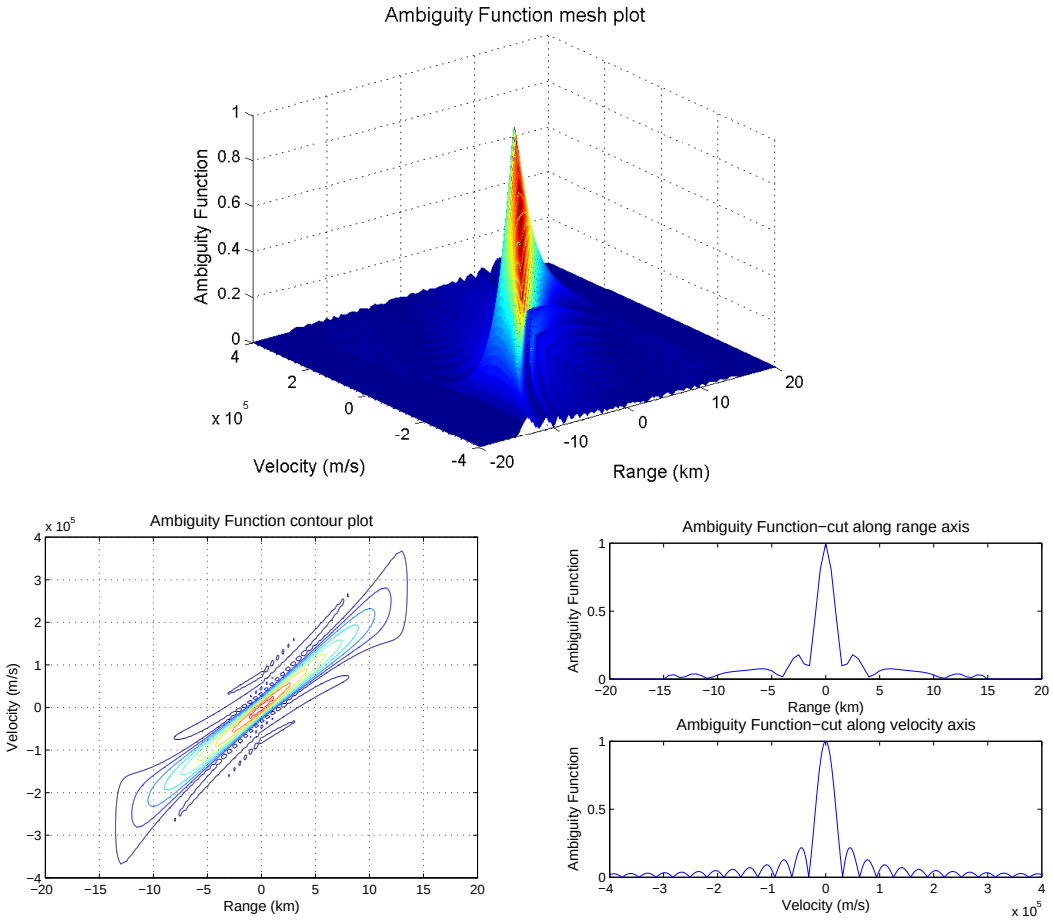

Figure 5.4: Ambiguity function of a linear FM pulse

where N is the number of pulses, and T_R is the pulse repetition period.

In this example, the filter is again matched to a moving target, V_a = 600 m/s, at R_a = 60 km. The whole train comprises three single rectangular pulses with 40 μs pulse length and 100 μs period. In Figure 5.5, it is shown that this transmitted waveform moves most of the volume underneath ambiguity diagram from the origin by forming other smaller peaks elsewhere, resulting in a rather narrow peak near the origin. This is significantly different from the above two examples, where only one main peak appear and the volume underneath the ambiguity diagram is mainly concentrated around the origin. This shows that the ambiguity function plots are able to provide information on range and Doppler resolution and ambiguity.

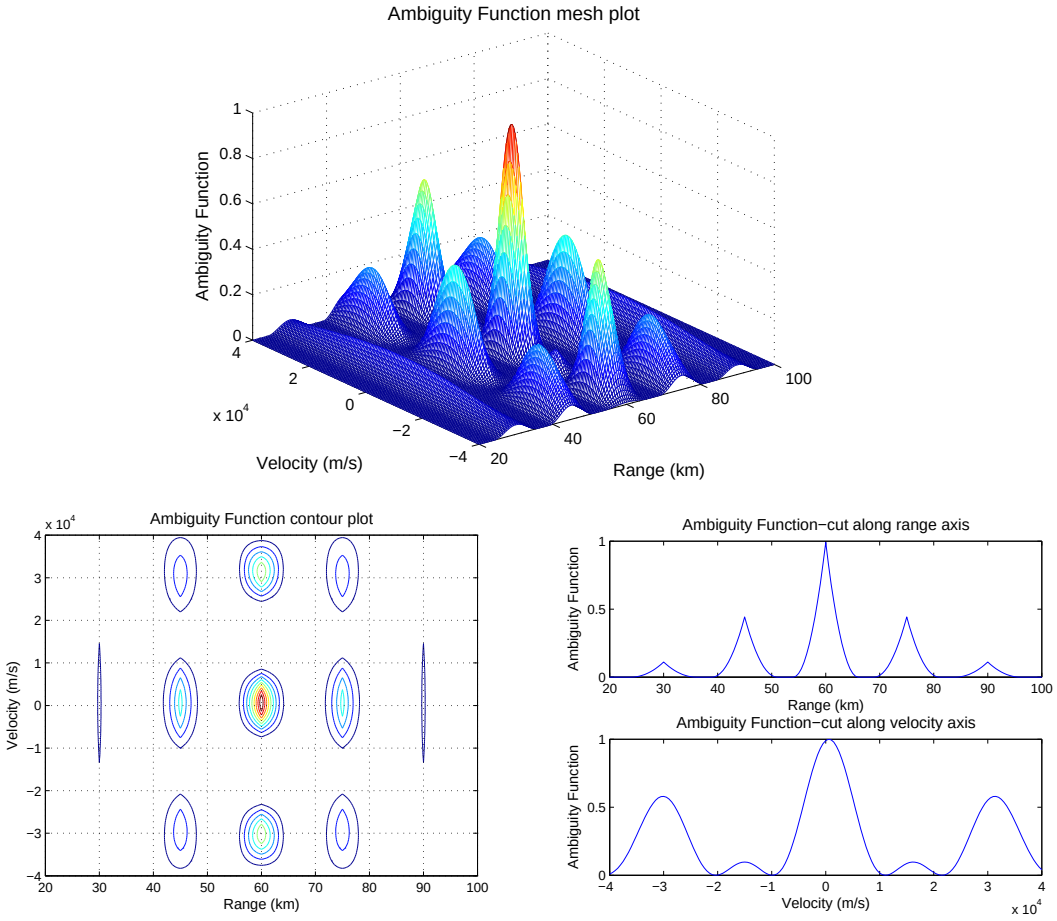

Figure 5.5: Ambiguity function of a train containing 3 pulses

It is worth mentioning that the shape of monostatic radar ambiguity function is dependent on the type of transmitted signal only and is not dependent on the range and velocity of the target. The latter two parameters only affect the displacement of the ambiguity diagram in the range-velocity plane. One can modify the ambiguity diagram to maneuver its volume in the delay-Doppler, or range-velocity plane by complicating the basic pulse signal. The ability to control the shape of the ambiguity diagram is very important, as it allows the radar designers to prevent signals from undesired targets or clutter to appear in the range and velocity windows of the targets of interests.

5.3 Bistatic radar ambiguity

5.3.1 Bistatic radar ambiguity function model

After examining monostatic ambiguity properties, bistatic ambiguity function are now presented, where the transmitter and receiver are spatially separated by a baseline distance L. A form of the bistatic ambiguity function was developed by Tsao [55]. This is attractive as it provides useful insight into the factors that subsequently govern the performance of the netted systems. It also leads itself to adaptation to encompass a form applicable to netted radar as is developed in Section 5.4

It is north-referenced coordinate system that is used to represent bistatic geometry [5], which is shown in Figure 5.6. This is a two-dimensional coordinate system confined to the bistatic plane formed by transmitter T_x, receiver R_x, and target, with a north-up orientation [55]. The look angle θ_T of the transmitter and the look angle θ_R of the receiver are measured positive clockwise from the north of the coordinate system. β and ϕ represent the bistatic angle and the angle formed by velocity vector and bistatic bisector, respectively. Finally, R_T and R_R are the range from transmitter to target and the range from receiver to target, respectively.

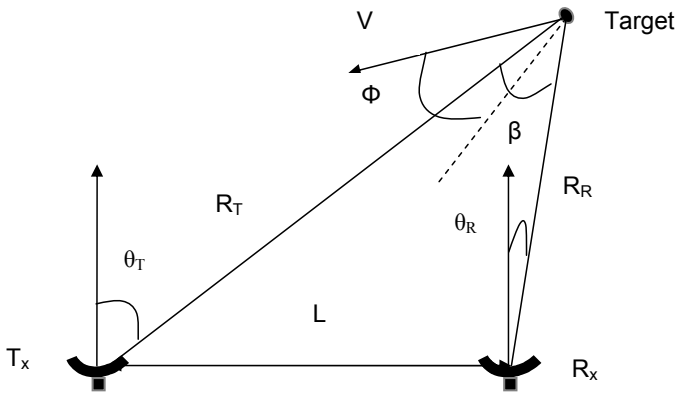

Figure 5.6: Bistatic radar north-referenced coordinate system

For bistatic radar, the transformation from delay-Doppler to range-velocity plane is not linear. This result in major differences between simple monostatic radar and bistatic radar ambiguity functions. When the calculation is referenced to the receiver, it can be expressed in terms of target-receiver range R_R, receiver look angle θ_R, baseline length L, velocity V and

angle ϕ, given by:

$$\tau = \frac{R_R + \sqrt{R_R^2 + L^2 + 2R_R L \sin\theta_R}}{c} \tag{5.20}$$

$$f_b = \frac{\omega_c V \cos\phi}{\pi c} \sqrt{\frac{1}{2} + \frac{R_R + L\sin\theta_R}{2\sqrt{R_R^2 + L^2 + 2R_R L \sin\theta_R}}} \tag{5.21}$$

where ω_c is the carrier frequency, f_b is bistatic radar Doppler shift, and $V\cos\phi$ is the magnitude of the projection of velocity vector along the bistatic bisector direction. Therefore, the bistatic ambiguity function is calculated by:

$$|\chi(R_R, \theta_R, L, V, \phi, \omega_c)|^2 = \left| \int_{-\infty}^{\infty} u(t) u^*(t-\tau) \exp(j2\pi f_b t) dt \right|^2 \tag{5.22}$$

Compared with the monostatic radar ambiguity function equations shown in Equation 5.6 to 5.8, it is seen that in bistatic radar cases, both delay and Doppler are defined by more factors that relates to the bistatic radar system geometry. Therefore, it is expected that the shape of bistatic radar ambiguity function will be dependent on bistatic radar system geometry.

5.3.2 Bistatic radar ambiguity function analysis

Bistatic radar ambiguity diagrams derived from the bistatic model developed in Section 5.3.1 will be presented in this section with respect to the range-velocity plane. The signal used for bistatic simulation is a coherent pulse train containing three rectangular pulses, with 40 μs pulse length, and 100 μs period. The carrier frequency is 3×10^8 rad/s. This is the same signal as used in [55], which is useful for clear illustration of ambiguity properties and provides a reason of cross-checking results. This signal is used in the rest of this chapter for the simulation unless stated otherwise. Other parameters defining the bistatic geometry are as follows: the baseline length is 100 km, and the target is 60 km away from the receiver with 600 m/s velocity along the bistatic bisector direction. The reference point is the receiver, which means that the range is calculated with respect to the receiver.

A group of four ambiguity diagrams and the geometry of the radar and the position of the target are shown for each of the cases in Figure 5.7 to Figure 5.10, with $\theta_R = 90^\circ, 45^\circ, -45^\circ, -85^\circ$, respectively, where the top left subfigure shows system geometry; the top right subfigure shows the bistatic radar ambiguity function three-dimensional mesh plot;

the bottom left subfigure shows the cuts along the range and velocity axes; and the bottom right subfigure shows the bistatic radar ambiguity function contour plot.

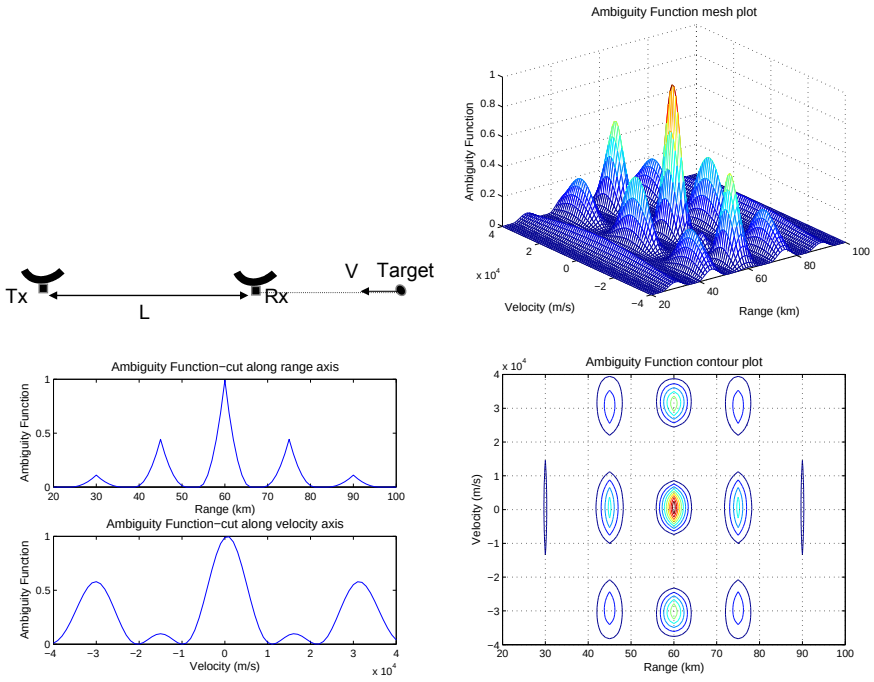

Figure 5.7: Bistatic ambiguity function for $\theta_R = 90°$

From Figure 5.7 to Figure 5.9, it is basically to move the target closer to the bistatic baseline. In Figure 5.7, it is shown that when the target lies on the extension of bistatic baseline, the bistatic ambiguity function is identical with the monostatic counterpart shown in Figure 5.5. In Figure 5.8 and Figure 5.9 it is shown that, when the target moves around the receiver, the relative position of the target with respect to the baseline changes, and the bistatic ambiguity diagram varies correspondingly. Also, it is observed that with decreased look angle θ_R, the resolution in both the range and velocity domain deteriorates, and the side-peaks corresponding to ambiguities move away from the main peak, showing a trade-off between the resolution and ambiguity performance.

Moving to the somewhat extreme final case in Figure 5.10, which shows that, when the target is very close to the bistatic baseline, resolutions in both range and velocity deteriorate dramatically. Therefore, the radar system is not capable of resolving targets. To verify if

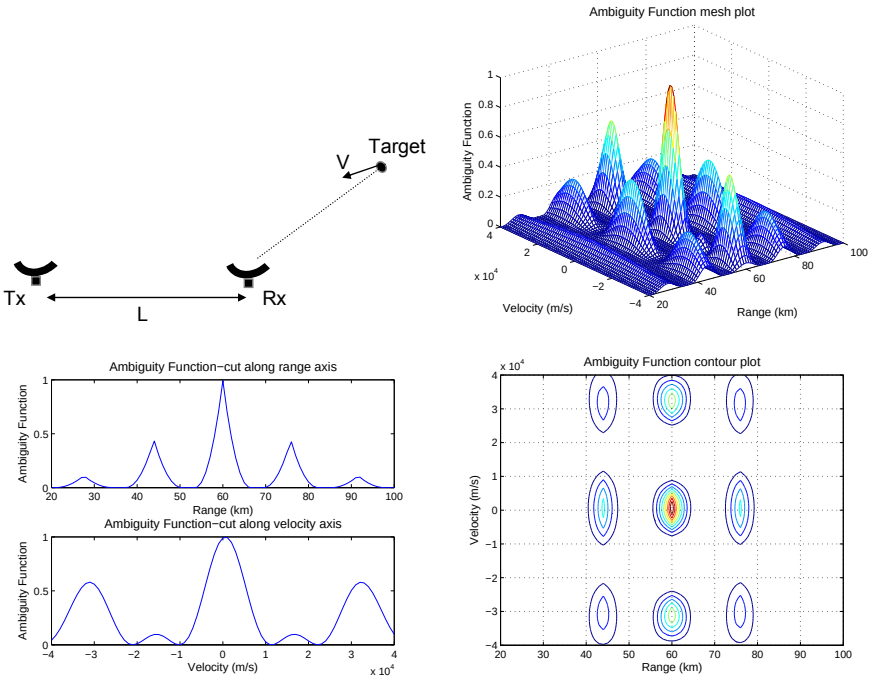

Figure 5.8: Bistatic ambiguity function for θ_R = 45°

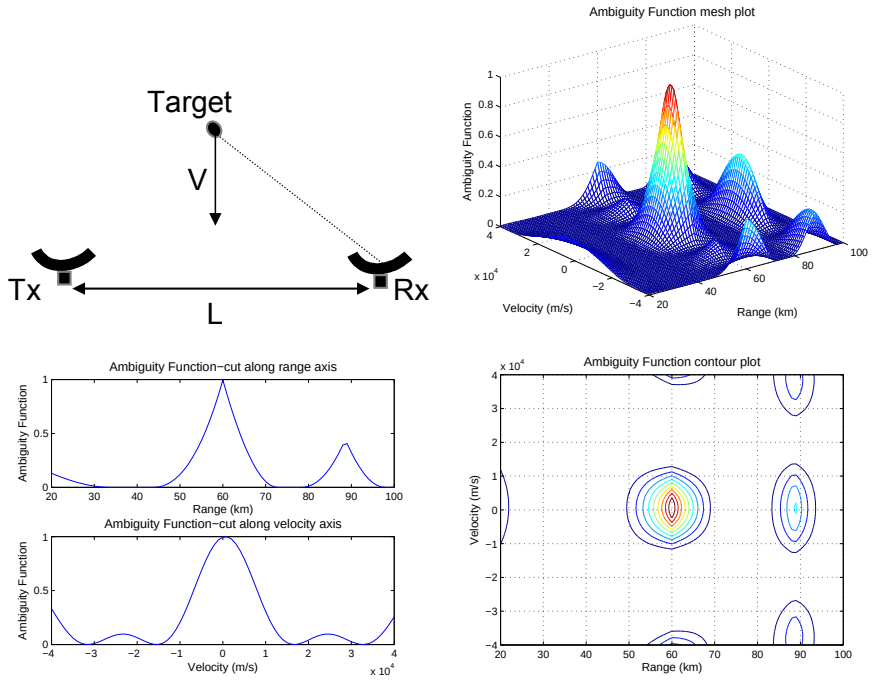

Figure 5.9: Bistatic ambiguity function for θ_R = -45°

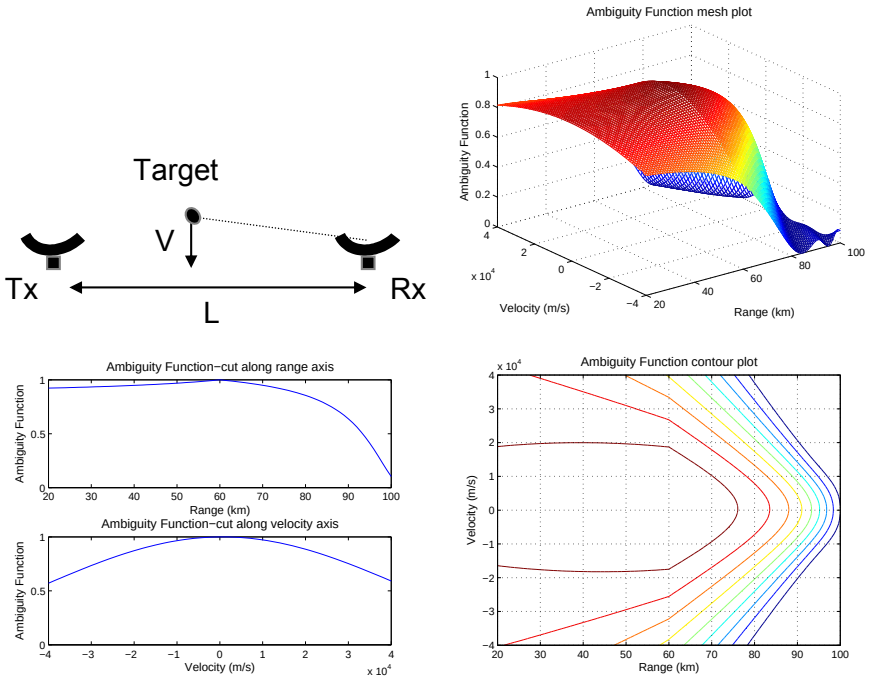

Figure 5.10: Bistatic ambiguity function for θ_R = -85°

this is a special case for this specific kind of signal, the following two sets of simulations are made with various kind of radar signals, but the same kind of geometrical parameters as is used in Figure 5.10, i.e. the baseline is 100 km long, and the target is 60 km away from the receiver with 600 m/s velocity along the bistatic bisector direction. In Figure 5.11, the transmitted signal is a single pulse. This is the same as the one used in Figure 5.3. In Figure 5.12, the transmitted signal is a linear FM pulse. This is the same as the one used in Figure 5.4. The reason of choosing these signal is just for the ease of making a comparison with the monostatic ambiguity function plots shown in Section 5.2. From these simulations it is clear to see that despite the transmitted signal being used, as long as the target is close to the bistatic baseline, the ambiguity function deteriorates. Therefore it is the system geometry, instead of the transmitted signal, that plays a rather important role in determining the bistatic radar ambiguity properties. This makes a big difference with the monostatic ambiguity function, where the shape of it is only dependent on the signal being used.

One more simulation is carried out to investigate the influence of the geometrical param-

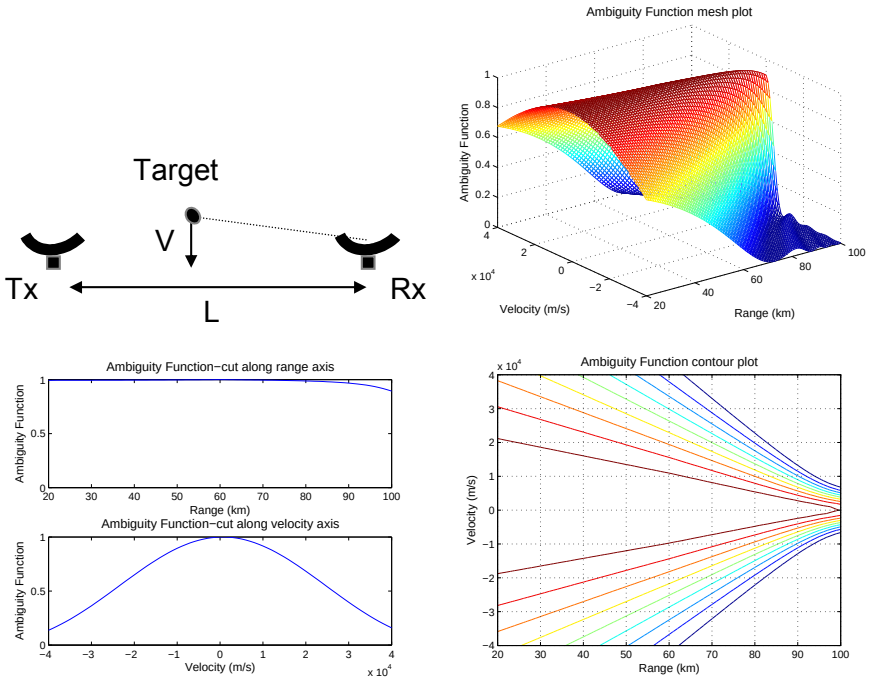

Figure 5.11: Bistatic ambiguity function for θ_R = -85°, single pulse

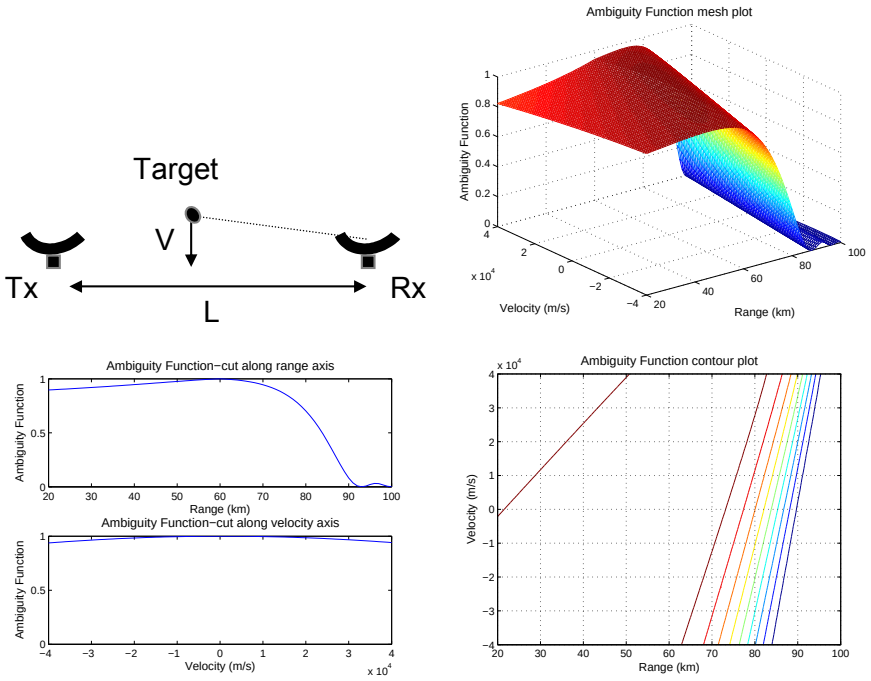

Figure 5.12: Bistatic ambiguity function for θ_R = -85° LFM

eter on the bistatic ambiguity function. This time the signal being used comes back to the one defined in the beginning of this section, i.e. a coherent pulse train containing three identical pulses. Figure 5.13 shows the ambiguity diagram of a bistatic radar system with shorter baseline compared to the former examples. In this simulation, the baseline length is 30 km, which is half of the target-receiver range R_R, and all the other parameters remain the same as in the previous examples. The look angle θ_R is -45°. It is shown that in this case the bistatic radar behaves as a monostatic one. The degradation of resolution does not exist. It is because that the target is so far away that the transmitter and receiver are approximately collocated.

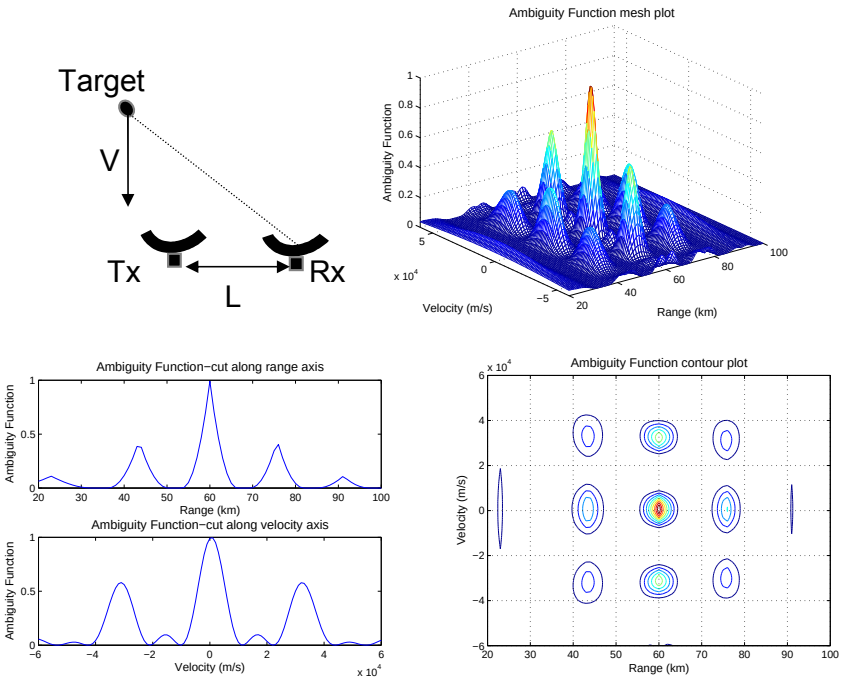

Figure 5.13: Bistatic ambiguity function for L = 30 km, θ_R = -45°

All the above examples demonstrated that the bistatic radar geometry plays an important role in the bistatic ambiguity function properties. This cannot be observed if the ambiguity function is plotted with respect to the conventional delay-Doppler plane, which disregards the bistatic geometry. Clearly, this will also be an important factor in the netted cases which, as been described already, can be thought of a series of connected bistatic systems.

5.4 Netted radar ambiguity

5.4.1 Netted radar ambiguity function model

The netted radar ambiguity function is going to be examined in this section, for both two-dimensional and three-dimensional topologies, where multiple transmitters and/or receivers are employed. An important assumption for this section is that the radar network is coherent, so that the echoes which arrive at different time intervals can be processed in phase.

A simple example of a netted radar topology is shown in Figure 5.14 in three-dimensional space. In effect a single additional transmitter has been added as this helps illustrate the effect of migrating from a bistatic radar case to a netted radar case.

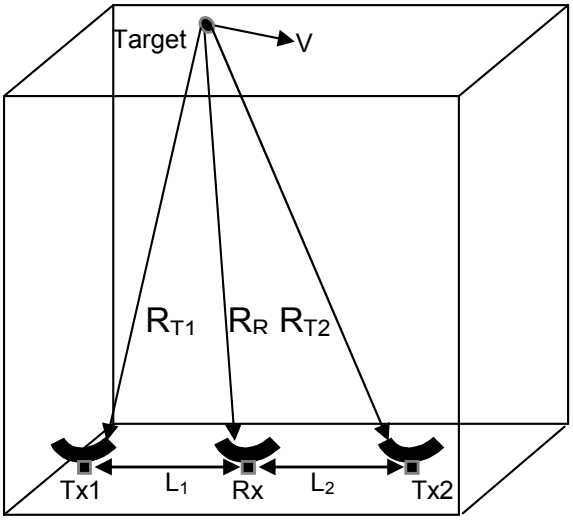

Figure 5.14: 3D netted radar topology

The netted radar ambiguity function is simply developed based on the bistatic radar ambiguity function. To account for the three-dimensional system geometry a vectorial approach is used to calculate the two key parameters, τ and f_b, for the ambiguity calculation. They are given by:

$$\tau = \frac{\left|\overrightarrow{R_T}\right| + \left|\overrightarrow{R_R}\right|}{c} \tag{5.23}$$

$$f_b = \frac{1}{\lambda}\left[\frac{d}{dt}\left(\overrightarrow{R_T} + \overrightarrow{R_R}\right)\right] = \frac{1}{\lambda}\left[\frac{\overrightarrow{R_T}\cdot\overrightarrow{V}}{\left|\overrightarrow{R_T}\right|} + \frac{\overrightarrow{R_R}\cdot\overrightarrow{V}}{\left|\overrightarrow{R_R}\right|}\right] \tag{5.24}$$

where $\overrightarrow{V}$ is the target velocity vector, whereas $\overrightarrow{R_T}$ and $\overrightarrow{R_R}$ are target to transmitter range vector, and target to receiver range vector, respectively.

The netted radar considered here is composed of N transmitters and one common receiver. This configuration provides the convenience that it is possible to calculate all the bistatic ambiguity functions with respect to the same reference point, i.e. the common receiver, and therefore gives the unified form of netted radar ambiguity function. As been mentioned already, the netted radar system can be treated as a set of connected bistatic radar systems. The weighted form of netted radar ambiguity function for the above system is developed by the following three steps: Firstly, to calculate the bistatic ambiguity function for each transmitter-receiver pair composing the netted radar system by:

$$\chi_i(\tau_i, f_{bi}) = \int_{-\infty}^{\infty} u(t)u^*(t-\tau_i)\exp(j2\pi f_{bi}t)dt \tag{5.25}$$

Secondly, to calculate the weighting factor according to the SNR contribution. Assuming that all the transmitters are identical and at receiving, the noise level for each transmitter-receiver pair is the same, the SNR will be proportional to the received signal power and therefore the weighting factor can be calculated by:

$$P_{Ri} = \frac{P_{Ti}G_{Ti}G_R\lambda^2\sigma}{(4\pi)^3(R_{Ti}R_R)^2}, i = 1, 2, \ldots N \tag{5.26}$$

The output of the matched filter is voltage which is proportional to the square root of the power, therefore, the weighting factor is calculated by:

$$w_i = \frac{\sqrt{P_{Ri}}}{Max(\sqrt{P_{Ri}})} \tag{5.27}$$

Finally, since the system is coherent, the overall netted radar ambiguity function weighted by received signal to noise ratio can be calculated by:

$$|\chi|^2 = \left|\sum_{i=1}^{N} w_i\chi_i\right|^2 \tag{5.28}$$

5.4.2 Netted radar ambiguity function analysis

This section is concerned with the netted radar ambiguity diagram examples, plotted using the models developed in Section 5.4.1, where the netted radar comprises N transmitters and one single receiver. All the baselines in the netted radar system are with the same length for simplicity. The transmitted signal is again a train of three pulses, which is the same as used in Section 5.3.2. Both the two-dimensional and three-dimensional netted radar ambiguity diagrams are presented for comparison. In the three-dimensional scenario, it is assumed that the transmitters and receiver are located in one plane, and the target is moving in another plane which is parallel to the transmitter/receiver plane. This is to take into account the third dimension of height which was omitted in previous work. In each example, the left figure shows the ambiguity function contour plot and the right figure shows the ambiguity function cuts along the range and velocity axes. Since it is not possible to show all cases, a limited set of results that highlight the forms of netted radar ambiguity function will be shown.

Figure 5.15 shows the netted radar system geometry used for the case where the target is far from all the original bistatic baselines and where two transmitters and one common receiver are employed. In this first example, the baseline length is 10 km and the target is 6 km away from receiver for two-dimensional simulation with 600 m/s velocity. The receiver look angle θ_R is -10°. Target is 10 km high for three-dimensional analyses. The ambiguity diagrams for

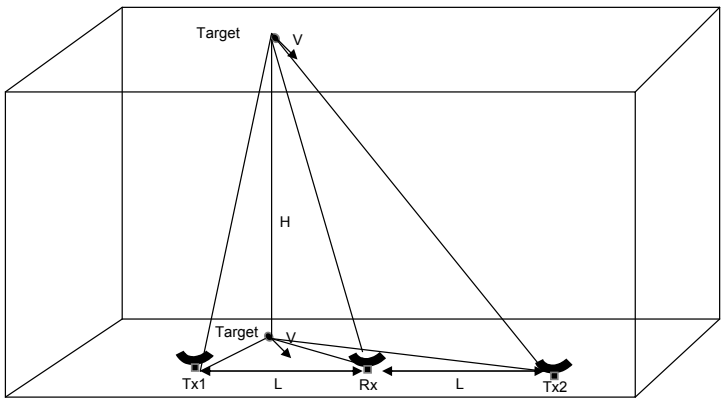

Figure 5.15: Netted radar topology - target far from baseline

two-dimensional and three-dimensional simulations for the above system geometry are shown

in Figure 5.16 and Figure 5.17, respectively. Because the target is far from all the original bistatic baselines, the two-dimensional ambiguity does not show severe deterioration. On the other hand, in the three-dimensional case, moving the target from the transmitter-receiver plane does not change the system resolution capability greatly.

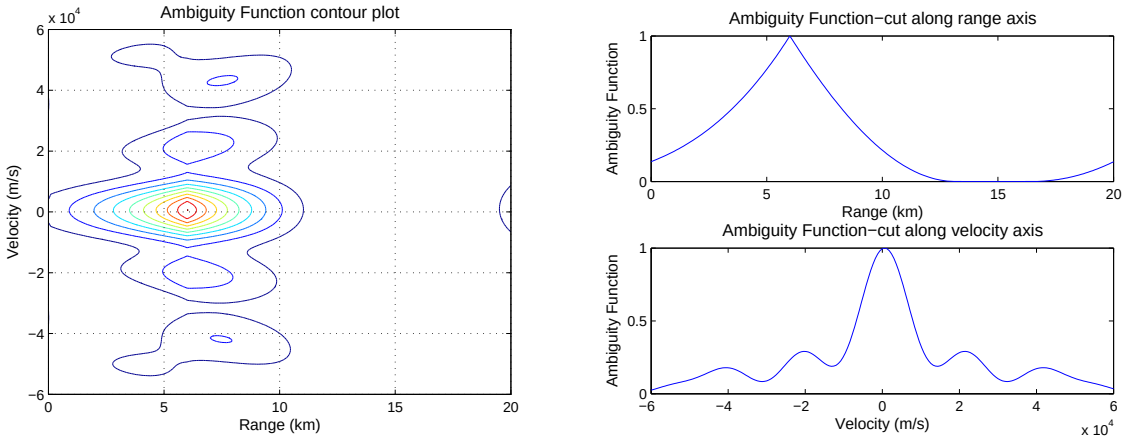

Figure 5.16: 2D Netted radar ambiguity - target far from baseline

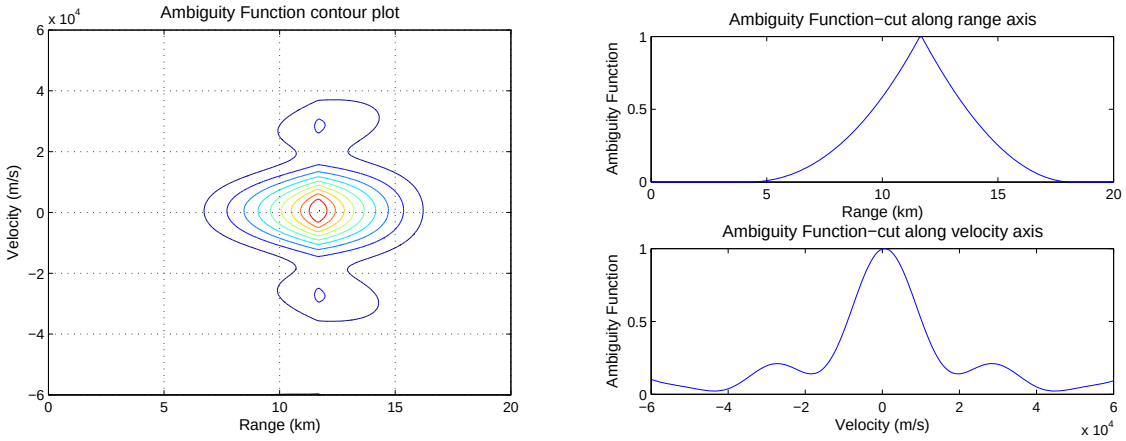

Figure 5.17: 3D Netted radar ambiguity - target far from baseline

Emphasis here is put on the cases where the target is located close to one of the original bistatic baselines, because this is where the deterioration in range and velocity resolution occurs in the bistatic cases (shown in Section 5.3.2). This arrangement is achieved by setting the receiver look angle θ_R as 80°, shown in Figure 5.18.

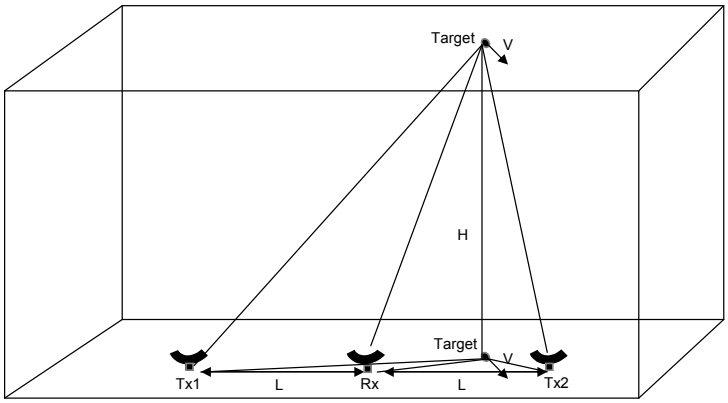

Figure 5.18: Netted radar topology - target close to baseline

In the first four examples of this arrangement, the baseline length is 10 km, the projection of the target on the ground plane is 6 km away from the receiver, and the target velocity is 600 m/s. Figure 5.19 shows the two-dimensional ambiguity diagram, while Figure 5.20, 5.21 and 5.22 show three-dimensional ambiguity diagrams with a target height of 20 km, 10 km and 2 km, respectively. Three-dimensional examples with different target heights are presented to show the effect of varying target height on the form of netted radar ambiguity properties. Figure 5.19 illustrates that in the two-dimensional netted radar scenario, when the target is located close to a bistatic baseline , the system resolution in both the range and velocity domains deteriorates dramatically. In this case, the netted radar is not capable of resolving target parameters. In Figure 5.20, the target is far enough from the transmitter-receiver plane, with a height of 20 km. Both range and velocity resolutions are improved greatly. However, if the target is not far enough from the transmitter-receiver plane, the improvement is not satisfactory. This is shown in Figure 5.21 and Figure 5.22. In Figure 5.21, where the target is 10 km high, resolution in both range and velocity domains are improved, compared to the two-dimensional case, but it is still not as good as the 20 km height one. In Figure 5.22, where the target is 2 km high, there is almost no improvement can be observed. In other words, the target should be far enough away from the transmitter-receiver baseline to achieve satisfactory improvement in range and velocity resolution.

The following examples show the ambiguity function of the netted radar with long base-

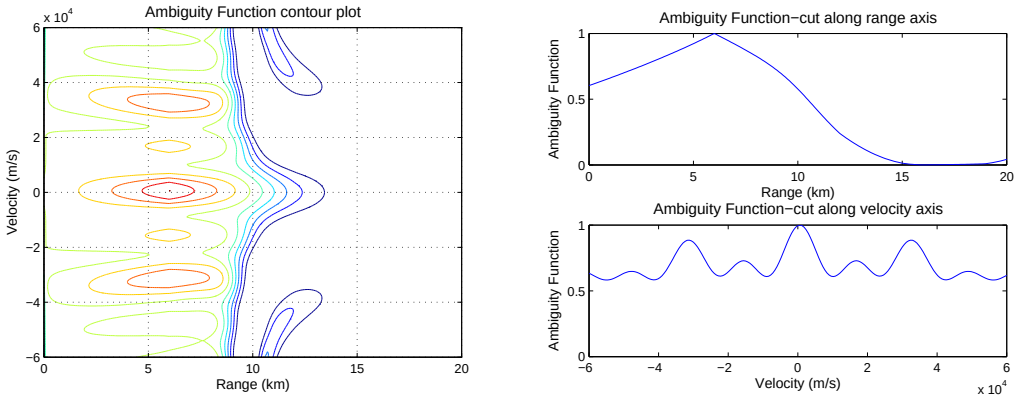

Figure 5.19: 2D Netted radar ambiguity - target close to baseline

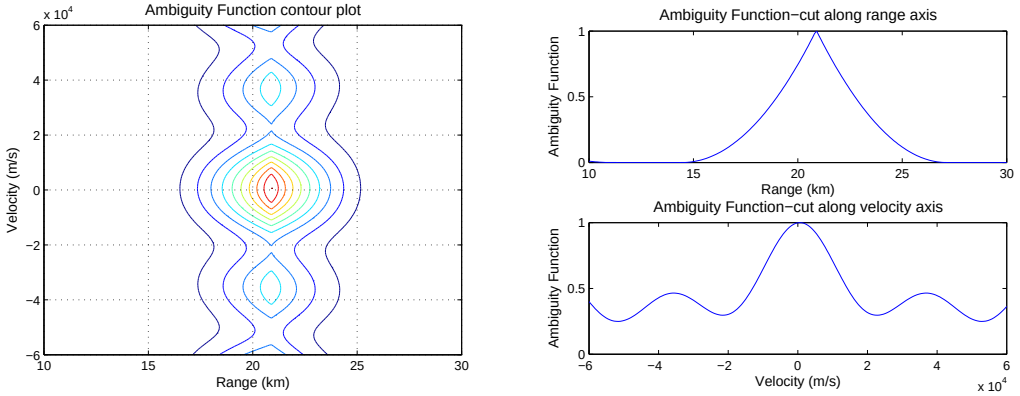

Figure 5.20: 3D Netted radar ambiguity - target close to baseline, H = 20 km

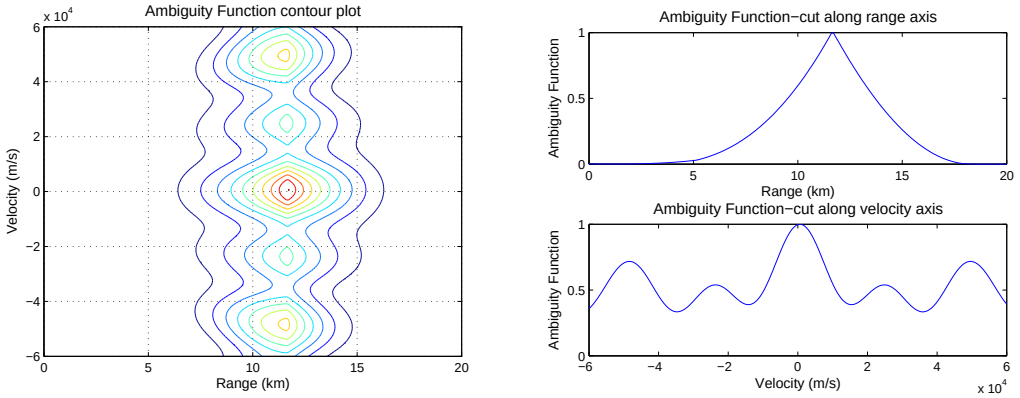

Figure 5.21: 3D Netted radar ambiguity - target close to baseline, H = 10 km

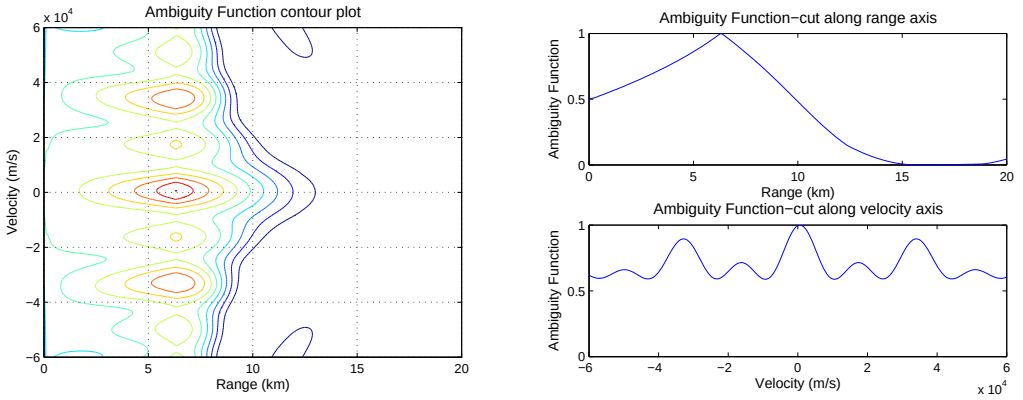

Figure 5.22: 3D Netted radar ambiguity - target close to baseline, $H = 2$ km

lines, where the baseline length is 100 km, the projection of the target on the ground plane is 60 km away from receiver with 600 m/s target velocity. Figure 5.23 shows the degradation of resolution in range and velocity domains for the two-dimensional netted radar case. Figure 5.24 shows the three-dimensional ambiguity function with target height of 20 km. It is observed that, although the absolute value of target height is big enough, because the relative value compared to baseline length is not big enough, satisfactory improvement of the range and velocity resolution is still not achievable.

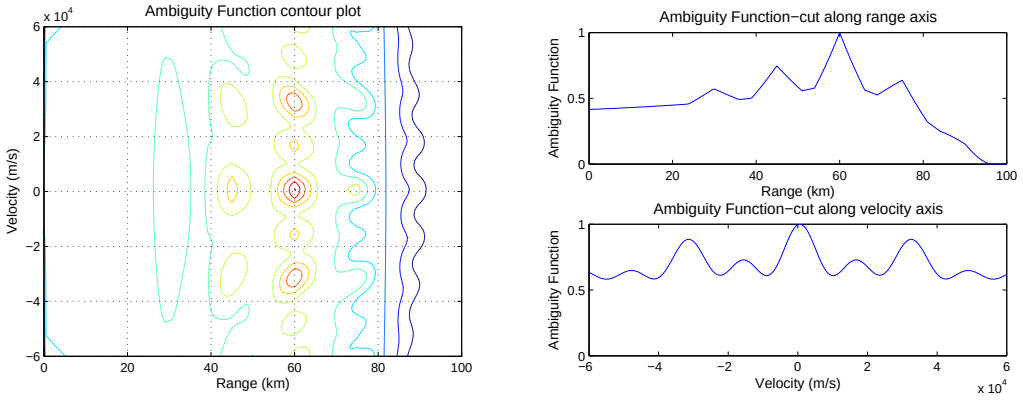

Figure 5.23: 2D Netted radar ambiguity - long baseline

A more complicated netted radar geometry is taken into account in the following examples, where four transmitters and one common receiver are employed. The two-dimensional

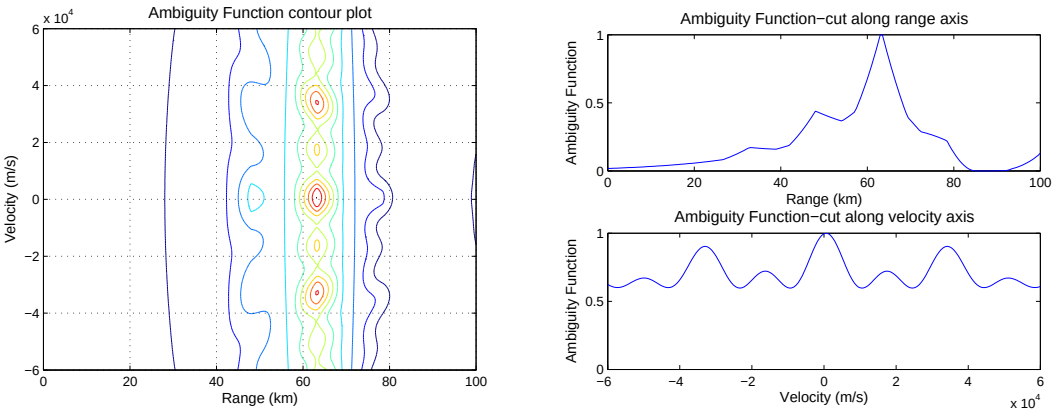

Figure 5.24: 3D Netted radar ambiguity - long baseline, H = 20 km

system topology of this configuration is shown in Figure 5.25. Only targets close to the baseline are simulated for comparison with the two transmitter topologies.

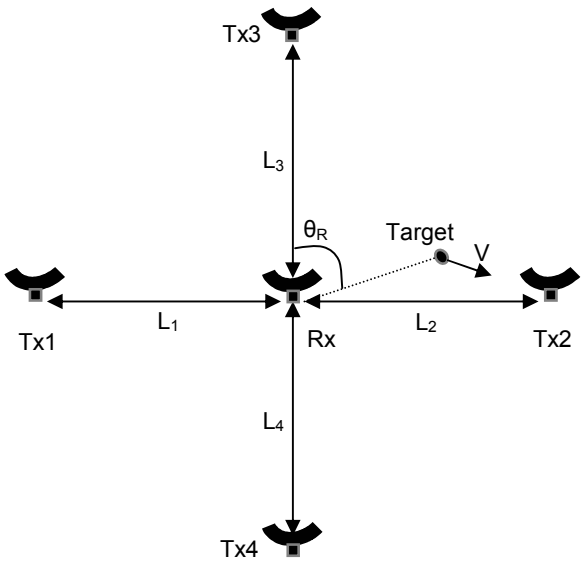

Figure 5.25: Netted radar topology - 4 transmitters 1 receiver

In the first example with four transmitters, the baseline length is 10 km, the target is 6km far from the receiver with 600 m/s velocity. Two-dimensional netted radar ambiguity function of this system geometry is shown in Figure 5.26. The target is 20 km high for the

three-dimensional case and three-dimensional netted radar ambiguity function of this system geometry is shown in Figure 5.27. It is observed that, the resolution in both the range and velocity domain is further improved compared to the case with two transmitters which is shown in Figure 5.20, especially in the velocity domain. In this four transmitter case, the sublobes that appear in the two transmitter counterpart are suppressed leaving only one main peak in the velocity domain.

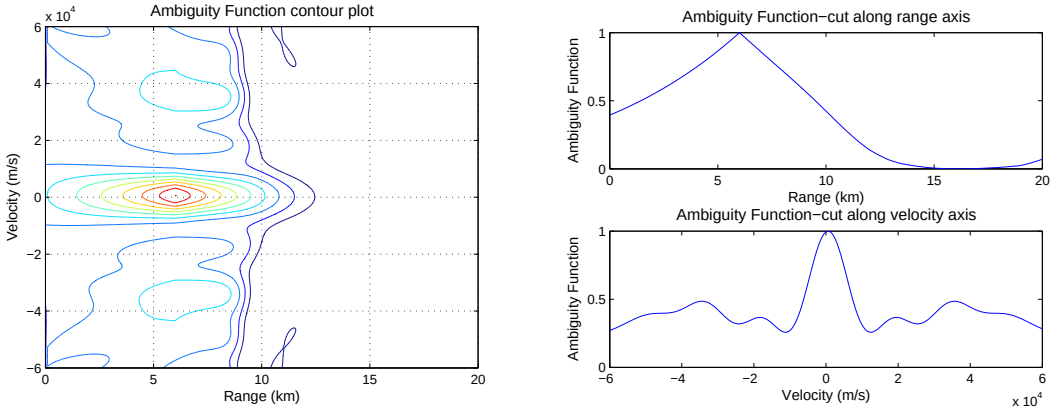

Figure 5.26: 2D Netted radar ambiguity - 4 transmitters

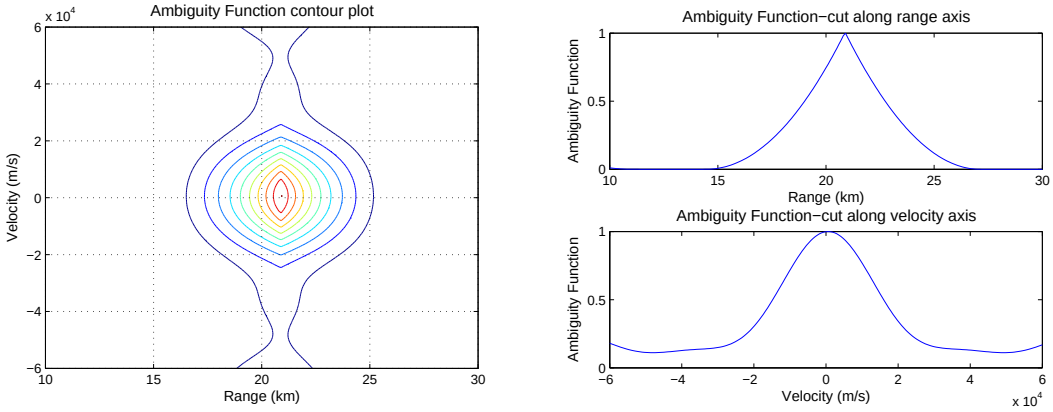

Figure 5.27: 3D Netted radar ambiguity - 4 transmitters, $H = 20$ km

The final example is used to show the effect of a long baseline of 100 km. The target is 60 km far from the receiver with a velocity of 600 m/s. Two-dimensional netted radar ambiguity function of this system geometry is shown in Figure 5.28. The target is 20 km high for the

three-dimensional case. Three-dimensional netted radar ambiguity function of this system geometry is shown in Figure 5.29. It is shown that the system range resolution capability in the three-dimensional case is improved compared with the two transmitter system which is shown in Figure 5.24. There is no obvious improvement in velocity resolution has been found. In this four transmitter case, although the baseline is long, a relatively sharp peak appears, while the three-dimensional system is capable of resolving some targets. It demonstrates that in the long baseline scenarios, when it is not possible to further increase the target height, adding more radar nodes may be another way to improve netted radar resolution capability.

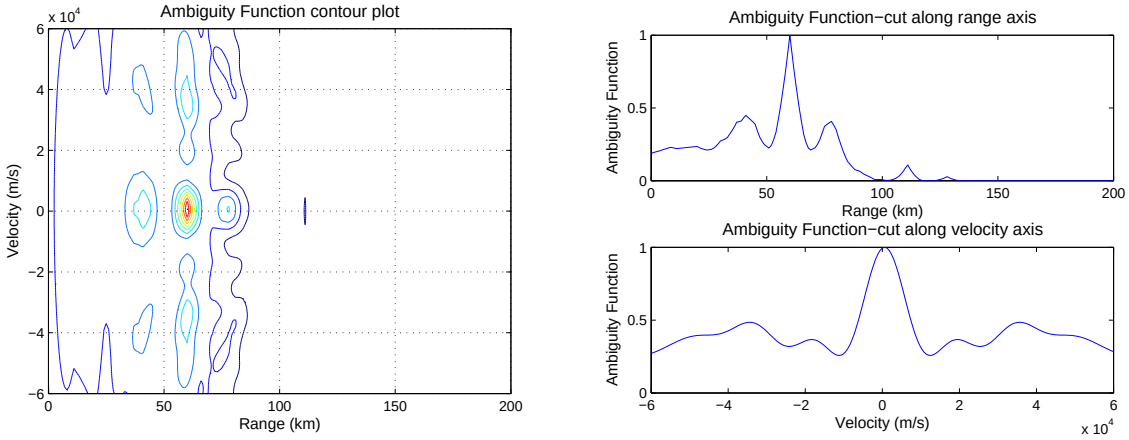

Figure 5.28: 2D Netted radar ambiguity - 4 transmitters, long baseline

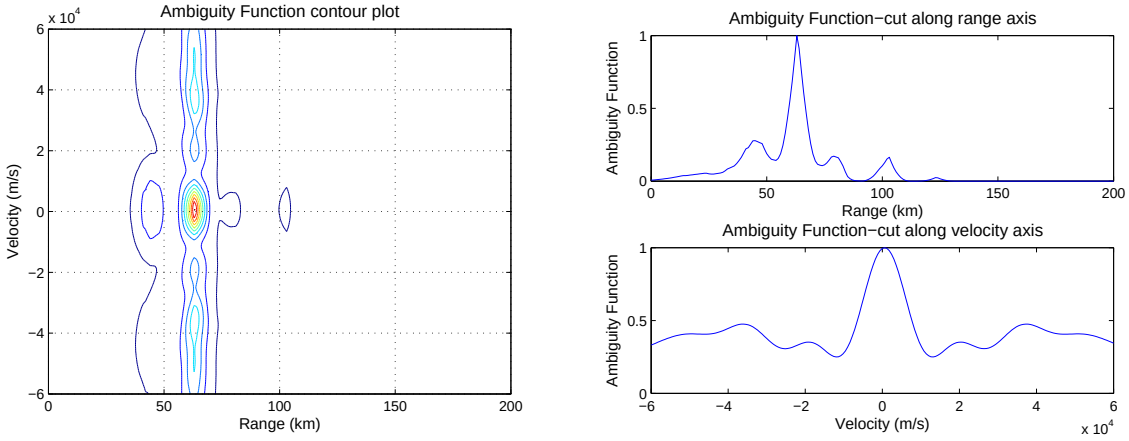

Figure 5.29: 3D Netted radar ambiguity - 4 transmitters, long baseline, $H = 20$ km

5.5 Conclusions

In this chapter, a form of the three-dimensional netted radar ambiguity function model has been developed and used to analyse netted radar ambiguity function as a function of network parameters especially system geometry. It is shown that the form of monostatic radar ambiguity function is dependent on the type of transmitted signal only. The bistatic radar ambiguity is greatly influenced by system geometry, which now includes the position and velocity of the target. Furthermore, the netted radar ambiguity function is strongly dependent on specific netted radar system geometry. When the target is close to the original bistatic baseline, large ambiguities are found in the two-dimensional cases. The three-dimensional geometry has a significant effect on the ambiguity properties, where the target height to baseline length ratio is the dominant factor, and smaller baselines perform better than longer baselines. Adding more nodes provides a more flexible netted radar system geometry and provides the possibility to further improve netted radar resolution capability. Therefore, it has been shown that the ambiguity function for a netted radar is complex and variable. This is an important aspect to understand in the design of any netted radar system.

Chapter 6

Netted Radar Ground Plane Effect

This chapter examines the influence of the ground plane on radar performance. Monostatic, bistatic and netted radar cases are considered separately in order to highlight the different behaviours as the level of distribution of the system increases. Each section includes formulation of mathematical models, examples of simulations and an analysis of simulation results.

In this chapter, only a perfectly flat conducting surface is going to be considered. This is to allow detailed insight to be gained for what amounts to the very low grazing angle cases. The monostatic and bistatic cases are considered first as these provide a useful reference for the more complex netted case.

6.1 Introduction

In most models examining radar performance, the target is assumed to be in the far-field. In radar applications the difference between near-field and far-field is that, when the target is in the near-field, the incepting wavefronts are curved, while when the target is in the far-field, which means the target is far enough from the radiating source, the wavefronts then can be assumed straight. Figure 6.1 shows an illustrative example of target in near-field and far-field. In this figure, it is seen that target A is in the near-field where the wavefronts are still curved, and target B is in far-field where the wavefronts are nearly flat. This far-field condition makes the calculation much simpler compared to the near-field condition. The following equation is normally used to meet the far-field assumption:

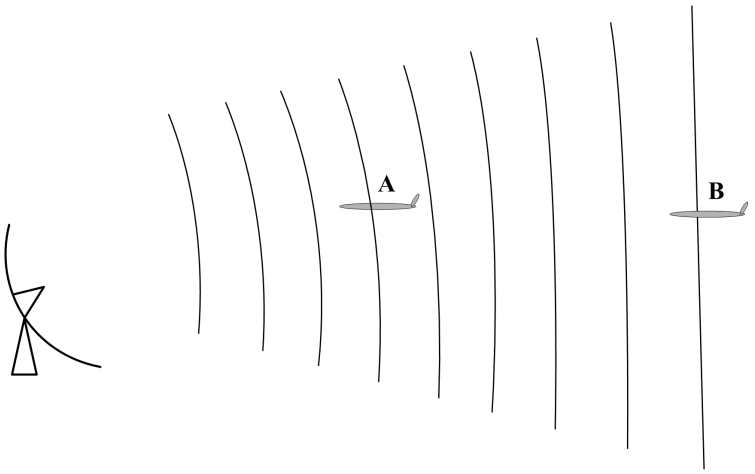

Figure 6.1: Near-field and far-field

$$R > \frac{2d^2}{\lambda} \tag{6.1}$$

where R is the distance between the target and the radiating source, d is the antenna aperture and λ is the transmitting wavelength.

To examine the performance of radar systems, one may conduct the tests indoors, considering the cost and convenience, plus the well-designed indoor chamber can eliminate unwanted returns and provides benign test environment. However, most experimental targets are just too big to allow us to do so. For example, if the antenna aperture is 2 m, for an S band radar with a 3 GHz operating frequency, $\lambda = \frac{c}{f} = \frac{3\times10^8}{3\times10^9}$ = 0.1 m. According to Equation 6.1, to meet the far-field assumption, the minimum distance between the target and radar is $\frac{2d^2}{\lambda} = \frac{2\times2^2}{0.1}$ = 80 m. The target must be no less than 80 m away from the radar. This is obviously very difficult to achieve in indoor laboratories. Therefore, in practice many radar tests are outdoor tests, where

the ground plane itself adds to the free space radar signals. Additionally, in many radar applications, the target is situated on or near the ground. This leaves the ground to be illuminated as well and hence there is a reflection component from the ground plane that contributes to the echo signal. For these reasons, it is important that the ground plane effect is understood in the case of netted radar to allow appropriate modelling strategies to be developed. Therefore, the ground plane effect on radar will be the main topic in this chapter.

Obviously, in radar applications, if the ground plane is presented, it will add in extra paths and smooth surfaces will behave differently from rough surfaces. Except for the case where the incepting signal is perpendicular to the ground plane, a smooth surface will result in strong forward scattering and weak back scattering. In contrast to this, a rough surface can result in weak forward scattering and strong back scattering. Figure 6.2 shows typical signal reflection from a rough surface. The Rayleigh criterion allows us to differentiate smooth surfaces from rough surfaces [76].

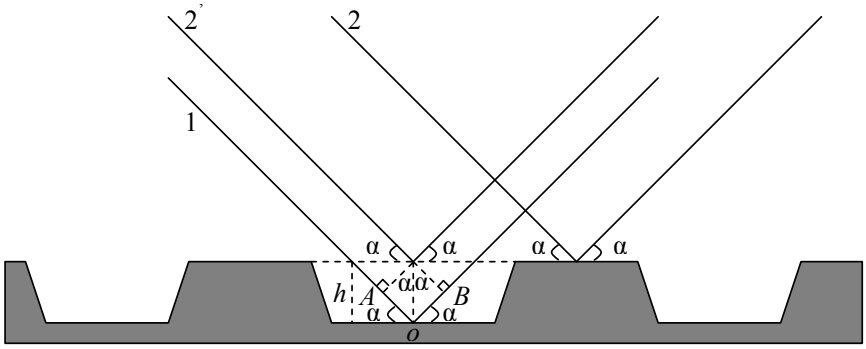

Figure 6.2: Rough ground plane

Under the far-field condition, two incident signals originated from a distant source can be seen as parallel. Then the signal will be reflected by either lower or higher ground surface with hight difference of h. As is shown in the figure, the difference of these two path lengths is the length of AOB, calculated by:

$$\Delta R = |AO| + |OB| = 2h \sin \alpha \tag{6.2}$$

Therefore the phase difference will be:

$$\Delta\phi = \Delta R\frac{2\pi}{\lambda} = \frac{4\pi h}{\lambda}\sin\alpha \tag{6.3}$$

A smooth surface will result in a zero or very small difference in phase, but any extra propagation distance does introduce a phase shift. When the phase difference caused by the difference in path length is increased to π, the two signals will cancel each other. In addition, according to the Rayleigh criterion, if the phase difference ϕ is greater than $\pi/2$, the surface is classified as rough surface, whilst, if the phase difference ϕ is smaller than $\pi/2$, it is seen as a smooth surface. In this way, a rough surface can also cause addition and subtraction of multiple wavefronts. Considering Equation 6.3 if $\frac{4\pi h}{\lambda}\sin\alpha < \frac{\pi}{2}$, i.e.

$$h < \frac{\lambda}{8\sin\alpha} \tag{6.4}$$

it is a smooth surface.

Equation 6.4 represents the Rayleigh criterion used to define a smooth surface. It is important to note that, even if the height variation of the surface is large, a small gazing angle will always result in a smooth surface. This implies that almost any surface can be seen as smooth at low grazing angles. This will be very useful when examining the reflection properties of the radar ground plane. In most cases of radar applications, the glazing angles are very small. In this thesis we focus on smooth surfaces only in order to gain an insight into the principle mechanism and effects on received signals in netted radar. A comprehensive analysis of the scattering characteristics of electromagnetic waves from rough surfaces is given in [77].

6.2 Monostatic radar ground plane effect

This section will briefly review the ground plane effect for the basic monostatic case, where the transmitting and receiving antennas are collocated. Figure 6.3 shows a typical monostatic radar geometry with ground plane. From this figure, it is seen that there are two kinds of different paths for the signal to travel between the radar antenna and the target. One is the direct path with length D. The other is the indirect path with length $I = S_1 + S_2$. In other words, the energy can be transmitted through either free space or with the reflection from the ground plane.

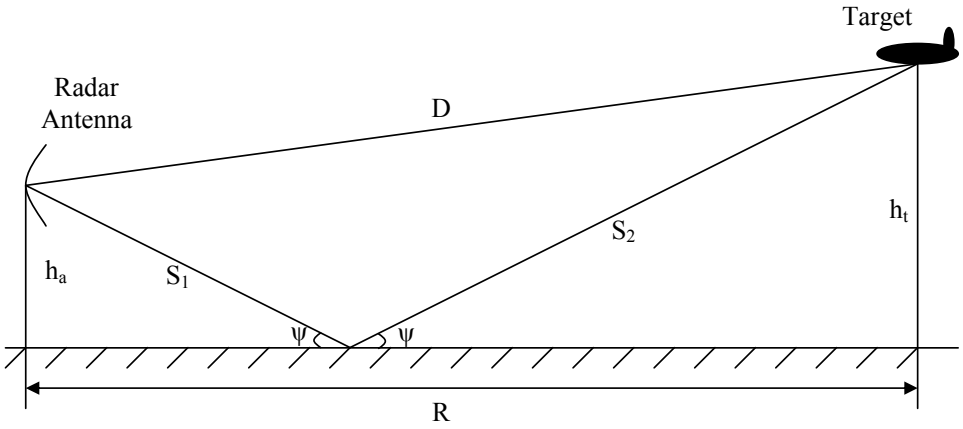

Figure 6.3: Monostatic radar ground plane effect

As there are two different paths for the signal to either go out to the target or come back to the antenna, this will results in four different round trip paths, shown in Figure 6.4, i.e. the direct path (Figure 6.4 (a)), the indirect path (Figure 6.4 (d)), and two of a combination of direct and indirect paths (Figure 6.4 (b) and (c)). Since the signal travelling along the opposite position via the direct and indirect paths will result in the same round trip path length, shown in Figure 6.4 (b) and (c), there will be three different round trip path lengths: (1) the direct path length $2D$; (2) the indirect path length $2I$; (3) the direct and indirect path length $D + I$.

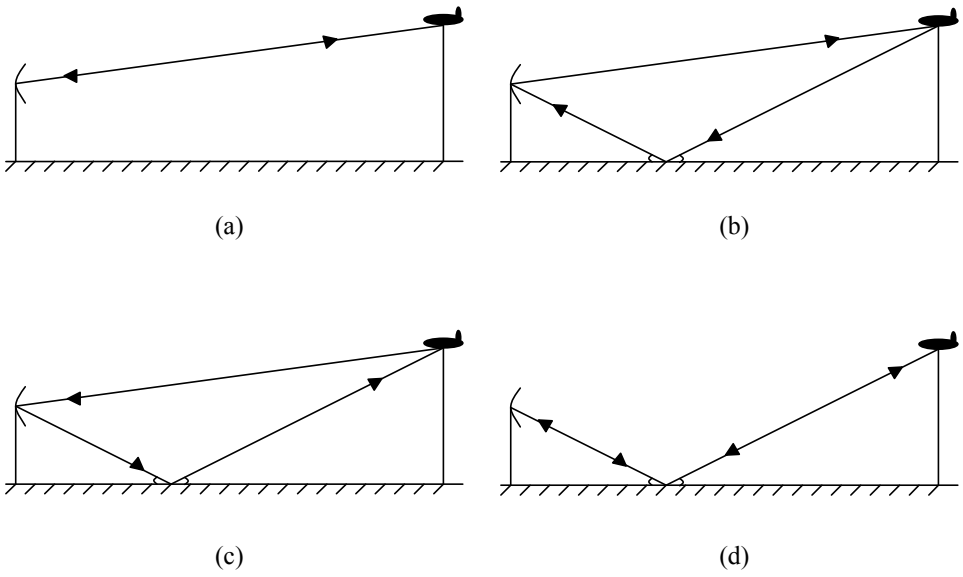

Figure 6.4: Monostatic radar paths

Each of these signals transmitted via four different paths will contribute to the total received signal. Therefore, the overall influence on the received signal can be obtained by summing up four separate contributions as is shown in Figure 6.4:

$$\sigma^{\frac{1}{2}} = \sigma_0^{\frac{1}{2}}\{\exp[i2kD] + 2\rho\exp[ik(D+I)] + \rho^2\exp[i2kI]\} \tag{6.5}$$

where

σ = RCS

σ_0 = free space RCS (as measured without ground plane)

k = wave number

ρ = reflection coefficient of the ground plane

D = direct path length

I = indirect path length

On the right hand side of this equation, the first term represents the free space return from the target; the second term represents two returns via direct and indirect paths, where the factor ρ represents a single reflection from the ground plane; the third term represents the indirect return from the target, where the factor ρ^2 represents the double reflection from the ground plane with the first from the radar to the target and the second from the target to the radar [56].

In Equation 6.5, if the phase reference point is changed to the first term, the RCS amplitude relationship can be simplified as:

$$\begin{aligned}\frac{\sigma}{\sigma_0} &= \left|1 + 2\rho\exp[ik(I-D)] + \rho^2\exp[2ik(I-D)]\right|^2 \\ &= |1 + \rho\exp[ik(I-D)]|^4\end{aligned} \tag{6.6}$$

With a perfectly conducting ground plane, i.e. the reflection coefficient $\rho = -1$, this can be further simplified as:

$$\begin{aligned}\frac{\sigma}{\sigma_0} &= |1 - \exp[ik(I-D)]|^4 \\ &= 16\sin^4[\frac{k}{2}(I-D)] \\ &= 16\sin^4[\pi\frac{(I-D)}{\lambda}]\end{aligned} \tag{6.7}$$

This relationship can be shown in Figure 6.5. This figure begins to show the effects brought out by the ground plane, although no specific parametres are taken into account yet. It is seen that with the ground plane effect included, the amplitude of the monostatic returned signal can be 16 times of the free-space returned signal, when the indirect and direct path length difference is an odd multiple of a half wavelength. On the other hand, it does fall to zero at some points when the $\frac{I-D}{\lambda}$ value is equal to an integer. In other words, the signal can be augmented or diminished by the ground plane, depending on the specific situation. This wide variability demonstrates very significant effect that multipath can have on radar performance even in the simple monostatic case.

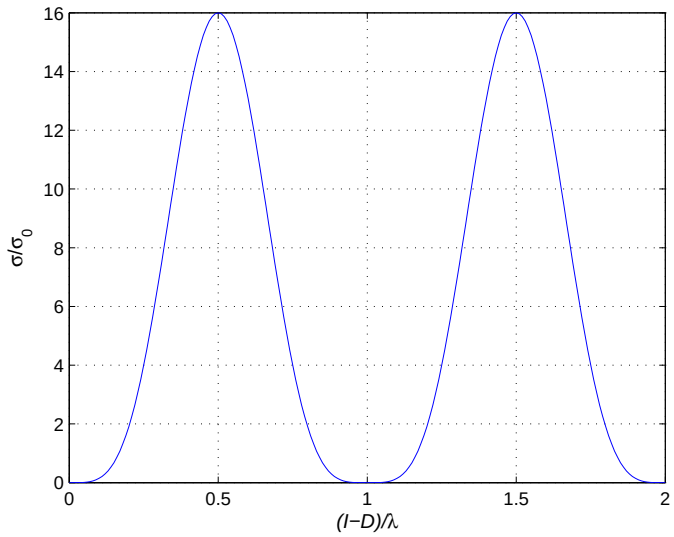

Figure 6.5: Influence of path lengths

From Figure 6.3 and Equation 6.7, it is seen that the magnitude of the returned signal will be affected mainly by four parameters: antenna height h_a, target height h_t, distance from antenna to target measured on the ground plane, i.e. the length of the projection of the direct path on the ground plane, and wavelength λ. A further analysis can be done to see the influence of these factors.

Considering the geometry shown in Figure 6.6, the direct and indirect path lengths can

be calculated by:

$$D = [(h_t - h_a)^2 + R^2]^{\frac{1}{2}} \tag{6.8}$$

$$I = [(h_t + h_a)^2 + R^2]^{\frac{1}{2}} \tag{6.9}$$

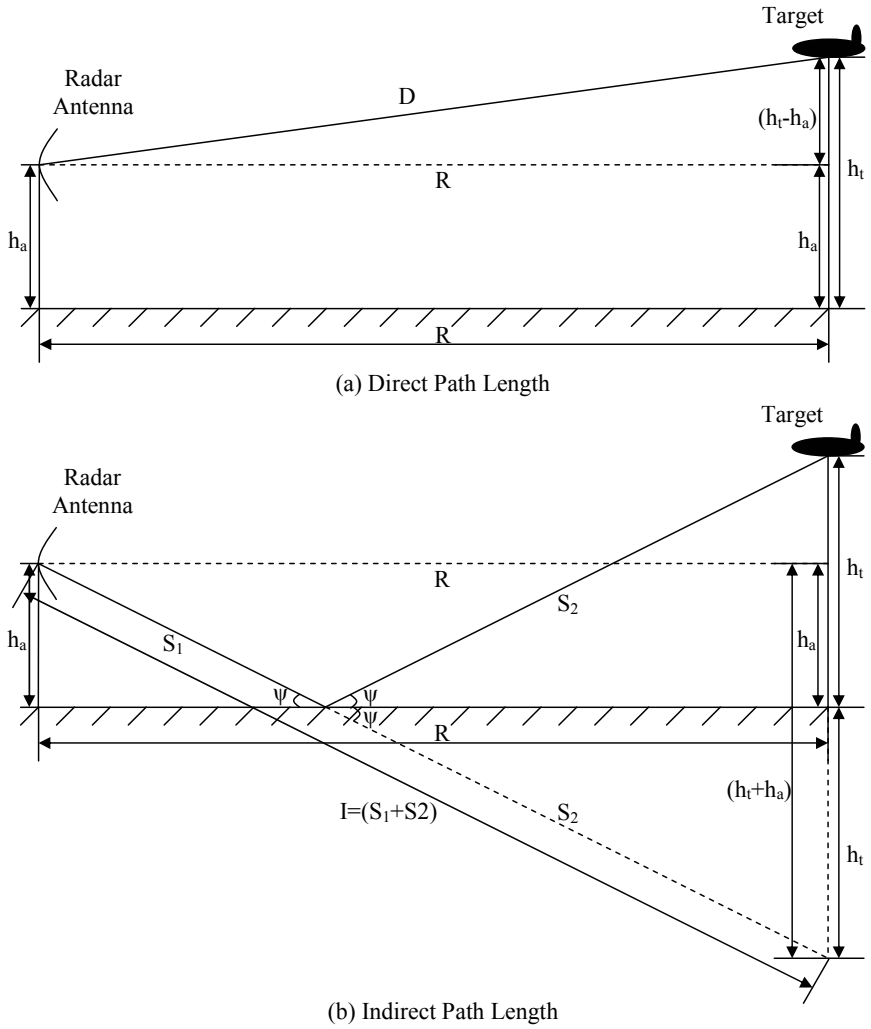

Figure 6.6: Direct and indirect path lengths

In practice, the values of h_t and h_a are almost always fairly small compared to the value

of R, in this case, the calculation can be approximated as:

$$D \approx R + \frac{(h_t - h_a)^2}{2R} \tag{6.10}$$

$$I \approx R + \frac{(h_t + h_a)^2}{2R} \tag{6.11}$$

As is seen in Figure 6.5, the maximum value of the returned signal can be achieved when:

$$I - D = \frac{\lambda}{2} \tag{6.12}$$

Substituting Equation 6.10 and 6.11 to 6.12, we will have:

$$I - D = \frac{2h_a h_t}{R} = \frac{\lambda}{2} \tag{6.13}$$

then

$$h_a h_t = \frac{R\lambda}{4} \tag{6.14}$$

This equation may be used as a guide to choose the parameters for outdoor radar testing to achieve maximum returned signal strength and therefore sensitivity. It might be too difficult to look at four variables all together, therefore the impact of each of the four parameters on the returned signal will be examined separately. In each of the following analysis three of the above four parameters will be fixed, and the remained one will be used as a variable to see the influence of every single parameter. The fixed values of the parameters are listed in Table 6.1.

Parameter(Unit)	Description	Value
h_a (m)	Antenna height	1.5
h_t (m)	Target height	1.5
R (m)	Length of the projection of the direct path on the ground	100
λ (m)	Transmitting wavelength	0.1
ρ	Reflection coefficient of the ground plane	-1

Table 6.1: Parameters used for monostatic ground plane effect simulation

Figure 6.7 shows the change of σ/σ_0 with range R. It is seen that with other selected parameters, the curve in relatively short range, i.e. within 60 m, changes rapidly. In this case,

it is good to choose a relatively long range, e.g. around 100 m. This will also make it easier to meet the far-field criterion. Figure 6.8 shows the change of σ/σ_0 with wavelength λ. It is shown that with relatively short wavelength, the curve changes very rapidly, for example, when the wavelength is less than 10 cm. On the other hand, with the relatively long wave length, the returned signal will be severely violated. Therefore, it is probably wise to choose a medium wavelength for outdoor test, for example, L or S band might be a good choice.

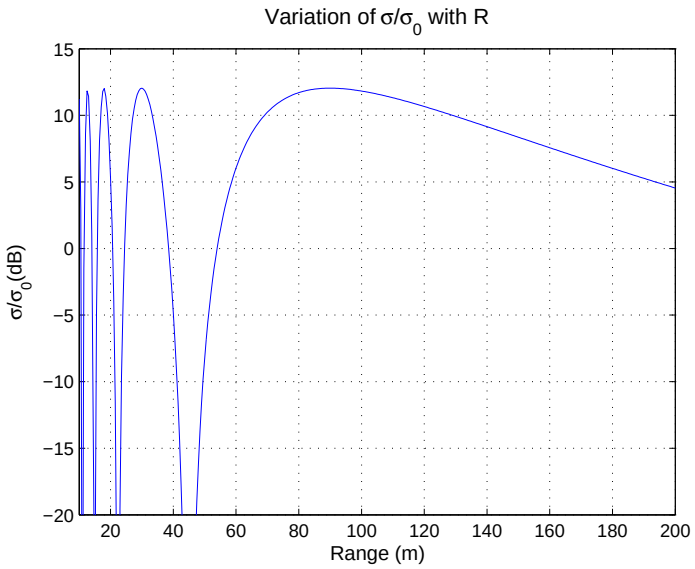

Figure 6.7: Monostatic σ/σ_0 variation with R

Figure 6.9 and Figure 6.10 show the change of σ/σ_0 with antenna height h_a and target height h_t respectively. From Equation 6.8, and 6.9, it is seen that the antenna height h_a and target height h_t play the same role in determining the direct and indirect path lengths due to the square calculation, and therefore the returned signal value defined in Equation 6.6. In this case, we should expect to see the same curve in these two cases. Actually, this is what we can see from Figure 6.9 and Figure 6.10, where the curve goes up and down with increasing intervals, when either the antenna height or the target height increases.

Up to now, the ground plane is assumed to be perfectly reflecting, i.e. $\rho = -1$. In the following simulation, the influence of the ground plane reflect coefficient will be examined. In Figure 6.11 the absolute value of the ground plane reflection coefficient is changing from

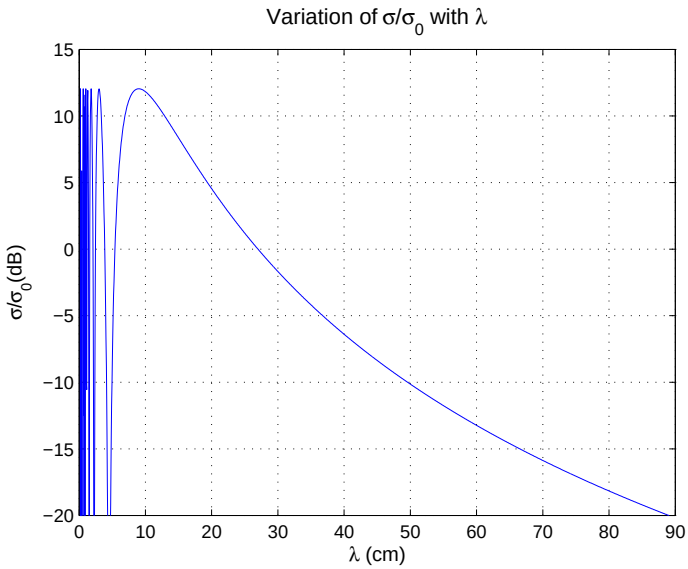

Figure 6.8: Monostatic σ/σ_0 variation with λ

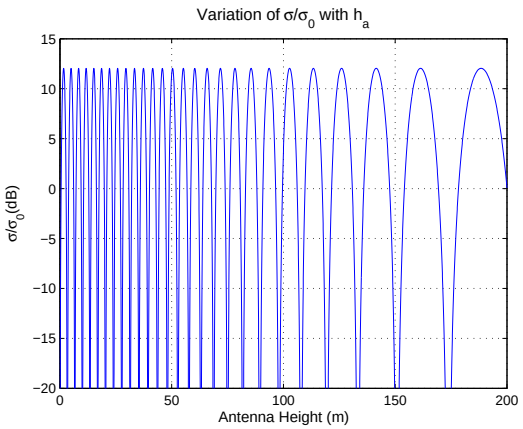

Figure 6.9: Monostatic σ/σ_0 variation with antenna height

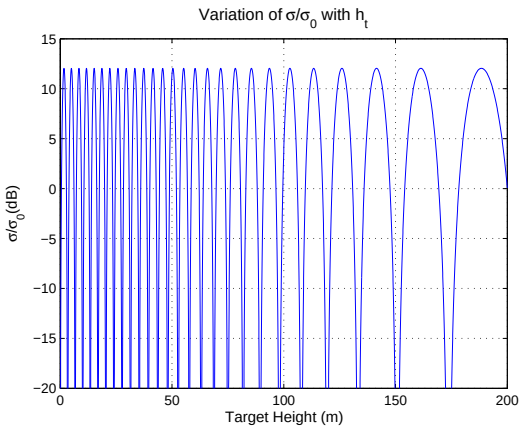

Figure 6.10: Monostatic σ/σ_0 variation with target height

0.7 to 1.0 with a step of 0.1 to examine the non-ideal ground plane effect against the perfect reflecting ground plane. It is seen that, a 10% deduction in the absolute value of the ground plane reflection coefficient will reduce the amplitude of the maximum returned signal by about 0.9 dB.

Now the influence of the ground plane on monostatic radar sensitivity will be examined.

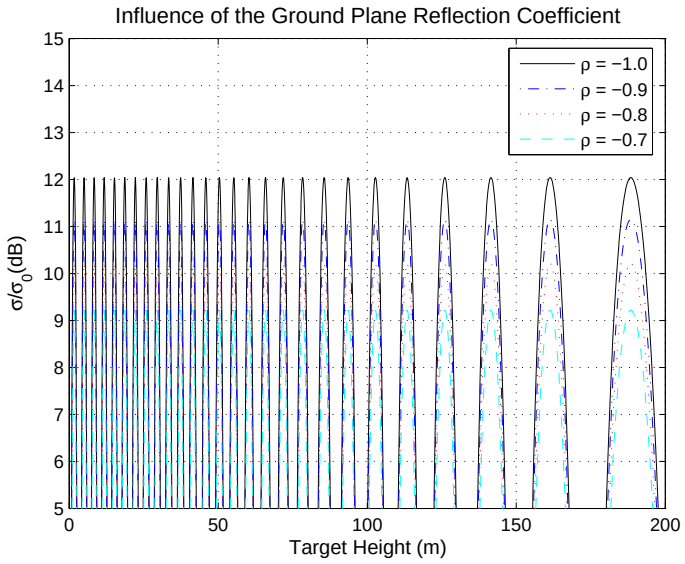

Figure 6.11: Influence of the ground plane reflection coefficient

From the above analysis, it is seen that, with the ground plane effect involved, the value of outdoor range RCS will be different from the actual target RCS. To reflect this influence the monostatic radar equation may be modified as:

$$SNR = \frac{P_t G_t G_r \frac{\sigma}{\sigma_0} \sigma_0 \lambda^2}{(4\pi)^3 k T_s B R^4 L} \tag{6.15}$$

where σ_0 is the free space RCS, and σ is the RCS with the ground plane effect.

Figure 6.12 shows a monostatic radar sensitivity map without the ground plane effect involved and Figure 6.13 shows the monostatic radar sensitivity map with the ground plane effect involved for the same system configuration. In this example, the values of radar parameters are the same as those listed in Table 4.1, and the ground plane related parameters are those listed in Table 6.1. Since the change of the target position on the X-Y plane will result in different range R, according to Figure 6.7 this will consequently result in a variation of the value of σ/σ_0, and therefore the sensitivity. As seen in Figure 6.13, the influence is geometry dependent. In this case, the monostatic sensitivity can be either greater or smaller than the free space one. Either with or without the ground plane effect considered, the monostatic sensitivity is always symmetrical with respect to the coordinate origin.

It is probably clearer to see the monostatic ground plane effect in one dimension. Figure

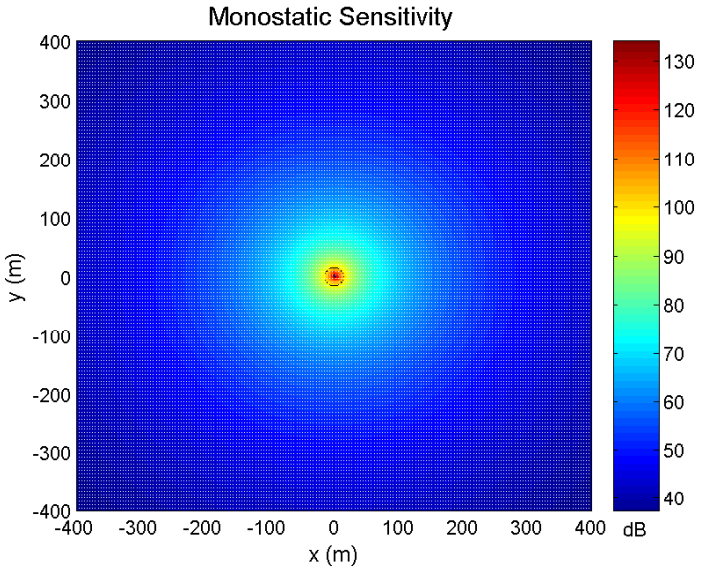

Figure 6.12: Monostatic sensitivity without ground plane effect

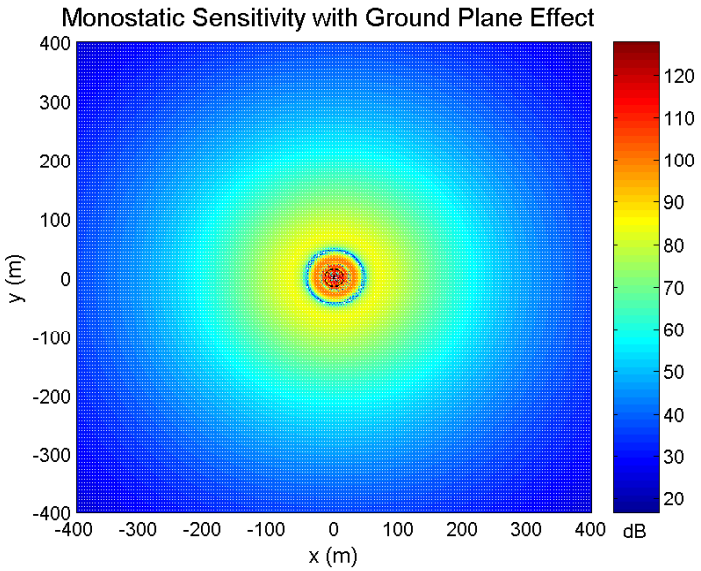

Figure 6.13: Monostatic sensitivity with ground plane effect

6.14 shows the variation of the monostatic sensitivities along X direction, i.e. with $y = 0$. Due to the symmetry of monostatic radar sensitivity, the variation of monostatic sensitivities along Y direction will be the same as that along X direction. It is seen that with the ground plane effect involved, the sensitivity value shows a tendency of fluctuation around the free space

value. Compared to free space sensitivity plot, the ground plane sensitivity curve along X direction is not consecutive, because with the ground plane considered, at some positions the deduction of the SNR is severe, i.e. the SNR can not reach the detection threshold. It is seen that with the ground plane included, the maximum sensitivity can be considerably increased. This is an advantage for target detection. However, at some points, the sensitivity is seriously violated.

Thus in this section, the potentially dramatic but, in principle, determinative effect of flat surface induced multipath can be seen on monostatic radar. In the next section, this is taken a step further by separately locating the transmitter and receiver in a bistatic configuration. Together these provide a lead into the more complex case of netted radar.

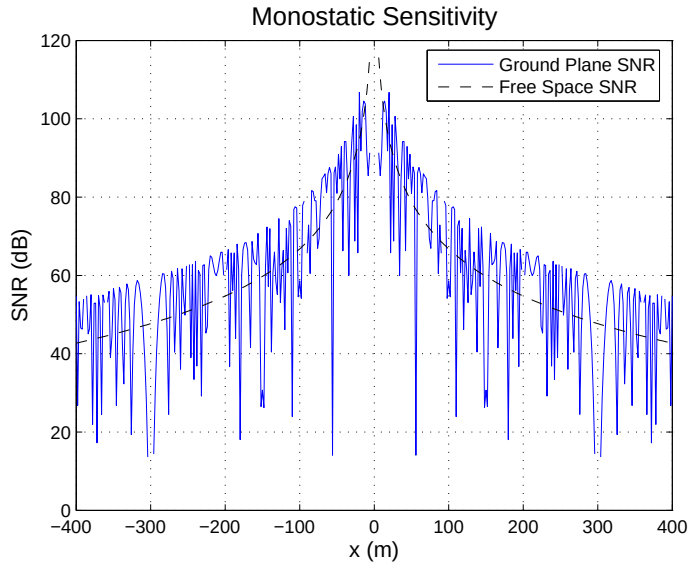

Figure 6.14: Influence of the ground plane effect - monostatic radar

6.3 Bistatic radar ground plane effect

Following the discussion of monostatic radar ground plane effect, this section will make a further step to examine bistatic radar ground plane effect, where the single transmitting and receiving antennas are spatially separated by a baseline. The bistatic radar ground plane effect model will be developed.

Figure 6.15 shows a typical bistatic radar geometry with ground plane. Similar to the monostatic case there are two different paths for the signal to travel between the radar antenna and the target: the direct path and the indirect path. The difference is, the transmitting antenna to target direct path length D_t can be different from the target to receiving antenna direct path length D_r, whist the transmitting antenna to target indirect path length I_t can be different from the target to receiving antenna indirect path length I_r, due to the spacial separation of the transmitting and receiving antennas.

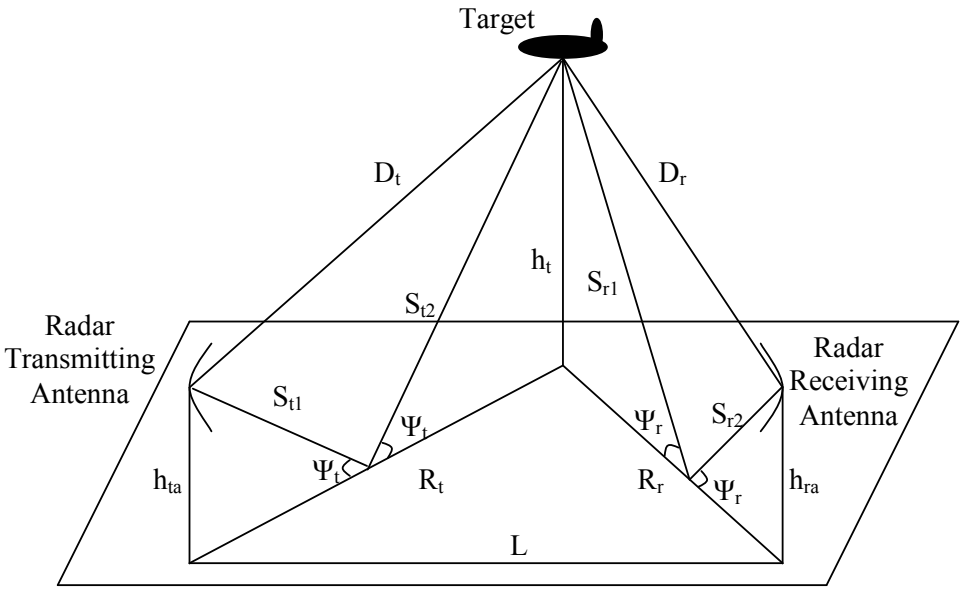

Figure 6.15: Bistatic radar ground plane effect

In bistatic case, again, there are two different kinds of paths for the signal to either go out to the target or come back to the antenna, i.e. direct and indirect paths, this will results in four different round trip paths, shown in Figure 6.16, i.e. the direct path (Figure 6.16 (a)), the indirect path (Figure 6.16 (d)) and two of a combination of direct and indirect paths (Figure 6.16 (b) and (c)). Therefore, there will be four different round trip path lengths: (1) the direct path length $D = D_t + D_r$; (2) the indirect path length $I = I_t + I_r$; (3) the direct and indirect path length $DI = D_t + I_r$; (4) the indirect and direct path length $ID = I_t + D_r$.

Each of these signals transmitted via the four different paths will contribute to the total received signal. Therefore, the overall influence on the received signal can be obtained by

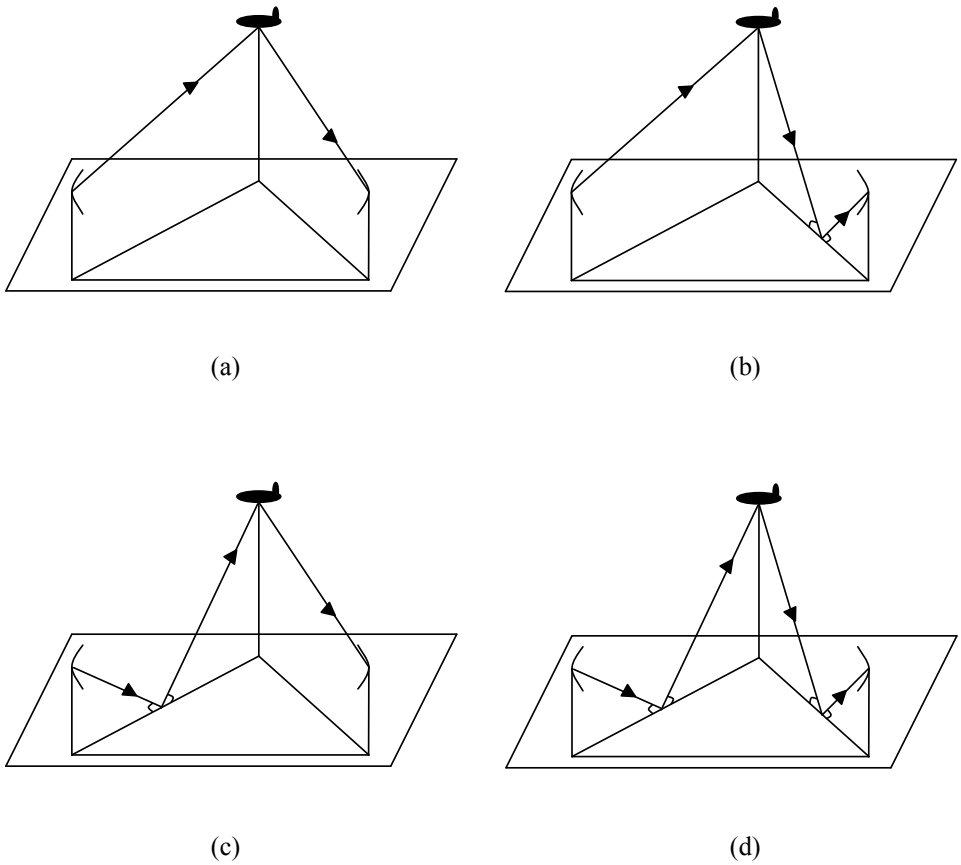

Figure 6.16: Bistatic radar paths

summing up the four separate contributions as is shown in Figure 6.16:

$$\left|\frac{\sigma_b}{\sigma_{b0}}\right| = \left|\exp[ikD] + \rho\exp[ik(D_t + I_r)] + \rho\exp[ik(I_t + D_r)] + \rho^2\exp[ikI]\right|^2 \quad (6.16)$$

where

σ_b = bistatic RCS

σ_{b0} = free space bistatic RCS (as measured without ground plane)

k = wave number

ρ = reflection coefficient of the ground plane

$D = D_t + D_r$ = direct path length

$I = I_t + I_r$ = indirect path length

On the right hand side of this equation, the first term represents the free space return from the target; the second and third terms represent two returns via direct and indirect paths, where

the factor ρ represents a single reflection from the ground plane; the last term represents the indirect return from the target, where the factor ρ^2 represents the double reflection from the ground plane with the first from the radar to the target and the second from the target to the radar.

According to Equation 6.8 and 6.9, the length of D_t, D_r, I_t and I_r can be calculated by:

$$D_t = [(h_t - h_{ta})^2 + R_t^2]^{\frac{1}{2}} \tag{6.17}$$

$$D_r = [(h_t - h_{ra})^2 + R_r^2]^{\frac{1}{2}} \tag{6.18}$$

$$I_t = [(h_t + h_{ta})^2 + R_t^2]^{\frac{1}{2}} \tag{6.19}$$

$$I_r = [(h_t + h_{ra})^2 + R_r^2]^{\frac{1}{2}} \tag{6.20}$$

where

D_t = transmitting antenna to target direct path length

D_r = receiving antenna to target direct path length

I_t = transmitting antenna to target indirect path length

I_r = receiving antenna to target indirect path length

R_t = length of the projection of transmitting antenna to target path on the ground plane

R_r = length of the projection of receiving antenna to target path on the ground plane

h_{ta} = transmitting antenna height

h_{ra} = receiving antenna height

h_t = target height

As with the monostatic case, the influence of every single parameter will be examined separately. Similarly, in each of the following simulations, one of the parameters will be left changing, and the other parameters will be fixed. In this bistatic case the target to receiving antenna range is used as range. As is seen in Chapter 5, in bistatic case when the target to receiver range and baseline length are given, the parameter angle θ_r will affect the transmitter to target range, and further relevant performance. Therefore, the influence of different θ_r will be shown. The fixed values of the parameters are shown in Table 6.2:

Parameter(Unit)	Description	Value
h_{ta} (m)	Transmitting antenna height	1.5
h_{ra} (m)	Receiving antenna height	1.5
h_t (m)	Target height	1.5
λ (m)	Transmitting wavelength	0.1
R_r (m)	Length of the projection of receiving antenna to target path on ground	70
θ_r (degree)	Receiver look angle	-45°
L (m)	Bistatic baseline length	100
ρ	Reflection coefficient of the ground plane	-1

Table 6.2: Parameters used for bistatic ground plane effect simulation

With given R_r, L and θ_r, R_t can be calculated by [55]:

$$R_t = (R_r^2 + L^2 + 2R_r L \sin\theta_r)^{\frac{1}{2}} \tag{6.21}$$

In Figure 6.17 influence of R_r is examined first. Three different receiver look angles are selected to make a comparison. The relevant two dimensional bistatic geometries are shown in Figure 6.18. It is seen that the shape of this curve is very similar to the monostatic counterpart. With other selected parameters, the curve in relatively short range changes rapidly. Therefore it is good to chose a relatively long range, for example a range greater than 50 m. It is also seen that the influence of receiver look angle is mainly in relatively long range. With increasing look angle, the bistatic σ/σ_0 decreases. In relatively short range, the influence of receiver look angle is trivial.

Figure 6.19 shows the change of bistatic σ/σ_0 with wavelength λ. Again, the shape of this curve is very similar to the monostatic one. With relatively short wavelength, the curve changes very rapidly, for example, when the wavelength is less than 10 cm. With the relatively long wavelength, the returned signal will be severely violated. Therefore, for a bistatic radar it is probably better to choose a medium wavelength for outdoor test, for example, again, L or S band might be a good choice.

Figure 6.20 and Figure 6.21 show the change of bistatic σ/σ_0 with antenna height and

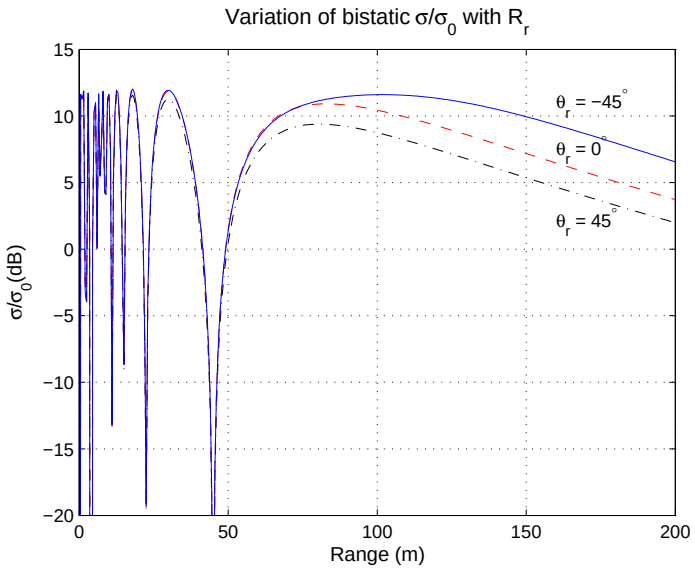

Figure 6.17: Bistatic σ/σ_0 variation with R_r

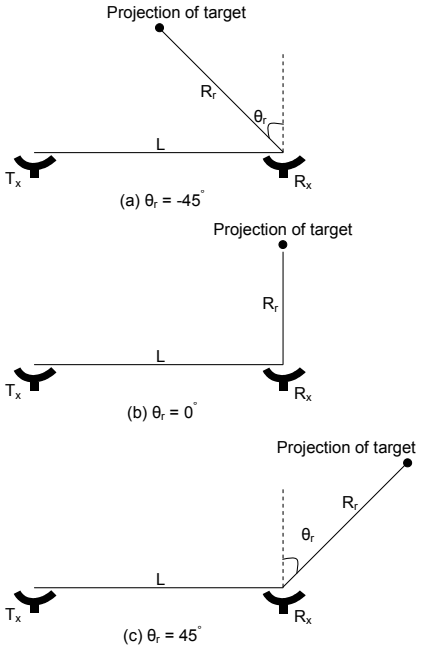

Figure 6.18: Bistatic radar geometry (change of θ_r)

target height respectively. In the bistatic case the transmitting and receiving antennae are assumed to be of the same height. From Equation 6.17 to 6.20, it is seen that the antenna height and target height play the same role in determining the direct and indirect path length

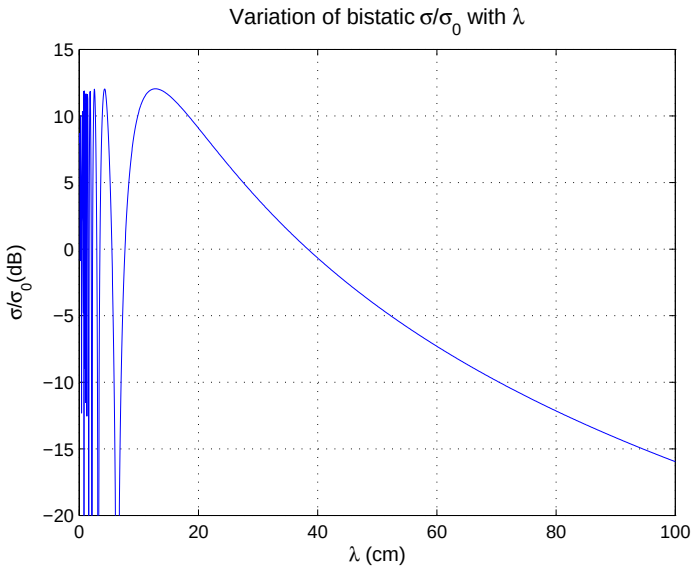

Figure 6.19: Bistatic σ/σ_0 variation with λ

due to the square calculation, and therefore the returned signal value defined in Equation 6.16. In this case, we should expect to see the same curve in these two cases. Actually, this is what we can see from Figure 6.20 and Figure 6.21, where the curve goes up and down with increasing intervals, when either the antenna height or the target height increases. This is also similar to the monostatic curves shown in Figure 6.9 and 6.10.

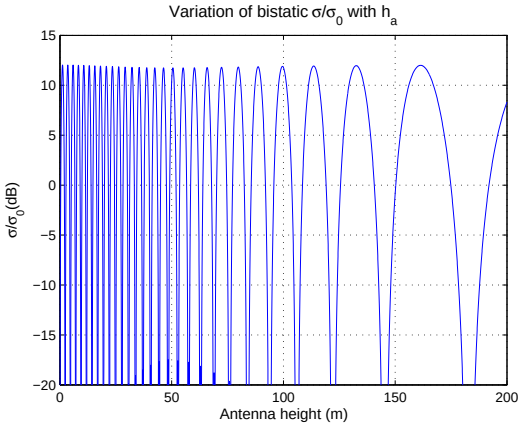

Figure 6.20: Bistatic σ/σ_0 variation with antenna height

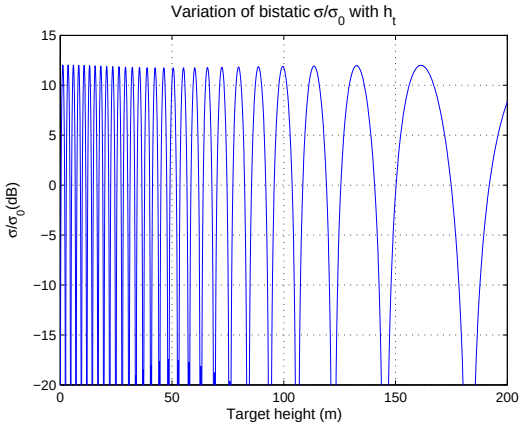

Figure 6.21: Bistatic σ/σ_0 variation with target height

Now the influence of the ground plane on bistatic radar sensitivity will be examined. From the above analysis, it is seen that, with the ground plane effect involved, the value of outdoor range bistatic RCS will be different from the actual target RCS. To reflect this influence the bistatic radar equation may be modified as:

$$SNR = \frac{P_t G_t G_r \frac{\sigma_b}{\sigma_{b0}} \sigma_{b0} \lambda^2}{(4\pi)^3 k T_s B R_t^2 R_r^2 L} \tag{6.22}$$

where σ_{b0} is the free space bistatic RCS, and σ_b is the bistatic RCS with ground plane effect. The value of σ_b/σ_{b0} can be calculated by Equation 6.16.

Figure 6.22 shows the bistatic radar sensitivity map without the ground plane effect involved and Figure 6.23 shows the bistatic radar sensitivity map with the ground plane effect involved for the same system configuration. In this example, the values of radar parametres are the same as those listed in Table 4.1, and the relevant ground plane related parametres are those listed in Table 6.2. Since the change of the target position on the X-Y plane will result in different range R_r, according to Figure 6.17 this will consequently result in a variation of the value of σ_b/σ_{b0}, and therefore the sensitivity. As seen in Figure 6.23, the influence is geometry dependent. In this case, the bistatic sensitivity can be either greater or smaller than the free space one.

Figure 6.24 and Figure 6.25 show the variation of the bistatic sensitivities in one dimension. The variation of bistatic radar sensitivity along X direction, i.e. with $y = 0$, is shown in Figure 6.24, and the variation of bistaitc radar sensitivity along Y direction, i.e. with $x = 0$, is shown in Figure 6.25. It is seen that in bistatic case, with the ground plane effect involved, the sensitivity value along both X and Y directions show a tendency of fluctuation around the free space value. Similar to the monostatic case, the ground plane included, the maximum sensitivity can be considerably increased and at some points. The sensitivity can also be seriously violated. Especially with long range, for example when the range in either X or Y direction is greater than 300 m, the ground plane affected bistatic sensitivity is reduced rapidly.

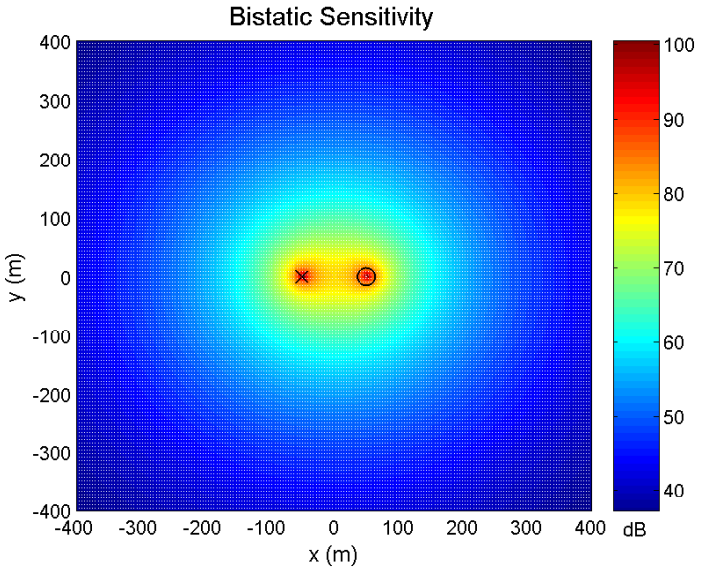

Figure 6.22: Bistatic sensitivity without ground plane effect

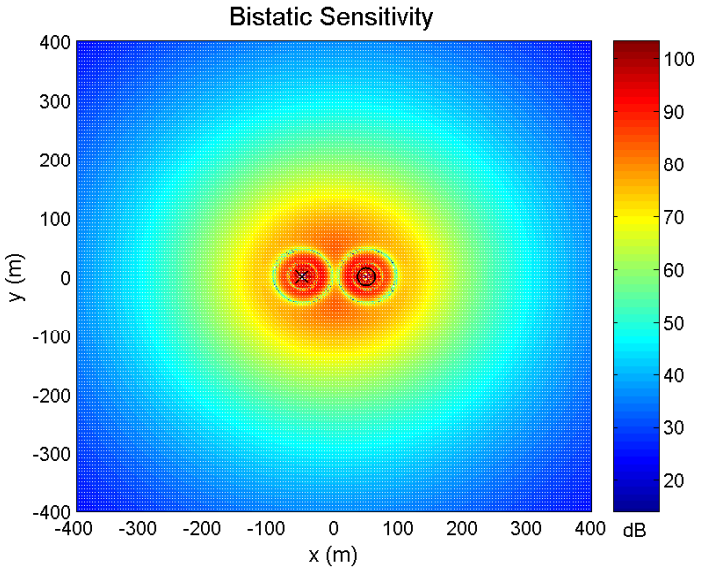

Figure 6.23: Bistatic sensitivity with ground plane effect

6.4 Netted radar ground plane effect

Based on the monostatic radar ground plane effect discussed in Section 6.2 and bistatic radar ground plane effect model developed in Section 6.3, netted radar ground plane effect model will be developed and analysed in this section.

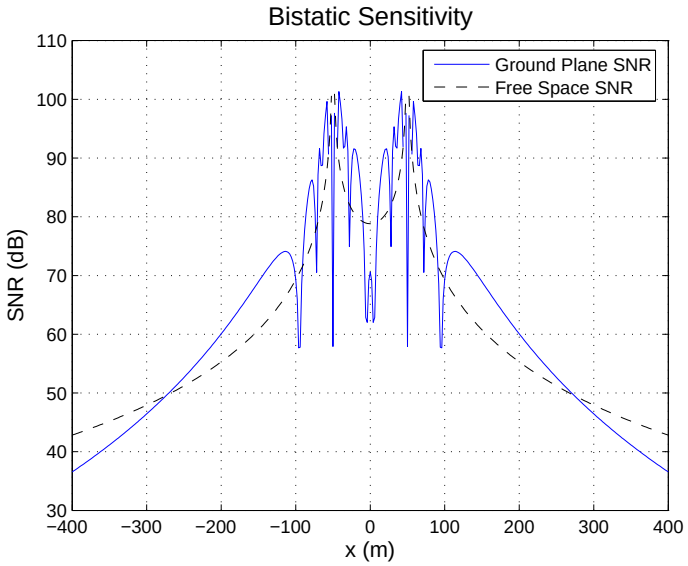

Figure 6.24: Influence of the ground plane effect - bistatic radar in X direction

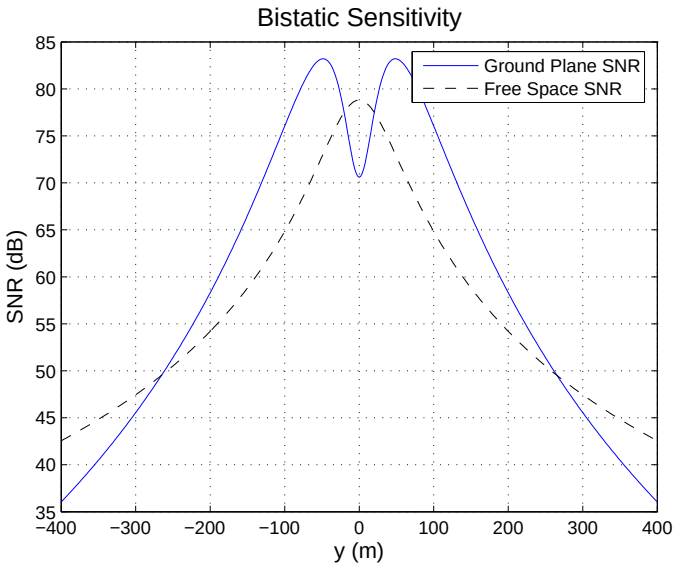

Figure 6.25: Influence of the ground plane effect - bistatic radar in Y direction

Figure 6.26 shows a simple netted radar geometry with the ground plane effect involved. This netted radar system is formulated by adding an extra node to the bistatic geometry shown in Figure 6.15. The three radar nodes here constitute nine radars including three monostatic and six bistatic radars. There is direct and indirect path for the signal to either going to the

target or coming back to the radar for each node.

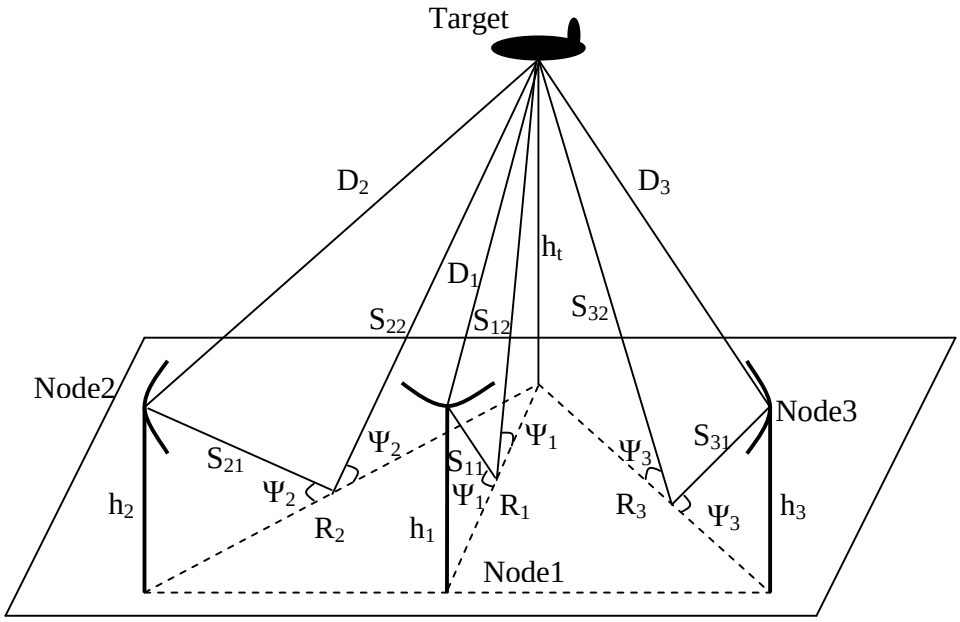

Figure 6.26: Netted radar ground plane effect

Figure 6.27 shows the possible paths for a monostatic radar in this netted radar configuration. It is seen that there are four possible paths for a round trip signal path for a monostatic radar. In this figure, it is only shown the possible paths for Node 2 monostatic configuration, and Node 1 and Node 3 monostatic configuration will have the same paths.

Figure 6.28 shows the possible paths for a bistatic radar in this netted radar configuration. It is seen that similar to the monostatic case shown in Figure 6.27 there are four possible paths for a round trip signal path for a bistatic radar. In this figure, it is only shown the possible paths for Node 1 and Node 3 bistatic configuration where Node 1 is transmitting and Node 3 is receiving. The possible paths for bistatic radar where Node 3 is transmitting and Node 1 is receiving can be derived by reverting the direction of all the arrows in Figure 6.28, and the possible paths for the other four bistatic radars in the network, i.e. Node 1 transmitting and Node 2 receiving, Node 2 transmitting and Node 1 receiving, Node 2 transmitting and Node 3 receiving, Node 3 transmitting and Node 2 receiving, will have similar paths with different bistatic angles.

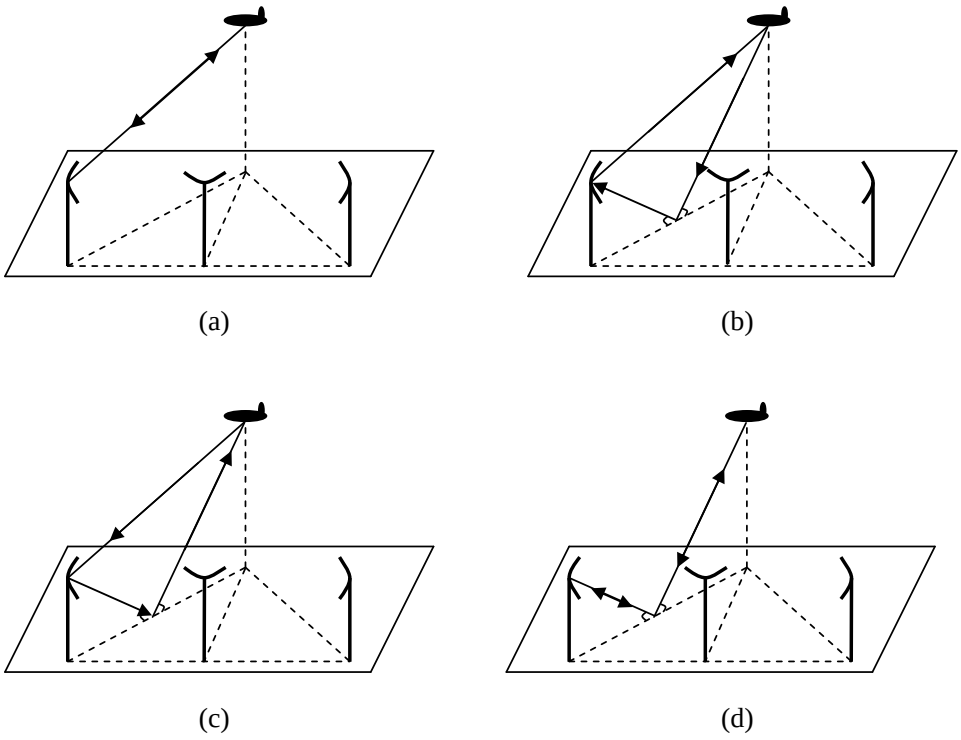

Figure 6.27: Netted radar paths - Node 2 monostatic

Again, the netted radar can be seen as a collection of monostatic and bistatic radar system. The ground plane affects the netted radar by influencing individual monostatic radars or bistatic radars that compose the netted radar. Therefore, with the ground plane effect involved the netted radar sensitivity Equation 4.17 can be modified as:

$$SNR_{total} = \sum_{i=1}^{m}\sum_{j=1}^{n} \frac{P_{ti}G_{ti}G_{rj}\frac{\sigma_{ij}}{\sigma_{ij0}}\sigma_{ij0}\lambda_i^2}{(4\pi)^3 kT_s B_i R_{ti}^2 R_{rj}^2 L_{ij}} \tag{6.23}$$

where σ_{ij0} is the free space bistatic RCS, and σ_{ij} is ground plane affected RCS, seen by ith transmitter and jth receiver.

A simple netted case is considered where the radar parameters for every transmitter-receiver combination are the same, then the netted radar equation can be written as:

$$SNR_{total} = \frac{P_t G_t G_r \sigma_0 \lambda^2}{(4\pi)^3 kT_s BL} \sum_{i=1}^{m}\sum_{j=1}^{n} \frac{\frac{\sigma_{ij}}{\sigma_0}}{R_{ti}^2 R_{rj}^2} \tag{6.24}$$

The netted radar sensitivities with the ground plane effect will be simulated and anal-

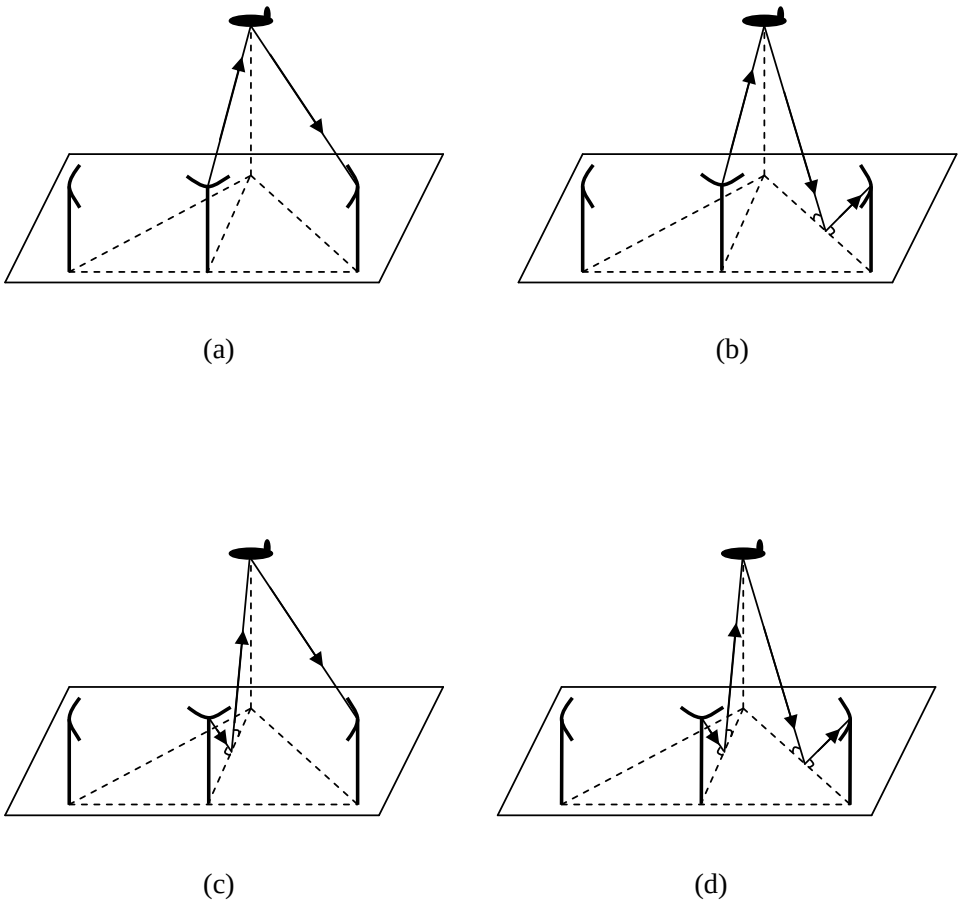

Figure 6.28: Netted radar paths - Node 1 to Node 3 bistatic

ysed in the rest of this section. This will focus on a netted radar composed of three identical transmitting units and three identical receiving units. This analysis will begin with the simplest case where all the transmitting and receiving nodes are collocated. The collocation of the transmitters and receivers of all radar nodes in a netted radar system is an important and particular geometry. Compared with monostatic radar, only the number of nodes in the system is changed. There is no change in system geometry. This limit the influence of other factors when we compare the performance of netted radar with monostatic radar.

For this netted radar configuration, Figure 6.29 shows the netted radar sensitivity map without the ground plane effect involved and Figure 6.30 shows the netted radar sensitivity map with the ground plane effect involved for the same system configuration. In this example,

the three radar nodes are all positioned on the ground plane at the coordinate origin (0, 0). The values of radar parameters are the same as those listed in Table 4.1, and the relevant ground plane related parameters are those listed in Table 6.2. It is seen that, as with monostatic and bistatic cases, the netted radar sensitivity with the ground plane effect involved also shows some fluctuation, especially around the area where radar nodes are places. For each individual spot in the surveillance area, the sensitivity could be either greater or smaller than the free space netted radar sensitivity.

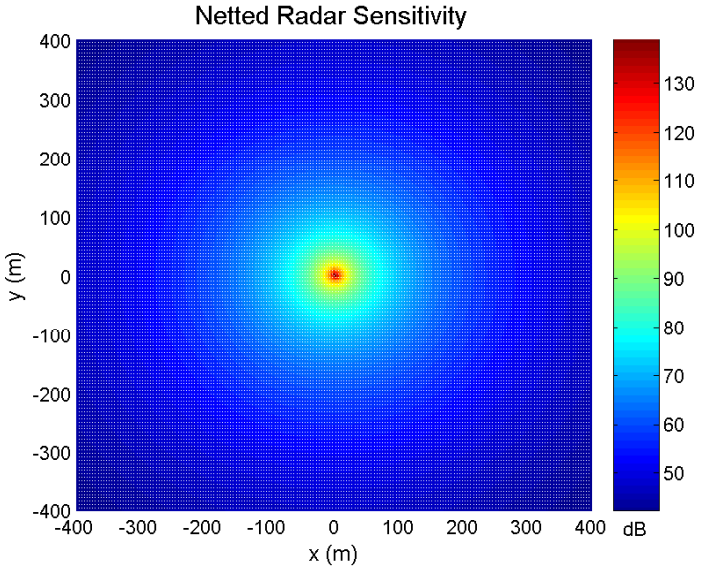

Figure 6.29: Netted radar sensitivity without ground plane effect - collocated netted radar

To look into the netted radar ground plane effect on netted radar sensitivity, the following simulations are made to compare free space and ground plane affected netted radar sensitivity in one dimension. Figure 6.31 and Figure 6.32 show the variation of the netted radar sensitivities in one dimension. The variation of netted radar sensitivity along X direction, i.e. with $y = 0$, is shown in Figure 6.31, and the variation of netted radar sensitivity along Y direction, i.e. with $x = 0$, is shown in Figure 6.32. It is seen that in this collocated netted radar case, with the ground plane effect involved, the sensitivity value along both X and Y directions are identical. This is expected as the system configuration is exactly the same in X and Y direction or any other direction. This netted radar sensitivity in one direction shows a tendency of fluc-

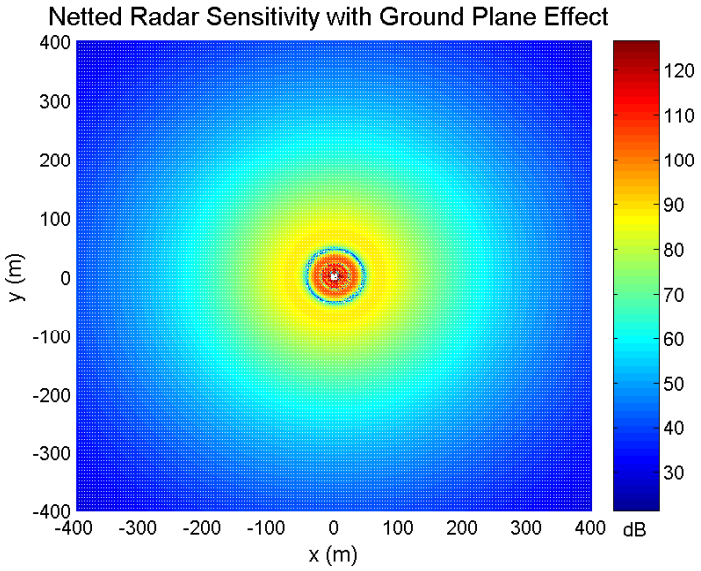

Figure 6.30: Netted radar sensitivity with ground plane effect - collocated netted radar

tuation compared with free space one where the netted radar sensitivity values are fluctuating around the free space sensitivity values. Similar to the monostatic and bistatic cases, with the ground plane included, the maximum sensitivity can be considerably increased and at some points. The sensitivity can also be seriously violated. Similar to monostatic cases with long range, for example, when the range in either X or Y direction is greater than 300 m, the ground plane affected netted radar sensitivity is reduced rapidly. Compared with the monostatic radar sensitivity in one dimension which is shown in Figure 6.14, it is seen that the netted radar sensitivity are less fluctuating than the monostatic ones. Some of the nulls shown in the ground plane involved monostatic radar sensitivity are filled up in this netted radar cases, and the netted radar sensitivity curve is smoother than the monostatic one. This is due to the addition of multiple ground plane effect. With more radar nodes involved, the multiple ground plane effects are cancelled with each other, resulting in a smoother sensitivity curve. The effect of netting randomizes the phase of returned signals. Therefore, compared with simple monostatic case, it gives better chance for the nulls to be cancelled when the returned signals are added up together to get the total sensitivity. This shows one aspect of the advantages of netted radar configuration over monostatic configuration. With netted radar configuration, when the ground

plane effect is involved, the sensitivity map is more stable than the monostaitc counterpart.

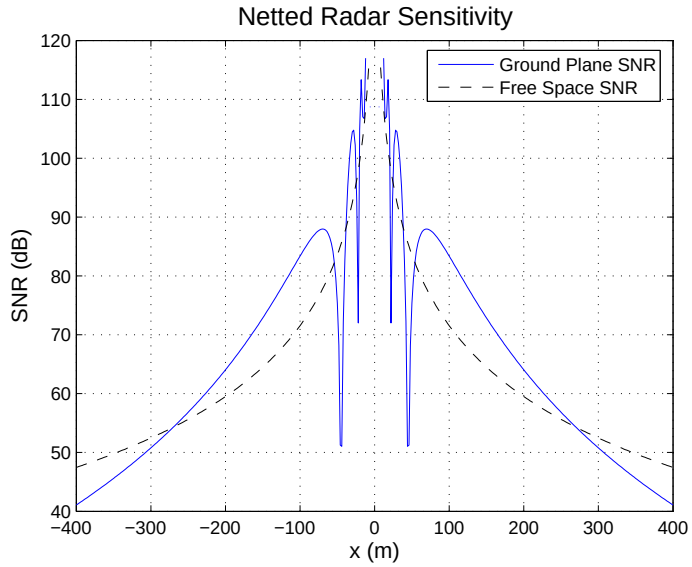

Figure 6.31: Influence of the ground plane effect - netted radar in X direction - collocated netted radar

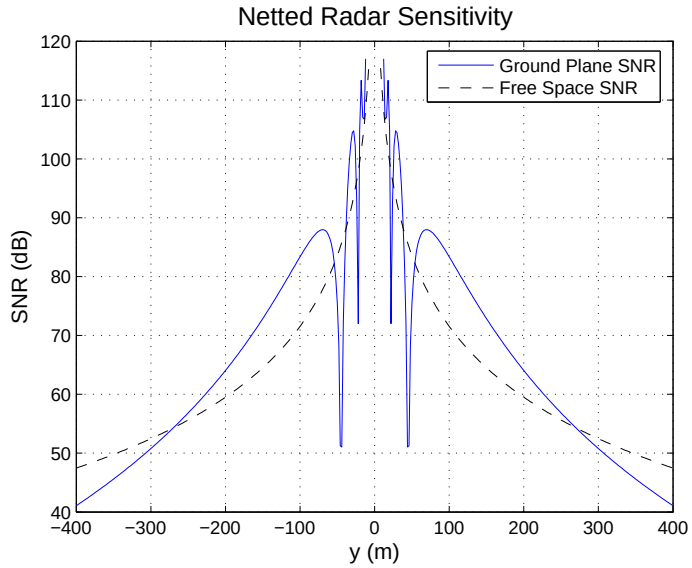

Figure 6.32: Influence of the ground plane effect - netted radar in Y direction - collocated netted radar

The next example shows ground plane affected netted radar sensitivity for a more complicated netted radar configuration where the three nodes are placed in one line along X axis at (-50, 0), (0, 0) and (50, 0) respectively. The three dimensional figure of this configuration can be found in Figure 6.26.

For this system configuration Figure 6.33 shows the netted radar sensitivity map without the ground plane effect involved and Figure 6.34 shows the netted radar sensitivity map with the ground plane effect involved. It is seen that some fluctuations are shown in this ground plane involved netted radar case, especially around the area where each radar node is placed.

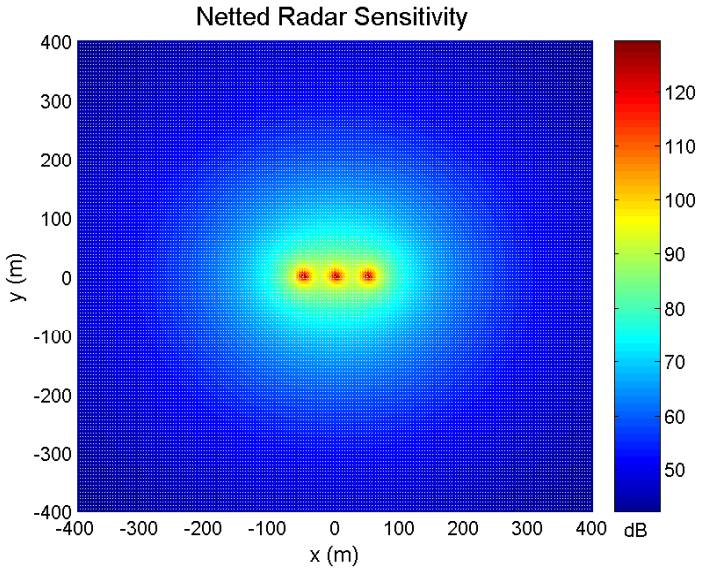

Figure 6.33: Netted radar sensitivity without ground plane effect - linear netted radar

Figure 6.35 and Figure 6.36 show the variation of the netted radar sensitivities in one dimension for this linear netted radar configuration. The variation of netted radar sensitivity along X direction, i.e. with $y = 0$, is shown in Figure 6.35, and the variation of netted radar sensitivity along Y direction, i.e. with $x = 0$, is shown in Figure 6.36. It is seen that in this netted radar case, the sensitivity in X and Y directions are different as the configuration of radar nodes are different when looking at the system from X and Y directions. However, the sensitivity in each direction is still symmetrical to the coordinate origin. With the ground plane effect involved, the sensitivity value along both X and Y directions show a tendency of

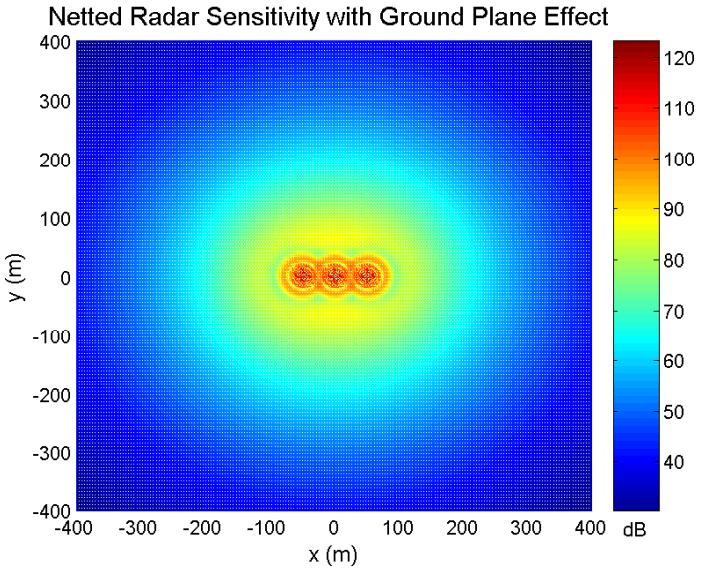

Figure 6.34: Netted radar sensitivity with ground plane effect - linear netted radar

fluctuation around the spots where the radar nodes are placed. Again, with long range, for example, when the range in either X or Y direction is greater than 300 m, the ground plane affected netted radar sensitivity is reduced rapidly.

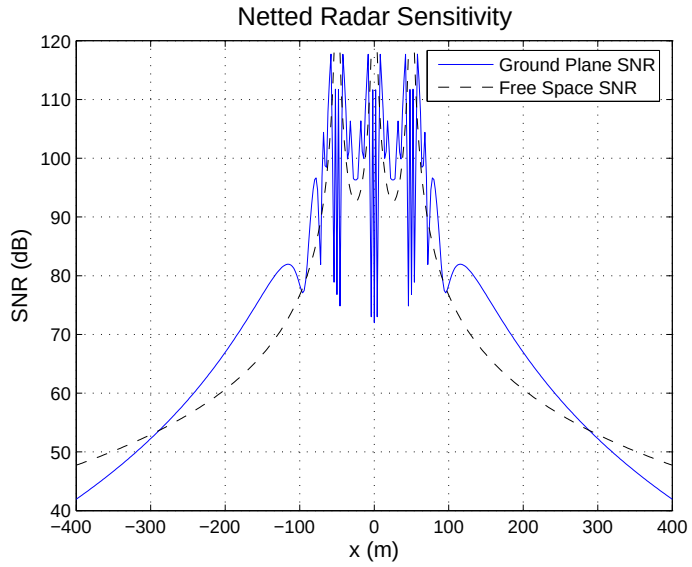

Figure 6.35: Influence of the ground plane effect - netted radar in X direction - linear netted radar

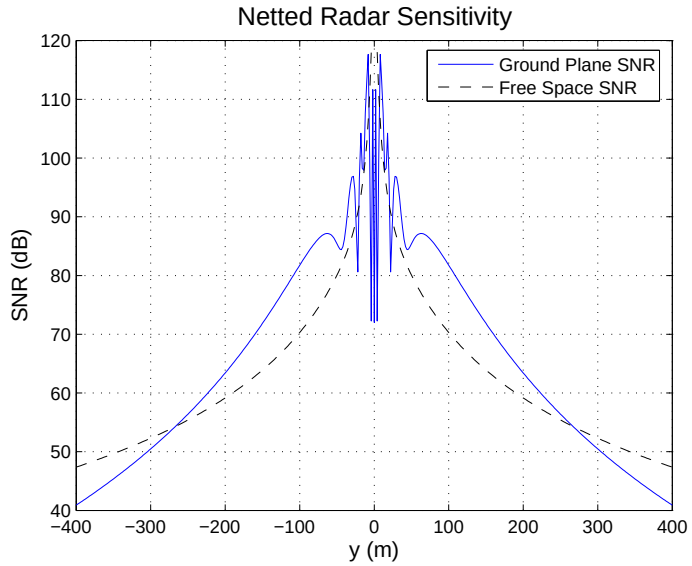

Figure 6.36: Influence of the ground plane effect - netted radar in Y direction - linear netted radar

The last example shows ground plane affected netted radar sensitivity for a dispersed netted radar configuration where the three nodes are placed at (-50, 0), (0, 50) and (50, 0) respectively to form a triangle.

For this system configuration Figure 6.37 shows the netted radar sensitivity map without the ground plane effect involved and Figure 6.38 shows the netted radar sensitivity map with the ground plane effect involved. Again it is seen that some fluctuations are shown in this ground plane involved netted radar case, especially around the area that each radar node is placed.

Figure 6.39 and Figure 6.40 show the variation of the netted radar sensitivities in one dimension for this dispersed netted radar configuration. The variation of netted radar sensitivity along X direction, i.e. with $y = 0$, is shown in Figure 6.35, and the variation of netted radar sensitivity along Y direction, i.e. with $x = 0$, is shown in Figure 6.36. It is seen that in this netted radar case, the sensitivity in X and Y directions are different as the configuration of radar nodes are different when looking at the system from X and Y directions. The sensitivity along X direction is still symmetrical to the coordinate origin, but the sensitivity along Y di-

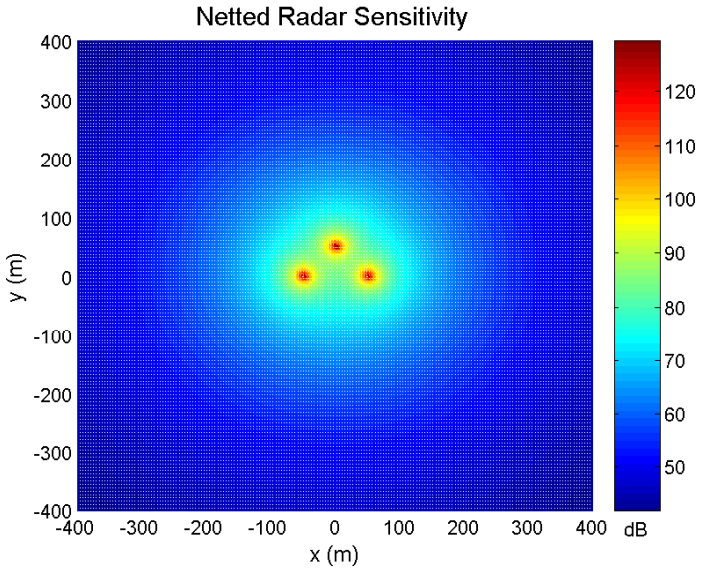

Figure 6.37: Netted radar sensitivity without ground plane effect - dispersed netted radar

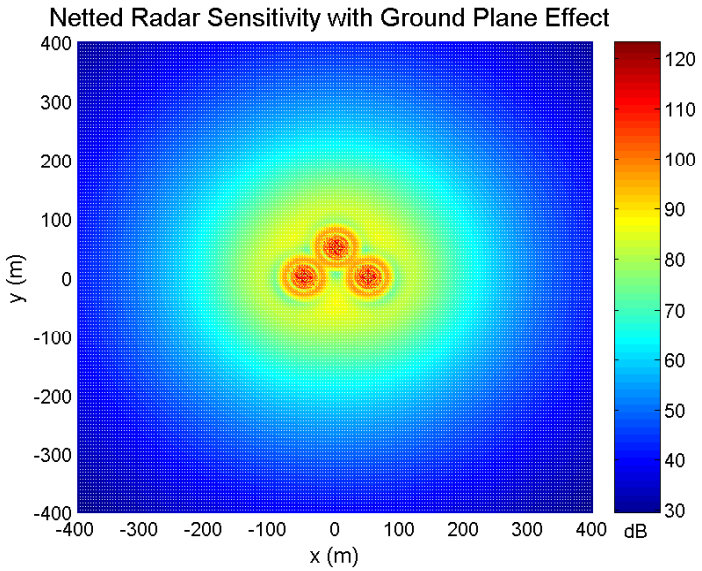

Figure 6.38: Netted radar sensitivity with ground plane effect - dispersed netted radar

rection is not symmetrical. This is due to the asymmetrical configuration of radar nodes in Y direction. Again, with the ground plane effect involved, the sensitivity value along both X and Y directions show a tendency of fluctuation around the spots where the radar nodes are placed. With long range the ground plane affected netted radar sensitivity is reduced rapidly.

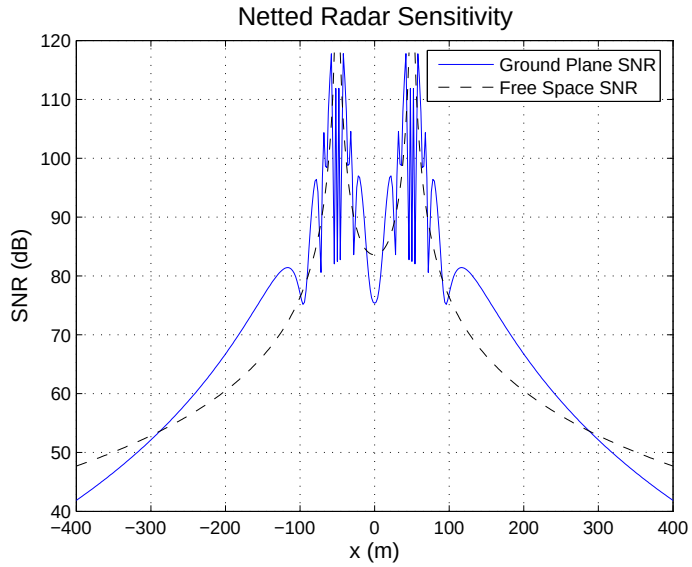

Figure 6.39: Influence of the ground plane effect - netted radar in X direction - dispersed netted radar

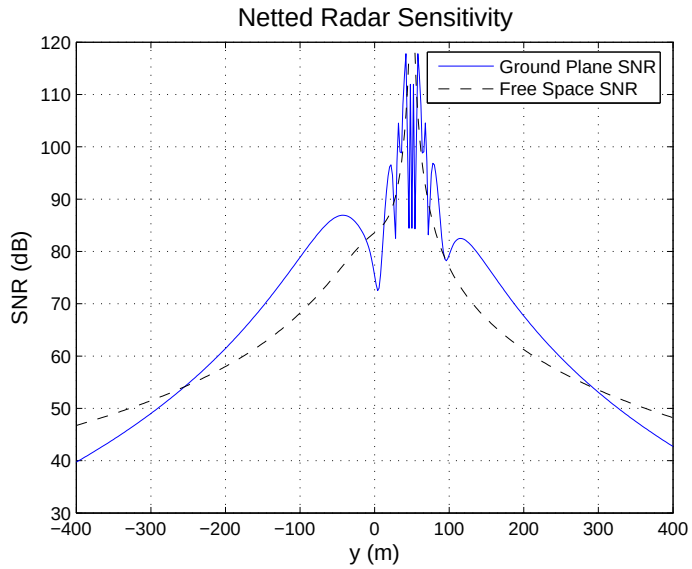

Figure 6.40: Influence of the ground plane effect - netted radar in Y direction - dispersed netted radar

6.5 Conclusions

In this chapter, a new form of the bistatic radar ground plane effect model has first been developed. Based on this model, the netted radar ground plane effect has been developed and

used to analyse the influence of ground plane on netted radar sensitivity. Monostatic radar ground plane effect was first reviewed where the RCS is affected by a few parameters such as wavelength, range, target and antenna height. This was then used to analyse the influence of ground plane on monostatic radar sensitivity where it has been shown that with the ground plane involved, the monostatic radar sensitivity is fluctuating dramatically, especially around the monostatic radar node. Null values of sensitivity have been observed. After this, a bistatic radar ground plane effect model has been developed and furthermore, a netted radar ground plane effect model has been developed. This has been used to analyse influence of the ground plane on netted radar sensitivity with various netted radar geometries. It has been shown that in netted radar cases, with ground plane involved, the sensitivity can be either greater or smaller than the free space one. The sensitivity is fluctuating, especially around the areas where the radar nodes are placed compared with the free space sensitivity for the same system configuration. Compared with monostatic case, some of the nulls that appear in the monostatic case disappear in the netted radar counterpart. The effect of netting randomizes the phase of returned signals. Therefore, compared with monostatic radar, netted radar provided better chance for the ground plane affected sensitivity curves to be smoothed. This shows one aspect of the advantages of the netted radar configuration where it offers a more stable sensitivity map with ground plane involved.

The ground plane potentially significantly influences the radar sensitivity, therefore the understanding of the influence of ground plane on netted radar performance is valuable for outdoor radar measurements. For example, when an actual netted radar system is deployed in real world situation, it can help to decide the system geometry where the sensitivity nulls can be avoided.

Chapter 7

Experimental Work

This chapter presents some field trial results to examine netted radar performance in practice. The experimental netted radar system used for the field trial was designed and developed by the UCL radar group. This chapter begins with an introduction to the experimental netted radar system, followed by a description of the field trials, and finally an analysis of experiment results.

7.1 Introduction

Some netted radar field experiments were performed using available resources to examine netted radar sensitivity performance in a real world situation and get collaboration with the netted radar theory. The prototype netted radar system used for the experiments was designed and constructed at UCL. The system has been developed over a number of teams to add extra capabilities. In the system design, COTS (Commercial off-the-shelf) components were used to keep capital costs very low compared to conventional commercial radar systems. An open and modular architecture is used to provide the flexibility to change or upgrade the system in the future. This is very important as the requirement for the system may change with the various potential experimental measurements in the future. The operating band is in the ISM band from 2.4 GHz to 2.45 GHz. The selection of this operating band came from two aspects. Firstly, components are readily available. Secondly, it is easy to get the netted radar to transmit in the license exempt band.

The UCL netted radar system consists of three nodes. Each node is capable of trans-

mitting and receiving. Node 1 is operating as a central node which has some extra functions including housing the distributed oscillator, transmitting the synchronisation pulse and operating the GUI compared with the other two nodes. Node 2 and Node 3 are identical. Figure 7.1 shows a picture of Node 1 in the netted radar system.

Figure 7.1: Netted radar node

Two sets of antennas are available for current netted radar system to meet the need of different experiment requirements. They are both 2.4 GHz parabolic antennas considering the high availability for use in ISM band. One set is 8° beamwidth antenna and the other set is 30° beamwidth antenna. Other operating parameters such as PRF, capture time and pulse length can also be chosen according to specific experiment requirement. The relevant parameters used for this experimental work will be specified in the experimental result section later in this chapter.

More details of the UCL netted radar hardware can be found in Appendix A.

7.2 Field trial environment

The netted radar field trials were carried out at the UCL Shenley Sports Ground at London Colney in Hertfordshire. Figure 7.2 shows a birds eye view of this trial field and the surrounding area. This relatively large flat grass field provides a low clutter trial environment. And it is quite easy to place radar nodes and targets anywhere within this area.

Since this test field is quite far from high population areas where high interferences would be expected, it was expected that the interference level would be low. However, it is still not possible to exclude all source of interferences. In Figure 7.2, it is seen that there are houses and supermarket/restaurant north of the motorway. They may become the source of interference due to the use of wireless networks which operate at 2.4 GHz that falls into the netted radar operating band. To roughly test the interference level of the field, a laptop computer was used to search for available WiFi networks. It turned out that although several wireless networks were found, the signal levels were still much lower than those typically seen in urban environment.

Typical trial geometry for the three radar nodes and a single target is shown in Figure 7.3. Since each node can be transmitting and receiving, (Figure 7.4 to Figure 7.6), and the netted radar is composed of three radar nodes, it can provide nine channels including three monostatic channels and six bistatic channels, shown in Table 7.1.

	Node 1 receiving	Node 2 receiving	Node 3 receiving
Node 1 transmitting	1 to 1 Monostatic	1 to 2 Bistatic	1 to 3 Bistatic
Node 2 transmitting	2 to 1 Bistatic	2 to 2 Monostatic	2 to 3 Bistatic
Node 3 transmitting	3 to 1 Bistatic	3 to 2 Bistatic	3 to 3 Monostatic

Table 7.1: Netted radar channels

The typical test range is around 120 m. Figure 7.7 shows a zoomed-in view of the test field with the experimental netted radar geometry. It is seen that the distance to the back of the test field is about another 120 m away from the target. Although it might be in the antenna main lobes, the return from the objects, i.e. trees etc., in these locations would still be easily

Figure 7.2: Test field and the surroundings

separable from the return of target of interests. It is also seen that the sides of the field are closer to the radar nodes compared to the back of the field. Since they are definitely not in the antenna main lobes, the return would also be separable. Therefore, in general, clutters from the edges of the field will be separable from the return signals from the target of interests.

It should be noted that in the field trial, for each node the transmitting and receiving antennas are separated by a length of 3 m to reduce feed through between them with transmitting antenna on the left-hand side and receiving antenna on the right-hand side (Figure 7.8). Also, all the antennas are manually adjusted so that the target is in the centre of the antenna main lobe to achieve best possible measurement results.

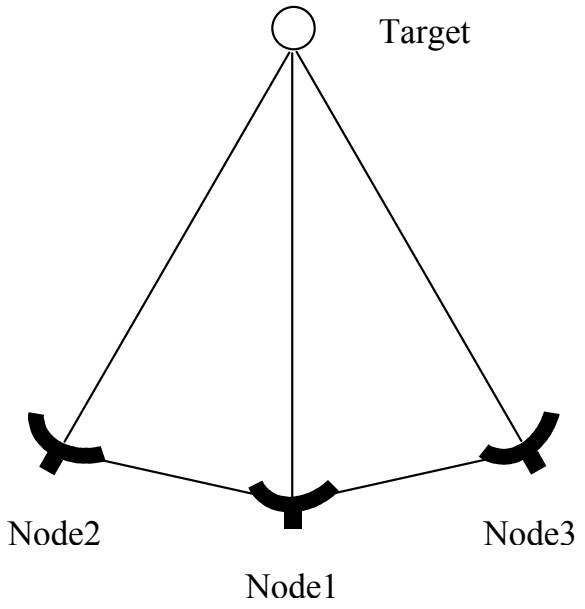

Figure 7.3: Field trial radar geometry

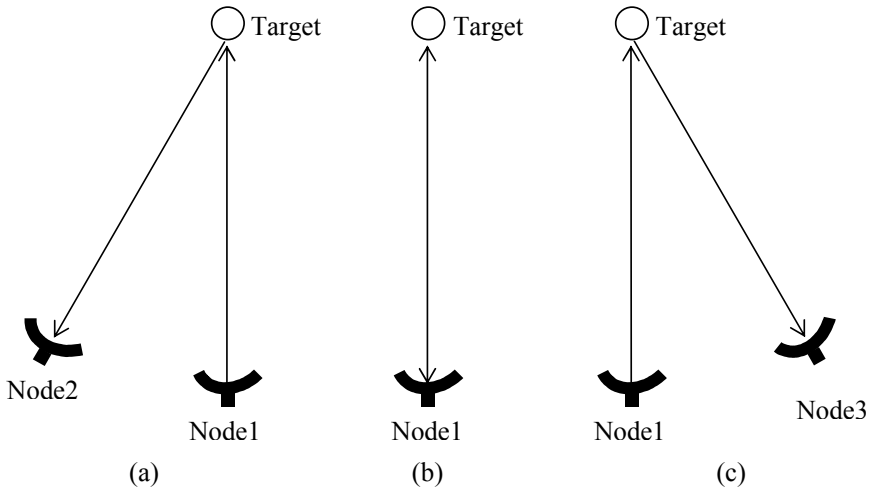

Figure 7.4: Node 1 transmitting (a) Node 1 receiving; (b) Node 2 receiving; (c) Node 3 receiving

7.3 Field trial experiments

The netted radar described in Section 7.1 was used to conduct a set of measurements to examine netted radar performance. This concentrates on range and sensitivity issues to relate closely to the theoretical aspects of this story. The experiments conducted for this thesis used

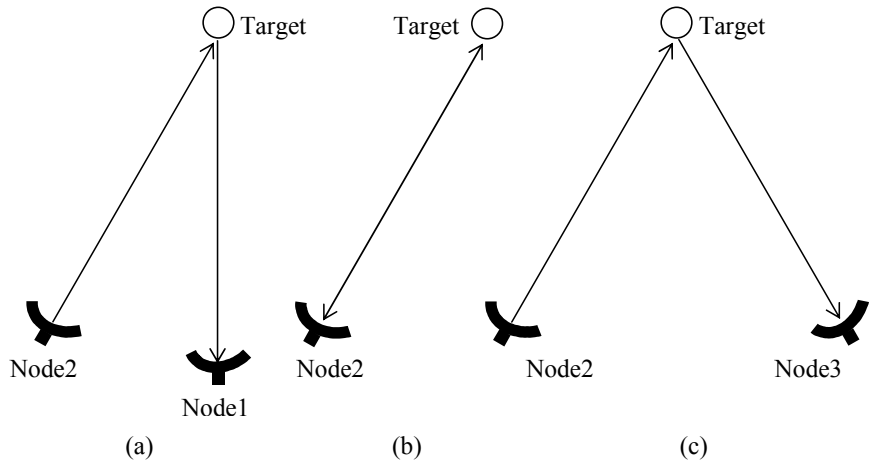

Figure 7.5: Node 2 transmitting (a) Node 1 receiving; (b) Node 2 receiving; (c) Node 3 receiving

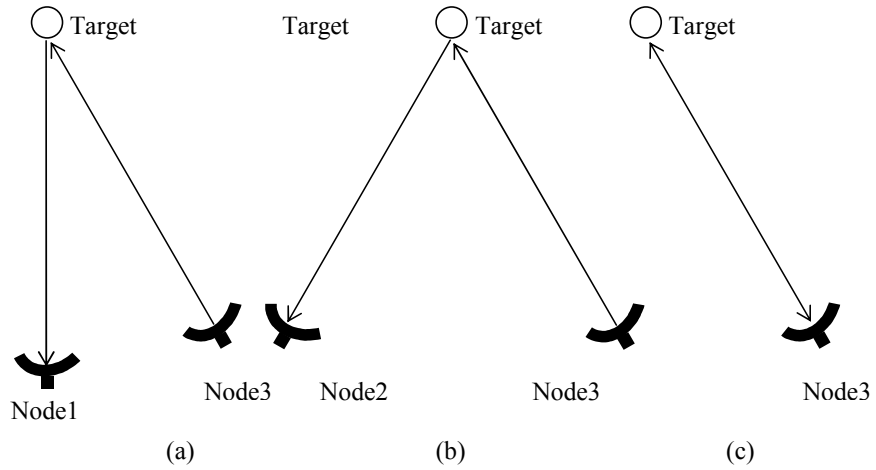

Figure 7.6: Node 3 transmitting (a) Node 1 receiving; (b) Node 2 receiving; (c) Node 3 receiving

the 8° beam antenna to get better gains. Figure 7.9 shows a picture of the netted radar in operation in the test field. In this picture, the closest node is Node 1 where Node 3 can be roughly seen as at the top right corner of this figure where it is connected to Node1 through a pair of 50 m red cables.

Before any measurements were taken, the noise level of the test field was measured to ensure that the noise model satisfied the assumptions for the following sensitivity measure-

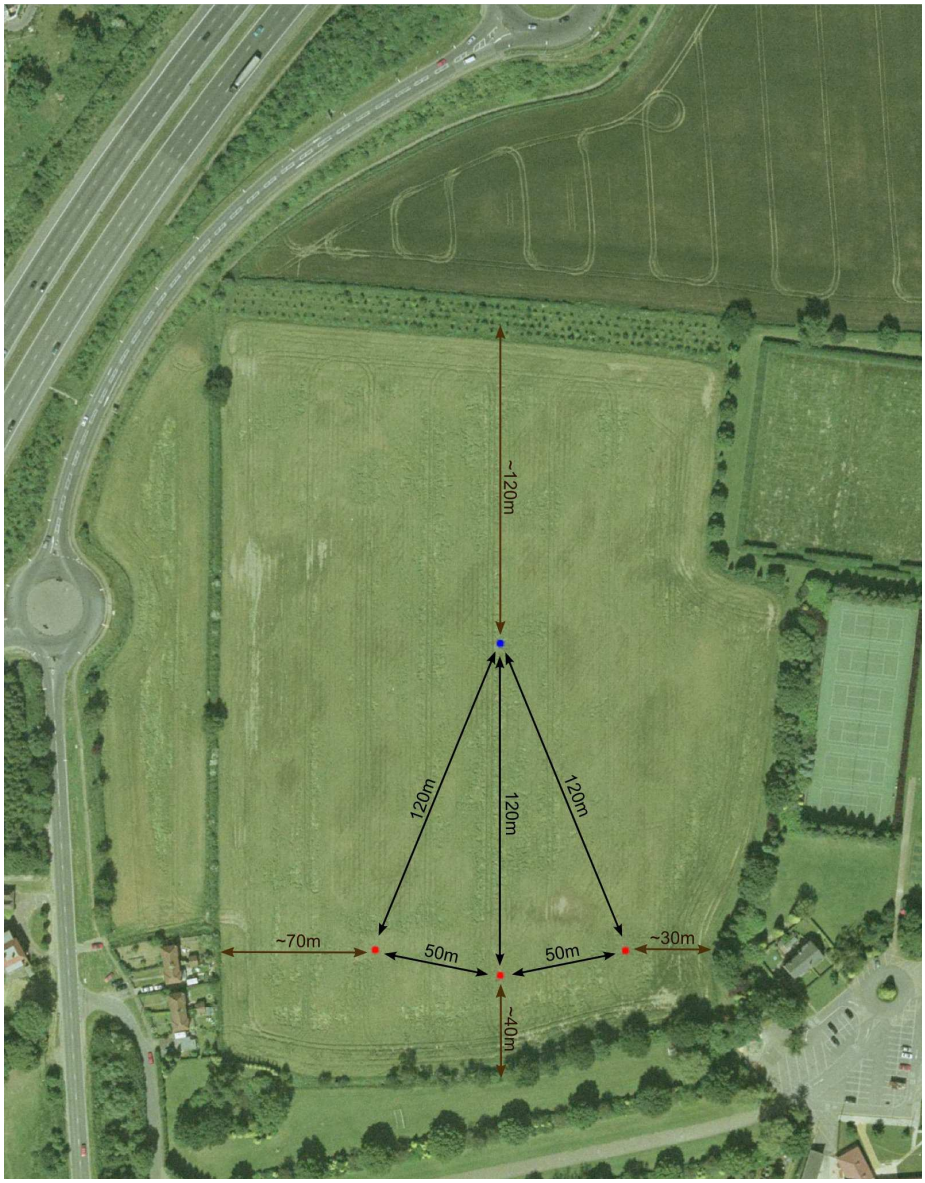

Figure 7.7: Zoomed-in test field view

ment. The noise was measured by turning off the transmitters and keeping the receivers on, i.e. the netted radar was in passive node. In this case, since there was no transmission from the netted radar itself, the returns measured at each receiver were noise only. It turned out that for the netted radar system the noise was Gaussian and white across the radar bandwidth. This satisfied the assumptions for noise conditions the netted radar sensitivity models were built on which are developed in Chapter 4.

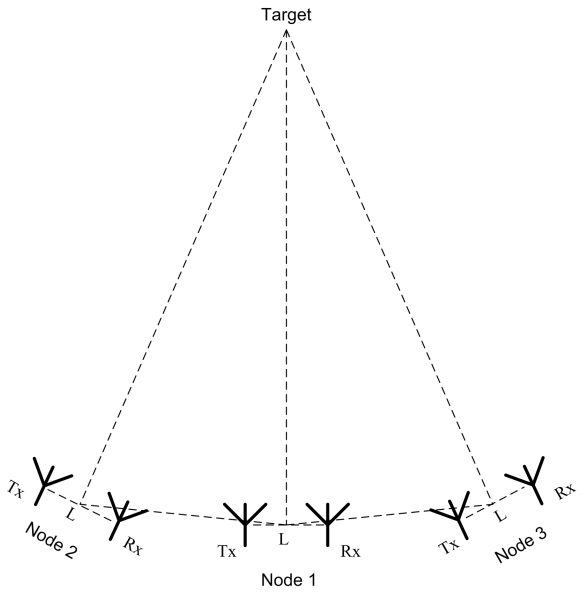

Figure 7.8: Separation of transmitting and receiving antennas

Figure 7.9: Netted radar in operation in the test field

7.3.1 Clutter measurements

After suitable noise conditions were established, the next step was to assess the clutter levels in the test field to determine the level to which minimum signal might be expected to be observed.

Since the test field was a relatively flat grass field, it was expected that it would provide low clutter. The clutter measurement was conducted by turning on all the transmitters and receivers but not placing any target in the field. In this case, the returned signals were due to the clutter from the test field rather than from any target.

Table 7.2 listed the netted radar system settings that were used for the measurement. The capture time was 1.28 μs. This corresponds to a two way test range of 192 m ($\frac{(1.28\times10^{-6})\times(3\times10^{8})}{2}$ = 192 m). Since all the transmitters and receivers were turned on and were enabled to receive signals transmitted from any receiver in the network, this provided nine channels as is shown in Figure 7.4 to Figure 7.6 including three monostatic and six bistatic channels. The number of pulse received by each node was 30,000. Since interleave was enabled, for each channel the total received number of pulses would be $\frac{30000}{3}$ = 10000.

Parametre	Value
Waveform	Up-chirp
PRF	30 kHz
Capture time	1.28 μs
Pulse length	0.6 μs
Interleave	Enabled
Number of pulses received	30,000
Bandwidth	40 MHz

Table 7.2: Experimental netted radar settings

Figure 7.10 to Figure 7.15 show the normalized matched filter output against range for the clutter measurement in the test field in nine different channels. It is the average of the summation over 10,000 samples for each channel. Each of the three monostatic profiles are plotted in individual figures. For the bistatic cases, the bistatic pair containing the same nodes are plotted in the same figure for easy comparison. In theory, since the parameters for such pair of nodes are exactly the same, the outputs should also be exactly the same due to reciprocity. In Figure 7.13 to Figure 7.15 it is seen that the profiles involving the same pairs of nodes are

very similar to each other, though not exactly the same.

It is seen that in each of the nine channels, the biggest response generally appears at around 240-250 m, which corresponds to the back of the trial field. As in Figure 7.7 it is seen that there are trees at around 250 m in the back of the test field. This could cause the clutter levels to rise at these range values. Between 150 m and 250 m, some other smaller peaks can be observed where the positions vary from profile to profile. These correspond to the sides of the trial field. Again, in Figure 7.7 it is seen that there are trees on both sides of the test field. Unlike the trees in the back of the test field which are almost evenly distributed, the trees on the sides of the test field are distributed more randomly. Also, the distribution of the trees on the left-hand side is different from that on the right-hand side. There are less trees on the left-hand side than on the right-hand side. For this reason, the positions of smaller peaks vary from profile to profile.

It is observed that in all the nine channels, from 120 m to 150 m in range, the responses are generally very low and flat. It is seen that the responses in these ranges are generally 20 dB lower than the biggest response in each channel where in Node 1 monostatic case, it is around 30 dB lower than the biggest response. This means that the test field in these ranges is relatively flat. It is likely to avoid influence of big clutters, if the target is placed in these ranges. Therefore, those ranges are where we place our targets for the range and sensitivity measurements in the next section.

7.3.2 Netter radar sensitivity measurements

In this section the measured netted radar sensitivity gain of a three node netted radar system is compared with the expected theory referenced to the monostatic case. After examining the noise and clutter levels for the experimental netted radar system and the test field, a single stationary target was placed in the test field to examine netted radar range and sensitivity. The target used was a cylinder mounted at the top of a tripod and was adjusted so that the centre of the cylinder target was about the same height as the centre of transmitting and receiving antennas. A picture of this target is shown in Figure 7.16. The cylinder target has the same geometry when it is viewed from any azimuth. Compared with some other targets which are

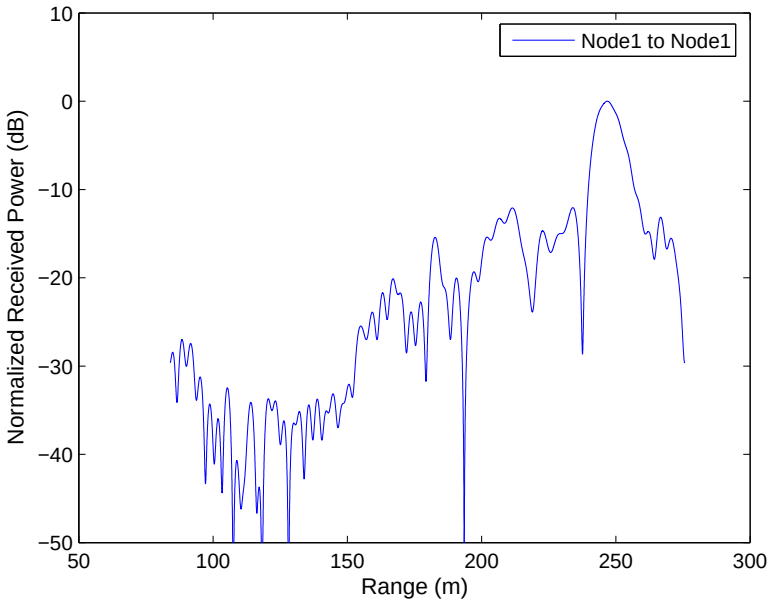

Figure 7.10: Clutter - Node 1 monostatic

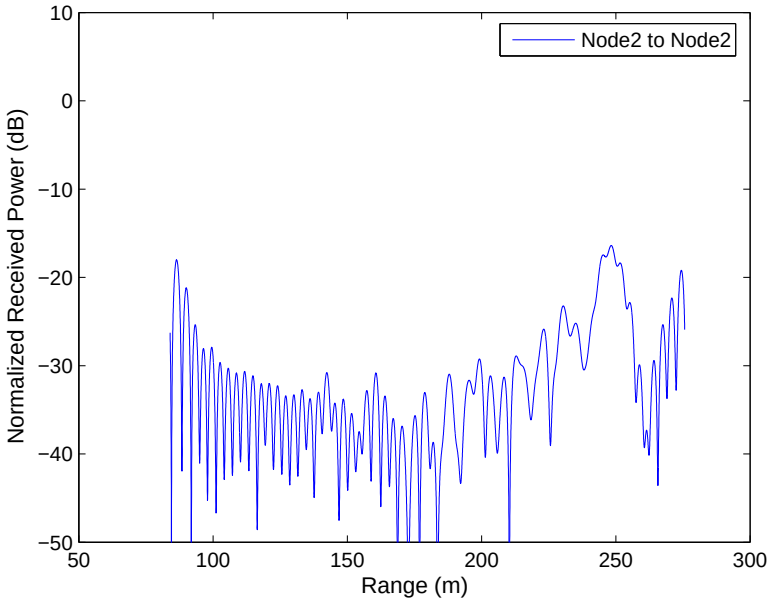

Figure 7.11: Clutter - Node 2 monostatic

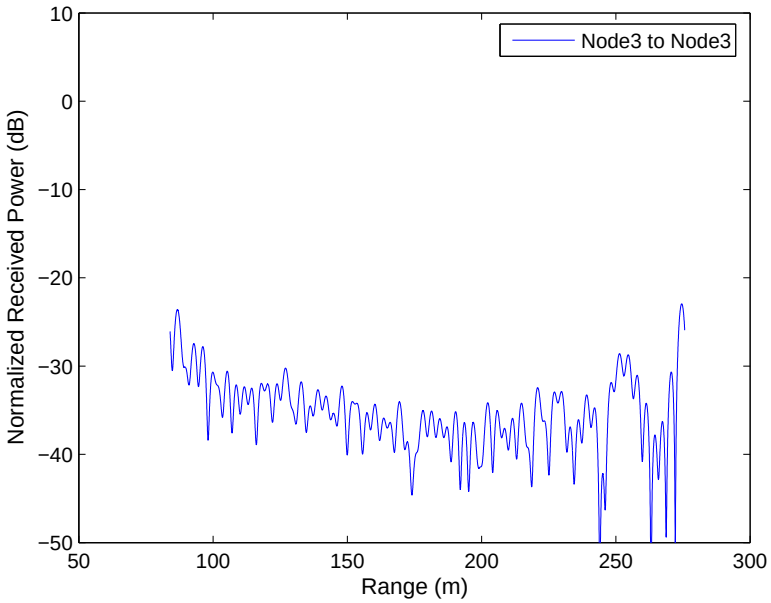

Figure 7.12: Clutter - Node 3 monostatic

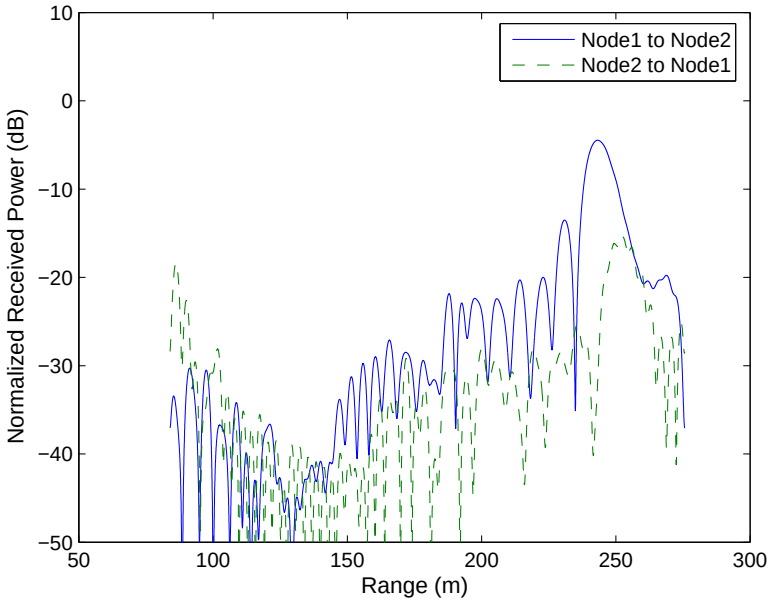

Figure 7.13: Clutter - Node 1 and Node 2 bistatic

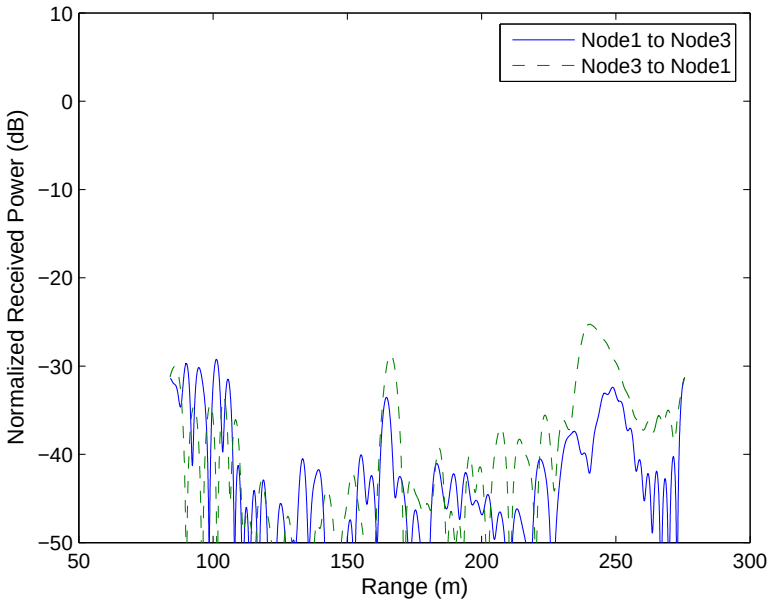

Figure 7.14: Clutter - Node 1 and Node 3 bistatic

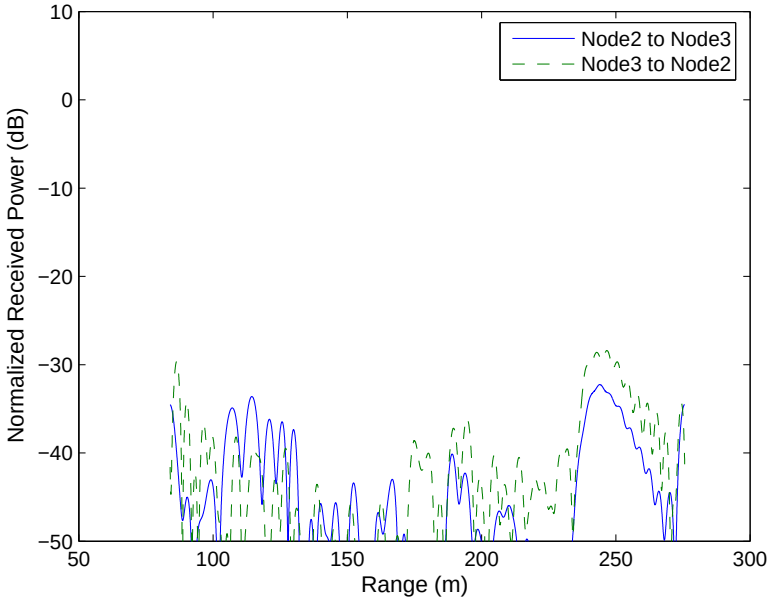

Figure 7.15: Clutter - Node 2 and Node 3 bistatic

also commonly used for radar trial, such as flat plate and corner reflector targets, this provides some kinds of symmetry which will allow easier analysis and comparison of the measurement results.

Figure 7.16: Cylinder target

The experimental netted radar geometry is shown in Figure 7.17. The arrangement of the radar nodes and target position is to provide symmetrical geometry. With this geometry, in theory, the performance of the bistatic radar composed by Node 1 and Node 2 and the performance of the bistatic radar composed by Node 1 and Node 3 should be exactly the same. The direct distance between neighbouring nodes was 50 m (L). The target was placed at 120 m for collaboration. When the target is at 120 m, $R = R_1 = 120$ m. When the target range R is greater than 120 m, R_1 will be slightly different from R, which can be easily calculated

through triangulation.

The target was placed at R = 130 m, R = 140 m and R = 150 m respectively to examine netted radar range and sensitivity. The radar settings for these measurements were the same as is listed in Table 7.2. Again, as for the clutter measurement in Section 7.3.1, all the transmitters and receivers were turned on and each receiver was enabled to receive signals from any of the transmitters, therefore nine channels were presented. Since the radar settings meet the conditions in Equation 4.18 and the noise meets the Gaussian white conditions, the sensitivity will be proportional to the received power. Therefore, normalized matched filter received power against range will be plotted for each of the profiles. From Figure 7.17, it is seen that, for the bistatic cases involving Node 1, since R and R_1 are slightly different, the expected two way range will be the average of these two.

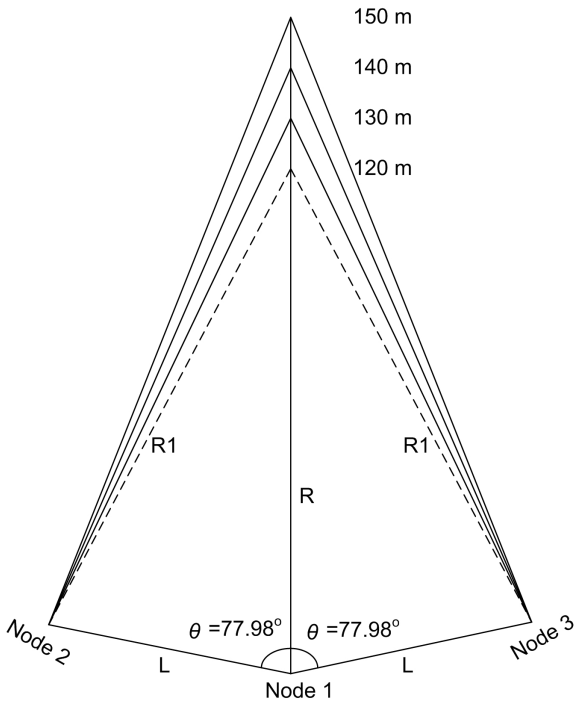

Figure 7.17: Experimental netted radar geometry

Figure 7.18 to Figure 7.23 show the normalized matched filter outputs for target at R = 130 m. This is again the average of 10,000 pulses. The same presentation as the clutter figures is used, i.e. the first three figures show the outputs for the three monostatic cases and the last

three figures show the outputs for the bistatic cases where the bistatic radars involving the same nodes are plotted in the same figure for easy comparison.

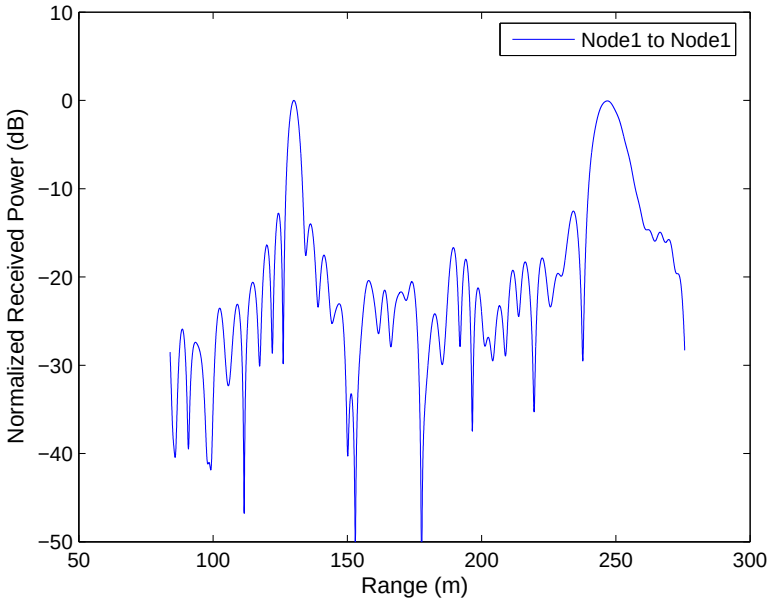

Figure 7.18: Target at 130 m - Node 1 monostatic

It is clearly seen that in each of these nine profiles, a relatively narrow and high peak appears at around 130 m on the range axis which corresponds to the cylinder target. This is more obvious if compared with the measurement for clutter shown in Figure 7.10 to Figure 7.15. It is also seen that for the bistatic pairs that involve the same radar nodes where in theory the outputs are expected to be exactly the same, the matched filter outputs generally well match to each other although slight differences are observed (Figure 7.21 to Figure 7.23). Especially for the bistatic pairs composed of Node 1 and Node 3, the two matched filter output curves representing Node 1 and Node 3 transmitting respectively are very similar to each other, shown in Figure 7.22.

Next, we examine the sensitivity of the netted radar system and begin by checking range measurement. Table 7.3 shows the expected two-way range for the nine radars comprising the netted radar. Table 7.4 shows the actual measured ranges for the corresponding radars. The measured range value corresponds to the biggest received power in range between 100 m and

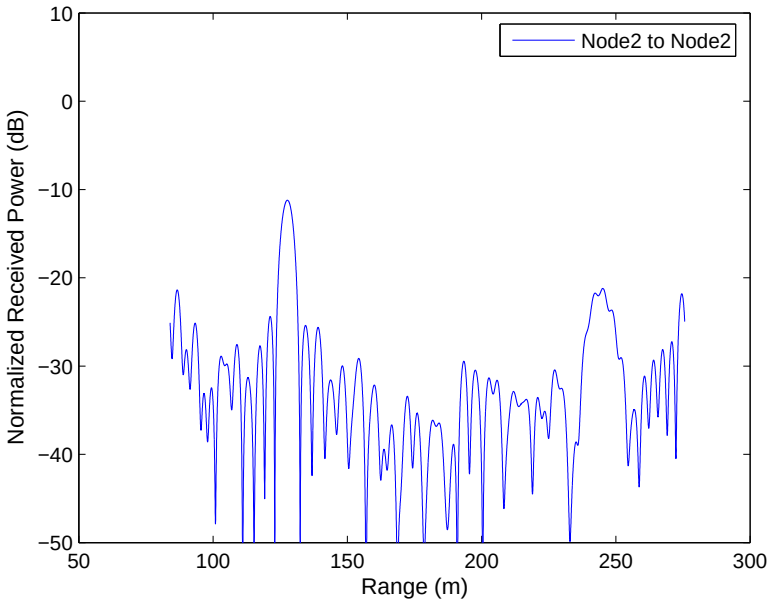

Figure 7.19: Target at 130 m - Node 2 monostatic

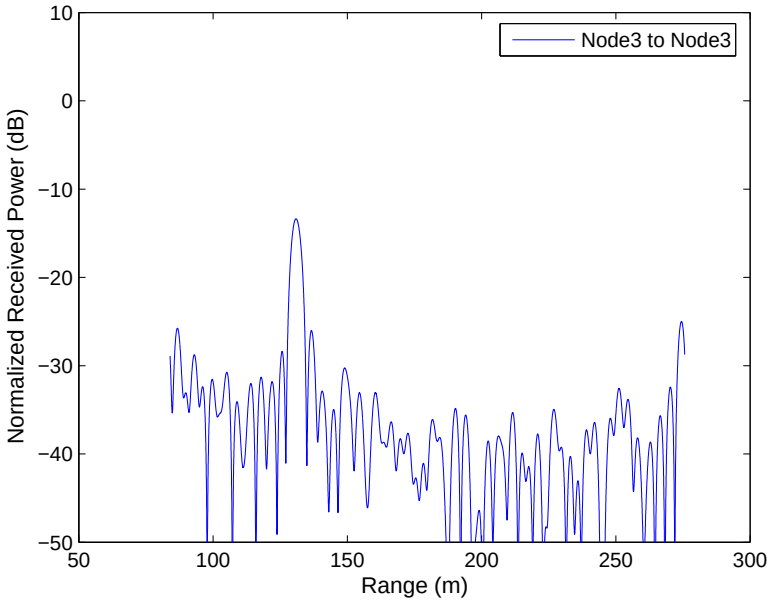

Figure 7.20: Target at 130 m - Node 3 monostatic

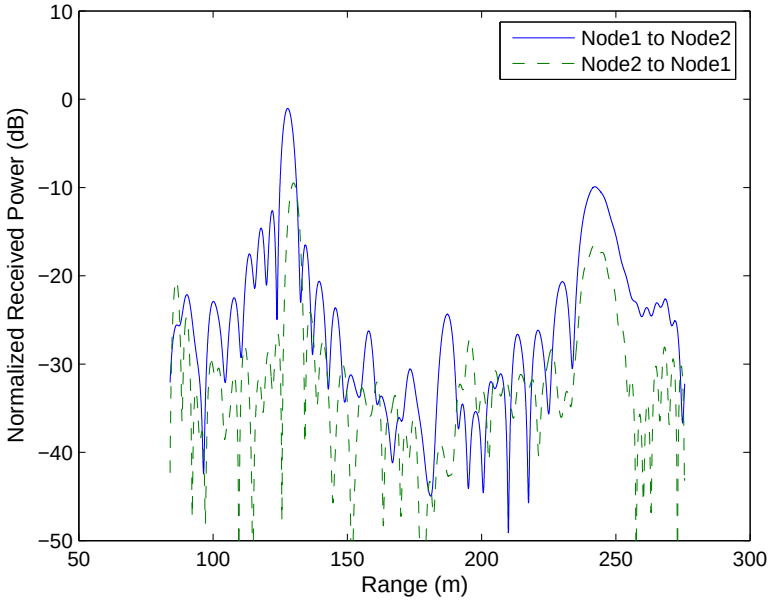

Figure 7.21: Target at 130 m - Node 1 and Node 2 bistatic

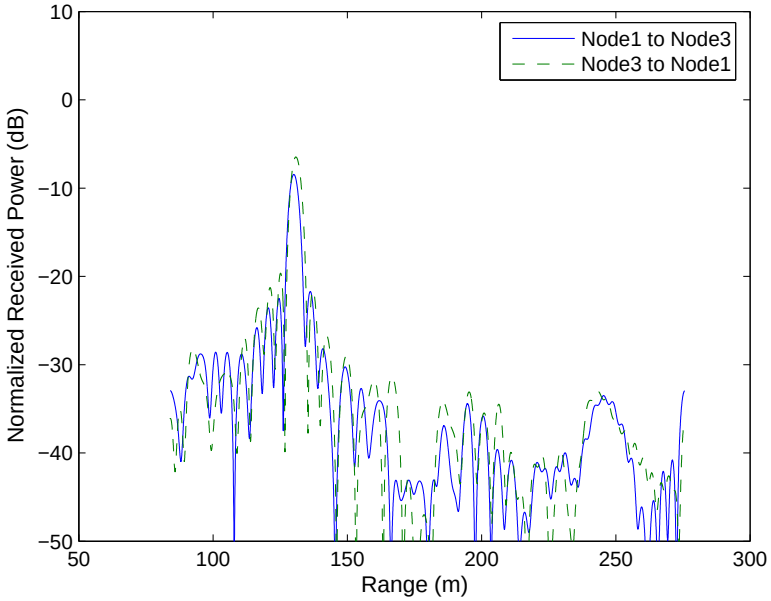

Figure 7.22: Target at 130 m - Node 1 and Node 3 bistatic

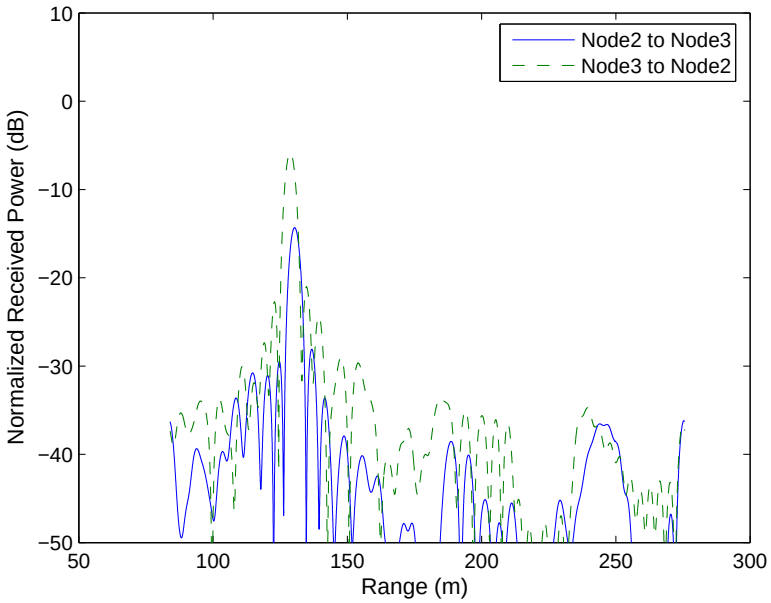

Figure 7.23: Target at 130 m - Node 2 and Node 3 bistatic

200 m. The number in parenthesis is the difference between measured value and expected value of range for each profile. It is seen that for the target at 130 m, the absolute value of the measurement error is between 0.1 m and 1.8 m. Considering the expected range is around 130 m, with this range of measurement error, the accuracy of range measurement of this netted radar system is satisfactory.

	Node 1 receiving	Node 2 receiving	Node 3 receiving
Node 1 transmitting	130 m	129.6 m	129.6 m
Node 2 transmitting	129.6 m	129.2 m	129.2 m
Node 3 transmitting	129.6 m	129.2 m	129.2 m

Table 7.3: Expected range - target at 130 m

After examining the ability of range measurement of the netted radar we are going to examine the sensitivity of the system. Table 7.5 shows the normalized matched filter output power in dB for the point where the cylinder target was located. The numbers in parenthesis is

	Node 1 receiving	Node 2 receiving	Node 3 receiving
Node 1 transmitting	130.1 m (0.1 m)	127.8 m (-1.8 m)	130.1 m (0.5 m)
Node 2 transmitting	130.0 m (0.4 m)	127.7 m (-1.5 m)	130.4 m (1.2 m)
Node 3 transmitting	130.8 m (1.2 m)	128.8 m (-0.4 m)	130.9 m (1.7 m)

Table 7.4: Measured range - target at 130 m

the actual value of the normalized matched filter output power corresponding to the dB values. If the dB value is P and the actual value is x, then the relation between these two is given by:

$$P = 10log_{10}x \tag{7.1}$$

and

$$x = 10^{(P/10)} \tag{7.2}$$

	Node 1 receiving	Node 2 receiving	Node 3 receiving
Node 1 transmitting	0 dB (1)	-1.04 dB (0.787)	-8.45 dB (0.143)
Node 2 transmitting	-9.49 dB (0.113)	-11.21 dB (0.076)	-14.32 dB (0.037)
Node 3 transmitting	-6.47 dB (0.225)	-5.85 dB (0.260)	-13.36 dB (0.046)

Table 7.5: Received power - target at 130 m

The three nodes in the netted radar system used for this experiment were identical. Since the power from individual monostatic and/or bistatic radar is considered to form the total netted radar sensitivity, i.e. no phase information is used, from Equation 4.24, the total netted radar sensitivity was expected to be N times of the single monostatic sensitivity. In the experimental netted radar system, there were three nodes. Theoretically the netted radar sensitivity was expected to have 3 times gain over the single monostatic radar sensitivity.

Now looking at the actual experimental measurement result for R = 130 m, the total netted radar sensitivity, given by the sum of the numbers in parenthesis in Table 7.5 is 2.687, which is 2.687 times of the Node 1 monostatic sensitivity. This is lower than the predicted 3 times gain of the theoretical value, but the netted operation still increases the total sensitivity

of the system compared to single monostatic case. If we look at the sensitivity for every single monostatic and bistatic radar in this table, it varies from case to case. The difference is up to about 14 dB. In this case, the ratio of the total netted radar sensitivity over single monostatic or bistatic sensitivity also varies from case to case.

The reason for the instability of the measured sensitivity could be complex. One reason could be the lack of knowledge of the initial phase of the transmitted signals and the accurate position of the antenna phase centre. In this case the coherency of the system can not be guaranteed. This could be improved by finding more accurate calibration method in the future. The antenna itself could also be a reason. In the experimental process, the antennas were manually adjusted to face the target. This may cause some uncertainty in the measurement. The cylinder target is supposed to have uniform RCS in all directions for monostatic and bistatic cases. This simple model can also cause inaccuracy. If a more complex target model is used, the accuracy can also be improved. Also, the target was manually adjusted and supposed to be in an upright position. If it is tilted, some unknown effects may also be added, because in this case, the RCS will vary for different bistatic radar pairs in the netted radar system even if the transmitter-receiver look angles are the same . The ground plane may also add in extra effect to the measured sensitivity. Additionally, the reflection from the tripod that was used to support the target may also interfere the measured return signals.

From the first set of experiments examining netted radar sensitivity where the target was placed at R = 130 m, it is seen that the actual measured netted radar sensitivity results are complex. Therefore, the same kind of experiments were conducted to further examine netted radar sensitivity experimentally. This time, the target was moved away from the radar nodes until R = 140 m. Figure 7.24 to Figure 7.29 show the normalized matched filter outputs for this new geometry. In each of the nine profiles, a clear peak can still be seen, but this time at around 140 m on the range axis which represents the reflection from the cylinder target.

Table 7.6 shows the expected two-way range for the nine radars comprising the netted radar. Table 7.8 shows the measurement results for the corresponding radars. It is seen that this time for target at 140 m, the absolute value of the measurement error is between 0.3 m and 1.8 m.

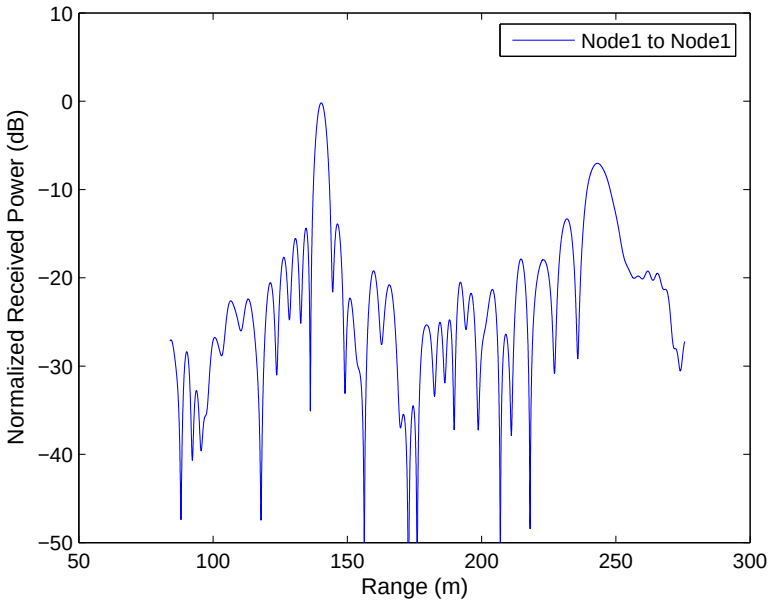

Figure 7.24: Target at 140 m - Node 1 monostatic

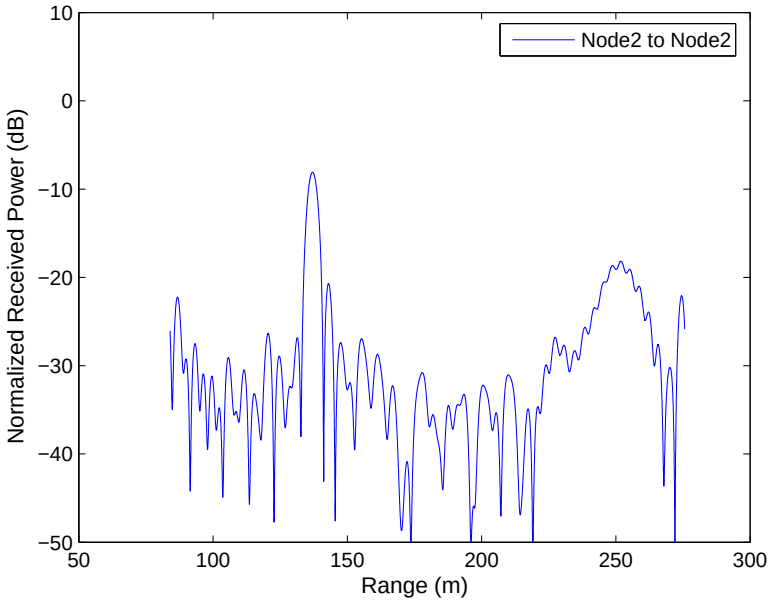

Figure 7.25: Target at 140 m - Node 2 monostatic

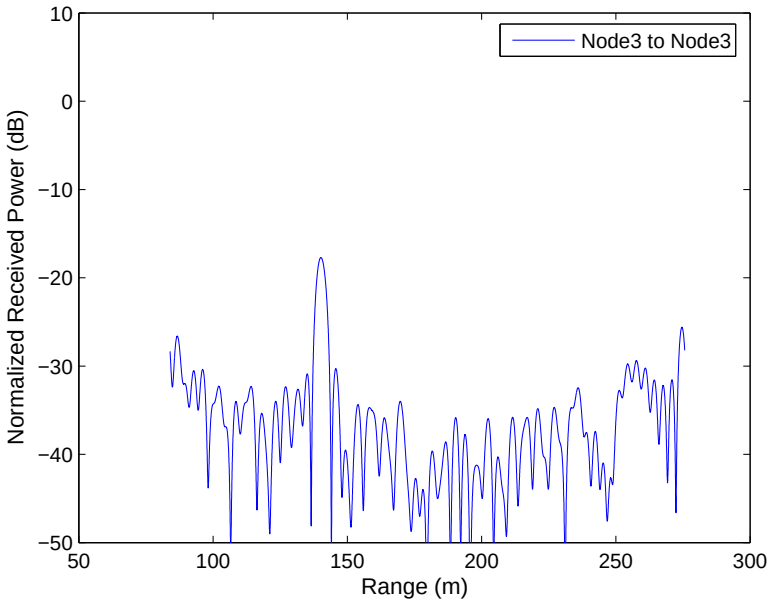

Figure 7.26: Target at 140 m - Node 3 monostatic

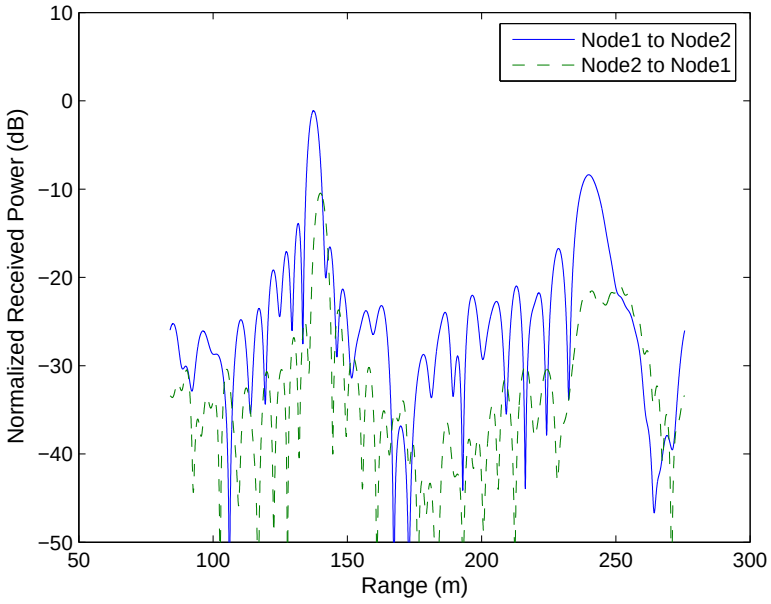

Figure 7.27: Target at 140 m - Node 1 and Node 2 bistatic

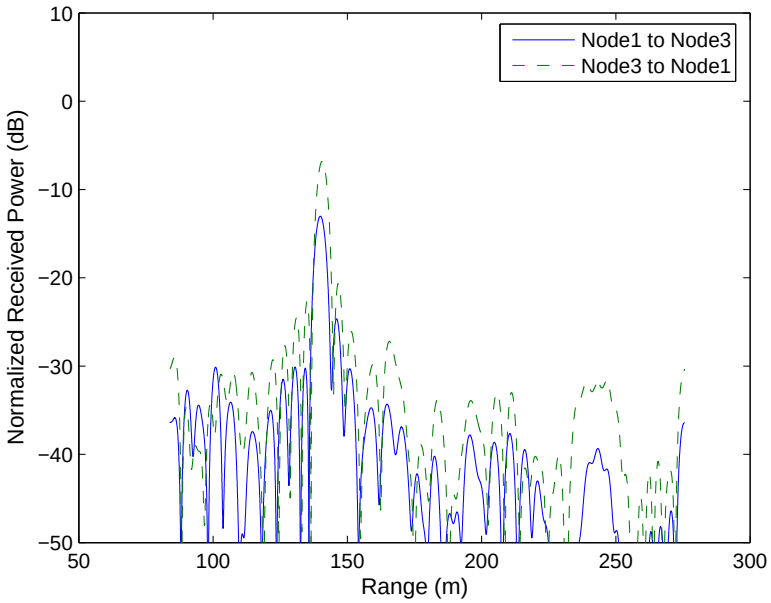

Figure 7.28: Target at 140 m - Node 1 and Node 3 bistatic

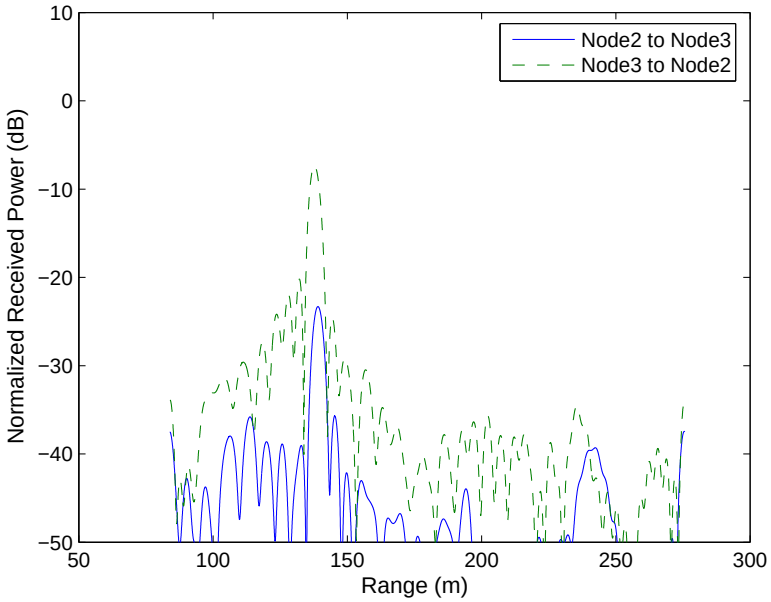

Figure 7.29: Target at 140 m - Node 2 and Node 3 bistatic

	Node 1 receiving	Node 2 receiving	Node 3 receiving
Node 1 transmitting	140 m	139.3 m	139.3 m
Node 2 transmitting	139.3 m	138.5 m	138.5 m
Node 3 transmitting	139.3 m	138.5 m	138.5 m

Table 7.6: Expected range - target at 140 m

	Node 1 receiving	Node 2 receiving	Node 3 receiving
Node 1 transmitting	140.3 m (0.3 m)	137.5 m (-1.8 m)	140.0 m (0.7 m)
Node 2 transmitting	140.0 m (0.7 m)	137.1 m (-1.4 m)	139.1 m (0.6 m)
Node 3 transmitting	140.6 m (1.3 m)	137.8 m (-0.7 m)	140.2 m (1.7 m)

Table 7.7: Measured range - target at 140 m

Now the total netted radar sensitivity for cylinder target at R = 140 m, given by the sum of the numbers in parenthesis in Table 7.8 is 2.440, which is 2.547 times of the Node 1 monostatic sensitivity. Again as in the R = 130 m case, this is lower than the predicted 3 times gain of the theoretical value, but the netted operation still increases the total sensitivity of the system compared to single monostatic case. Variation of the sensitivity could also be seen for different monostatic or bastatic radar in the system.

	Node 1 receiving	Node 2 receiving	Node 3 receiving
Node 1 transmitting	-0.19 dB (0.958)	-1.12 dB (0.773)	-13.03 dB (0.050)
Node 2 transmitting	-10.47 dB (0.090)	-8.10 dB (0.155)	-23.30 dB (0.005)
Node 3 transmitting	-6.82 dB (0.208)	-7.36 dB (0.184)	-17.71 dB (0.017)

Table 7.8: Received power - target at 140 m

Lastly, the target was moved further away from the radar nodes to a position where R = 150 m. Figure 7.30 to Figure 7.35 show the normalized matched filter outputs for this new geometry. In most of the profiles, a clear peak can be seen at around 150 m on the range

axis which represents the reflection from the cylinder target. An exception occurred in Node 3 monostatic case where the peak representing the cylinder target can not be very clearly identified. Here two small peaks appear at around 150 m in range axis with similar heights (Figure 7.32). This, on the other hand, shows one aspect of the advantages of netted radar system over traditional monostatic and bistatic radars. When one channel in the network is faulty, other channels can still be used to decide target location.

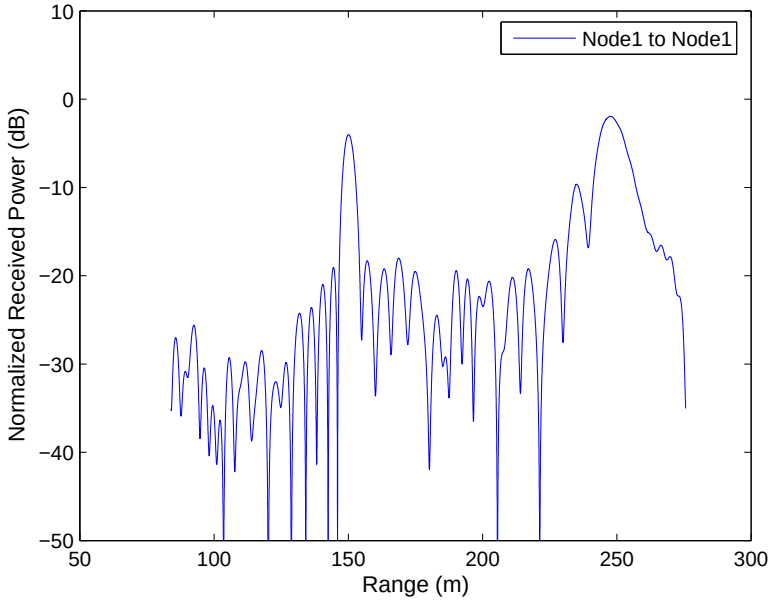

Figure 7.30: Target at 150 m - Node 1 monostatic

Table 7.9 shows the expected two-way range for the nine radars comprising the netted radar. Table 7.11 shows the measurement results for the corresponding radars. It is seen that now for target at 150 m, the absolute value of the range measurement error is between 0.1 m and 3.3 m.

Now the total netted radar sensitivity for the cylinder target at R = 150 m, given by the sum of the numbers in parenthesis in Table 7.11 is 1.068, which is 2.690 times of the Node 1 monostatic sensitivity. This is again lower than the predicted 3 times gain of the theoretical value, but the netted operation still increases the total sensitivity of the system compared to single monostatic case. Variation of the sensitivity can still be seen for different

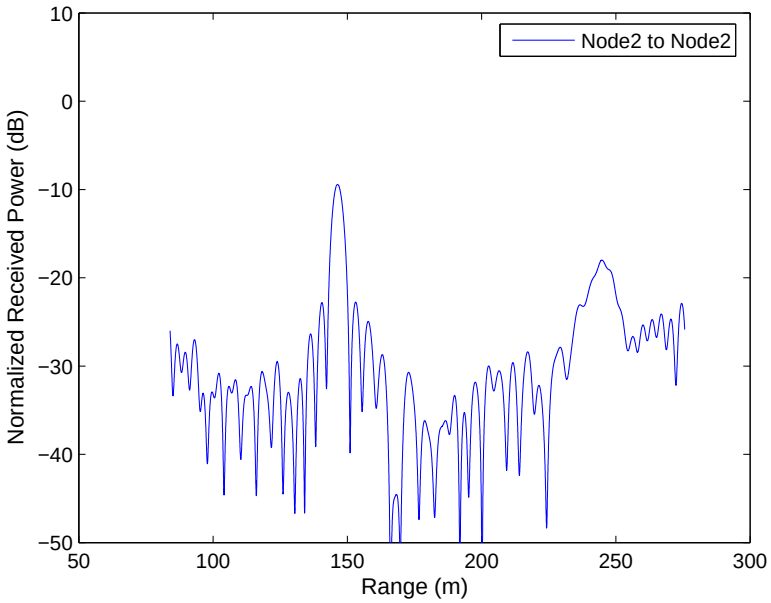

Figure 7.31: Target at 150 m - Node 2 monostatic

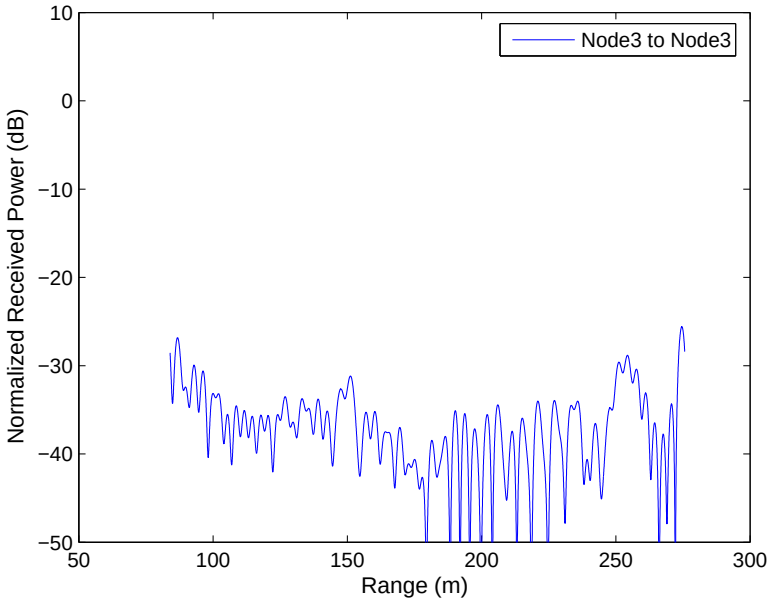

Figure 7.32: Target at 150 m - Node 3 monostatic

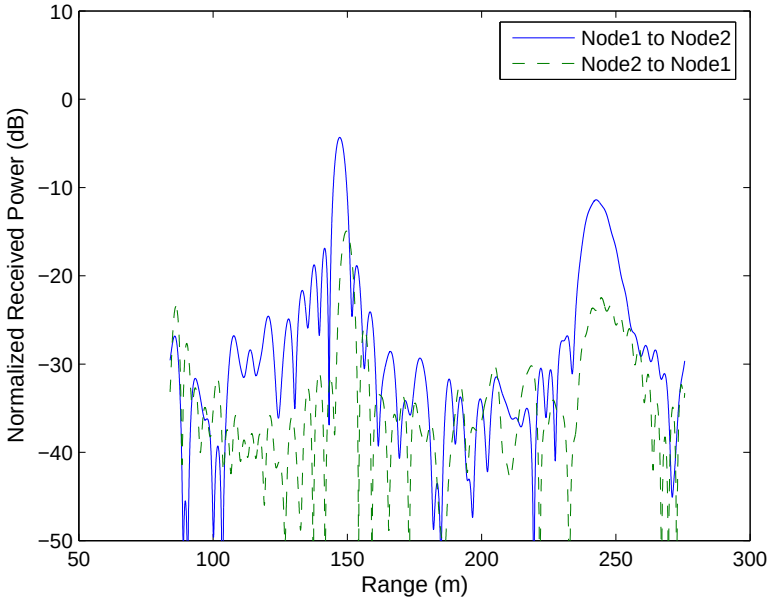

Figure 7.33: Target at 150 m - Node 1 and Node 2 bistatic

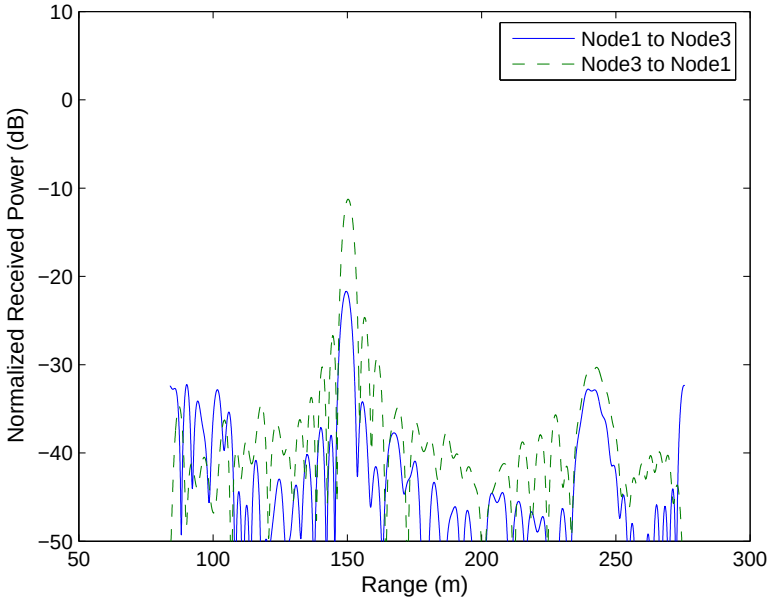

Figure 7.34: Target at 150 m - Node 1 and Node 3 bistatic

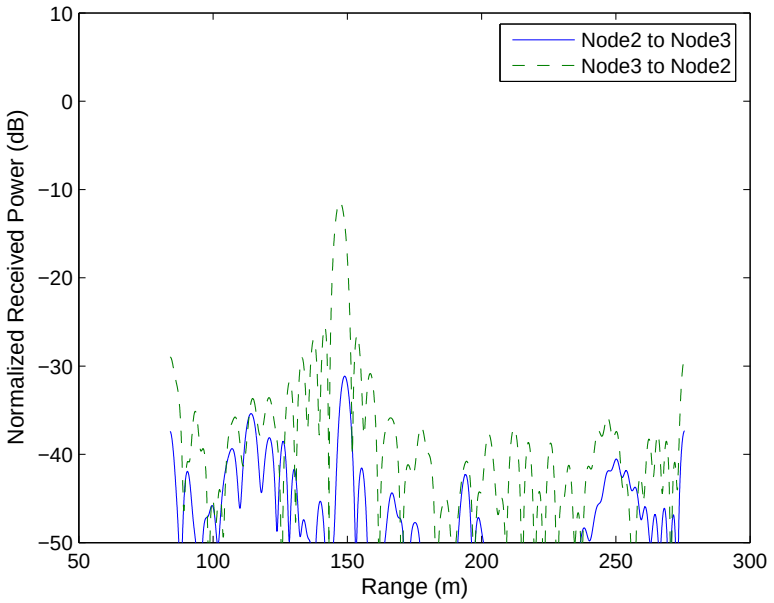

Figure 7.35: Target at 150 m - Node 2 and Node 3 bistatic

	Node 1 receiving	Node 2 receiving	Node 3 receiving
Node 1 transmitting	150 m	149.0 m	149.0 m
Node 2 transmitting	149.0 m	147.9 m	147.9 m
Node 3 transmitting	149.0 m	147.9 m	147.9 m

Table 7.9: Expected range - target at 150 m

	Node 1 receiving	Node 2 receiving	Node 3 receiving
Node 1 transmitting	150.1 m (0.1 m)	147.2 m (-1.8 m)	149.6 m (0.6 m)
Node 2 transmitting	149.7 m (0.7 m)	146.4 m (-1.5 m)	149.1 m (1.2 m)
Node 3 transmitting	150.3 m (1.3 m)	147.3 m (-0.6 m)	151.2 m (3.3 m)

Table 7.10: Measured range - target at 150 m

monostatic or bastatic radars in the system. It is observed that in this set of measurement, obvious degradation of sensitivity occurred whenever Node 3 was receiving (Figure 7.32, 7.34

and 7.35). This was possibly due to a fault on the Node 3 receiving channel at the time when this set of data were taken.

	Node 1 receiving	Node 2 receiving	Node 3 receiving
Node 1 transmitting	-4.0 dB (0.397)	-4.33 dB (0.369)	-21.70 dB (0.007)
Node 2 transmitting	-14.94 dB (0.032)	-9.43 dB (0.114)	-31.15 dB (0.001)
Node 3 transmitting	-11.26 dB (0.075)	-11.41 dB (0.072)	-31.18 dB (0.001)

Table 7.11: Received power - target at 150 m

Now looking at the field trial results for cylinder target at R = 130 m, R = 140 m and R = 150 m together, it is seen that the errors for range measurement range from 0.1 m to 3.3 m. This is quite satisfactory considering the actual range of the target of interests is from 130 m to 150 m. The sensitivity measurement for netted radar is generally greater than the single monostatic or bistatic ones in the system. This supports the netted radar sensitivity model developed earlier in this work. The sensitivity measurement for single monostatic and bistatic radar in the system varies from case to case due to various reasons. The total netted radar sensitivity decreased when the target was moved away from the radar nodes which was as expected from the netted radar Equation 4.18.

7.4 Conclusions

In this chapter, a set of netted radar field experiment results has been presented and analysed. This is the first experiment to get collaboration with netted radar theory. The noise level and clutter condition were analysed before putting the target in the field. The field trial focused on the measurement of range and sensitivity with a single stationary cylinder target. The measurement was repeated for three times with the target at three different locations in the test field. It has been shown that the range measurement was quite satisfactory. In the sensitivity measurement results, it has been shown that the sensitivity gain has been achieved in netted radar system compared with the monostatic case. The overall netted radar sensitivity generally decreases with range. This strongly supports our theoretical models developed in Chapter 4.

Complexity has been observed in netted radar sensitivity measurements. The sensitivity measurement was found to vary from case to case. This could be due to a number of reasons, for example, the lack of knowledge of the initial phase of the transmitted signal, the inaccuracy of the antenna phase centre, the simplified model for target RCS and the ground plane effect.

It is possible to improve the sensitivity measurement results from two major aspects. Firstly, it can be improved by upgrading the netted radar hardware. For example, better synchronization method and hardware will reduce the timing error. A more accurate collaboration method will reduce the measurement error caused by the system itself. The improvement of stability of the netted radar hardware will reduce the random errors occurred in the process of measurement. Secondly, it can be improved by applying improved signal processing method to reduce the inaccuracy caused by the signal processing method itself.

The comparison between the measurement results and those from the theoretical model also suggests that the theoretical model developed for calculating netted radar sensitivity can also be improved to better represent real netted radar sensitivity. For example, the RCS model can be improved by considering the conditions of the actual target rather than using a point target model. Clutter and noise levels can be further investigated and included in the analysis of netted radar sensitivity.

This set of netted radar field experiment has verified the advantage of a netted radar system in providing sensitivity gains compared with monostatic radar in a real world situation. It has also revealed the complexity in performing netted radar field experiments. This provides valuable guidance for further netted radar theoretical development and field experiments where more practical theoretical models can be developed and improved experimental methods can be applied.

Chapter 8

Conclusions and Future Work

This chapter first summarizes and discusses main results and findings in the scope of this research work. Then the principle achievements and novel contributions accomplished in netted radar are pointed out. Finally the potential directions for further investigation are discussed.

8.1 Conclusions

The research work presented in this thesis has built a framework for investigating and examining fundamental aspects of netted radar performance. Three fundamental aspects of netted radar performance have been discussed: netted radar sensitivity, the netted radar ambiguity function and the netted radar ground plane effect. In discussion of each of the above issues, mathematical models have been developed and simulation results have been presented and analysed. Finally field trial results have been presented to examine netted radar performance in practice.

Before discussing any of the topics of interest, an introduction has been given to briefly introduce the netted radar concept, to discuss the potential value of this research work, to address the main objectives and to point out the overall structure of this thesis. This was followed by a comprehensive literature review to emphasize the necessity and importance of this research work. After this, some fundamental aspects of monostatic radar, bistatic radar and netted radar in existing literature were discussed to set the scene of this research.

The investigation began with discussing netted radar sensitivities which in simple term can be defined as received signal to noise ratio because radar sensitivity indicates the ability of

a radar system to detect the presence of a target which is always the most important function for any radar system. Any other functions such as ranging, imaging and tracking should be based on the detection of a target. Since radar sensitivity is an indicator of the target detection ability of radar system, it is fundamental when evaluating netted radar performance.

In discussion of netted radar sensitivity, monostatic and bistatic radar equations and sensitivity were first reviewed as a starting point for developing a netted radar equation and sensitivity model. Here a three-dimensional simulation method showing the radar sensitivity envelope has been developed to better understand radar sensitivity performance in three-dimensional space. The netted radar equation has been developed for a fully netted coherent netted radar system by summing sensitivity contributions from every bistatic radar pair that comprises the netted radar system where collocated transmitter and receiver pair is seen as a special bistatic radar case.

Simulation results have shown that netted radar sensitivity has a strong dependency on the system geometry, i.e. the positions of radar transmitters and receivers that comprise the netted radar system. For the exemplar ground based netted radar system, the dispersion of radar nodes provides an enlarged coverage area in the first two dimensions, i.e. the ground plane, but reduced coverage in the third dimension of height. This shows that for a netted radar system overall emitted power is conserved and is traded between the horizontal and vertical dimensions of coverage. It has also been shown that compared with traditional monostatic and bistatic radar systems, netted radar can offer a more flexible arrangement of radar nodes, i.e. system geometry, so that it provides a way to configure netted radar system to form desired coverage area. This extra degree of freedom may be extremely valuable. For example, in hilly terrain the possibility for a ground based netted radar to achieve a line of sight in a particular zone can be bigger than monostatic and bistatic radars. Therefore, netted radar topology provides a more efficient way to utilize the transmitted power.

In developing the simulation of the netted radar ambiguity function, monostatic and bistatic radar ambiguity functions were first reviewed. For bistatic radar case the degradation of ambiguity properties that occurs when the target is located close to the bistatic baseline regardless of the form of transmitted signal has been addressed. Subsequently, a form of the

netted radar ambiguity function model was developed by considering the netted radar system as a collection of bistatic radars. Therefore, each bistatic component contributes to the overall netted radar ambiguity function. A three-dimensional simulation model has been developed which can be applied where the geometry formed by radar nodes and the target is in three-dimensional space while two-dimensional netted radar geometry can be seen as a special case of the three-dimensional one.

It has been shown that the netted radar ambiguity function has a strong dependency on the system geometry defined by the positions of the radar nodes and the target. In the two-dimensional netted radar case, when the target is close to any of the original bistatic baseline, this bistatic pair becomes dominant in determining the overall netted radar ambiguity and large ambiguities result. In the three-dimensional netted ambiguity model, the target height to baseline length ratio is an important factor, and smaller baselines perform than longer baselines. Adding more nodes to the netted radar system provides a more flexible way to arrange the system geometry and the possibility to further improve netted radar ambiguity properties. Compared with the monostatic and bistatic cases, the three-dimensional netted radar system can provide a more flexible way to control ambiguity properties.

To develop the analysis of the netted radar ground plane effect, monostatic radar ground plane effect was first reviewed, where factors such as wavelength, range, target and antenna heights that affect monostatic radar RCS were analysed separately. This was used to examine the influence of the ground plane on monostatic radar sensitivity. After this, a novel bistatic radar ground plane effect model has been developed and used to examine influence on bistatic radar sensitivity. Finally the influence of ground plane on netted radar sensitivity was analysed in detail by considering each bistatic radar that comprises the netted radar system.

It has been shown that for a specific point in the netted radar surveillance area the sensitivity value can be either greater or smaller than free space one. Fluctuations of sensitivity values have been observed, especially around the areas where the radar nodes are placed compared with free space sensitivities for the same system geometry. It has also been shown that some of the nulls that appear in monostatic radar case disappear when a netted radar system is applied. This has demonstrated that netted radar configuration offers a more stable sensitiv-

ity map when the ground plane is taken into account compared with monostatic and bistatic radars.

Lastly, field trial results using a prototype netted radar system developed by UCL radar group have been presented to examine netted radar performance. The experiments focused on netted radar range and sensitivity measurement. Satisfactory range measurement results have been achieved using this system. It has been shown that the netted radar sensitivity increases compared with monostatic and bistatic radars and the overall sensitivity decreases with range. This matched the theoretical model developed for netted radar sensitivity. It has also been observed that the real world netted radar sensitivity is complex and variable. Possible ways to improve netted radar sensitivity measurement have been identified including upgrading the netted radar hardware and improving the theoretical model calculating netted radar sensitivity.

8.2 Main achievements and contributions

In this work, a framework for investigating fundamental aspects of netted radar performance has been built. Three fundamental aspects of netted radar performance have been investigated comprehensively, including netted radar sensitivity, the netted radar ambiguity function and the netted radar ground plane effect. Field trials have been conducted to examine netted radar range and sensitivity performance in a real world situation.

Through development of three-dimensional netted radar sensitivity models and analysis of netted radar sensitivity with various system configurations, it has been learnt that compared with traditional monostatic radar, netted radar can offer sensitivity gains considering the same level of total transmitted power. Netted radar can also offer a more flexible arrangement of the coverage area for the whole system compared with monostatic radar. This provides a new degree of freedom in radar system design which will be extremely valuable for deploying a real radar system in a specific surveillance area, for example, in hilly terrain. Therefore, the total emitted power is more efficiently used in a netted radar system.

Through development of three-dimensional netted radar ambiguity function models and analysis of netted radar ambiguity performance with different system configurations, it has been learnt that the netted radar ambiguity function is strongly dependent on the specific netted

radar system geometry. Compared with the monostatic case, the flexibility of arranging radar nodes in a netted radar system can offer a better way to control the radar system ambiguity properties. The ambiguity function for a netted radar system is complex and variable. This is important to learn in the design of a netted radar system.

Through development of the ground plane effect models for a netted radar system and analysis of ground plane affected netted radar sensitivities, it has been learnt that compared with the monostatic case a netted radar can offer a more stable sensitivity map when the ground plane effect is involved. This is very useful as it can help determine the system geometry when deploying a netted radar in an outdoor test environment to avoid multipath ground plane effect nulls.

From the netted radar field experiment results, it has been verified that the improvement of the sensitivity that netted radar can offer over a monostatic radar system can be realised in practical radar applications. This strongly supported the theoretical models developed in this work. Complexity and difficulties in performing netted radar experiment have also been identified. This is valuable to learn for development of netted radar theory and design of netted radar experiment method where more practical influencing factors can be included.

To summarize, from the theoretical development results of this work it has been shown that compared with monostatic radar, netted radar can offer advantages in fundamental aspects of radar performance such as sensitivity, ambiguity and the ground plane affected sensitivity. From the experimental results, it has been demonstrated that some of the advantages theoretically offered by a netted radar system such as sensitivity gains are indeed realizable in a real world situation. Therefore, this work has formed the basis for some very new aspects of netted radar studies and provided guidance for future netted radar studies.

8.3 Future work

Some of the most fundamental aspects influencing netted radar system performance have been investigated in this work. In the future, the framework that has been built within this work can be further extended. There are still many areas that might be of interests for future investigation. This can be classified into two categories. One is to further investigate the fundamental

aspects that have been covered in this work, and the other one is to explore other fundamental aspects that have not been studied in this work.

To further investigate netted radar sensitivity, the following aspects might be of interests. A more complex RCS model can be built to replace the current point target model. This will better represent the actual situation of the target used as in practice a perfect point target is almost impossible to obtain. More system geometries can be further investigated. Since netted radar offers more flexible arrangement of radar nodes than monostatic and bistatic radar, the system geometry can be tailored to meet the needs of different requirements. For example, in a hilly area, the netted radar nodes might be mounted at places of different heights to achieve a specific line of sight. The sensitivity for this kind of configuration can be further discussed. More factors that may affect netted radar sensitivity, such as clutter, noise could also be further discussed.

In the netted radar ambiguity function area, more cases of system geometry could be included in future studies, for example, a netted radar system that the nodes are mounted at places of different heights. Variation of radar parameters could also be considered to achieve better ambiguity function, for example, using different transmitted power in different transmitters. In this way it might be possible to mitigate the dominant effect caused by the bistatic pair where the target is close to the bistatic baseline and therefore achieve better system ambiguity function. Incoherent netted radar ambiguity function might also be included in future studies, where the radar nodes comprising the netted radar system do not have a common knowledge of phase of the transmitted signals.

In the study of netted radar ground plane effect, rough surfaces might be considered in the future. For a rough surface, the ground plane is not perfectly conducting and a specific area which is illuminated by radar signal is composed of many small facets. When the radar signal hits the ground, it is reflected by all the small facets and the direction of the reflected signal will be various. Therefore, the reflected signal will be the sum of the reflection from all the small surfaces. In this way, a rough surface may offer the possibility to cancel more nulls that occur in flat surface cases and provide better netted radar sensitivity map for outdoor radar tests.

More field trials could also be conducted in the future. Netted radar sensitivity could be further examined with changed system geometry. Netted radar ambiguity and ground plane effect could be included in future field trials. Various radar and geometrical parameters could be considered. The trial could also be taken place in a different environment, for example, in a lower clutter place to exclude influence of other factors.

Other fundamental aspects of netted radar performance may include detection of multiple targets and tracking of moving target. The work accomplished in this thesis has focused on single target. However multiple targets will also be the case in many practical radar applications. Therefore, investigating the ability of netted radar to detect and distinguish different targets would also be important. And the possibility for netted radar to improve tracking performance over traditional monostatic and bistatic radar would also be of interest. The beginning point for investigation of netted radar tracking performance may be formulation of tracking algorithm.

Finally, the potential application areas for netted radar system need to be further identified. This is a very important step to link the netted radar research with industry usage. Only in this way, can research in netted radar system gain practical values.

Appendix A

UCL Experimental Netted Radar System

The hardware design of UCL netted radar system is reviewed below. This netted radar system is composed of three nodes. Each node is capable of transmitting and receiving. Node 1 is operating as a central node which has some extra functions including housing the distributed oscillator, transmitting the synchronisation pulse and operating the GUI compared with the other two nodes. Node 2 and Node 3 are identical.

A block diagram for Node 1 is shown in Figure A.1, which is the central node. A block diagram for Node 2 and Node 3 is shown in Figure A.2.

Basically a standard 19 inch equipment rack is used for each of the netted radar node where various modules are split between two rack-mount cases contained in it. This design effectively alleviated some of the reliability problems shown in the initially designed system due to loose connectors etc.. This also made the nodes easy to transport without damaging the boards. This is very convenient considering that the netted radar system will be regularly taken to an outdoor environment for experiments and sometimes in more rural settings. It should be noted that several other small designs were made to make the netted radar system more portable and suitable for field trials. For example, a miniature low-power display screen is used to run the GUI for data display and processing. Several fans are used around the case for cooling. And each node will be placed in a tent when necessary for waterproofing considering the low-cost approach. The main purpose of all the above-mentioned designs is to avoid system crashes and bugs due to lack of system reliability and stability.

Considering that the netted radar will be taken to outdoor environment for field trial all the

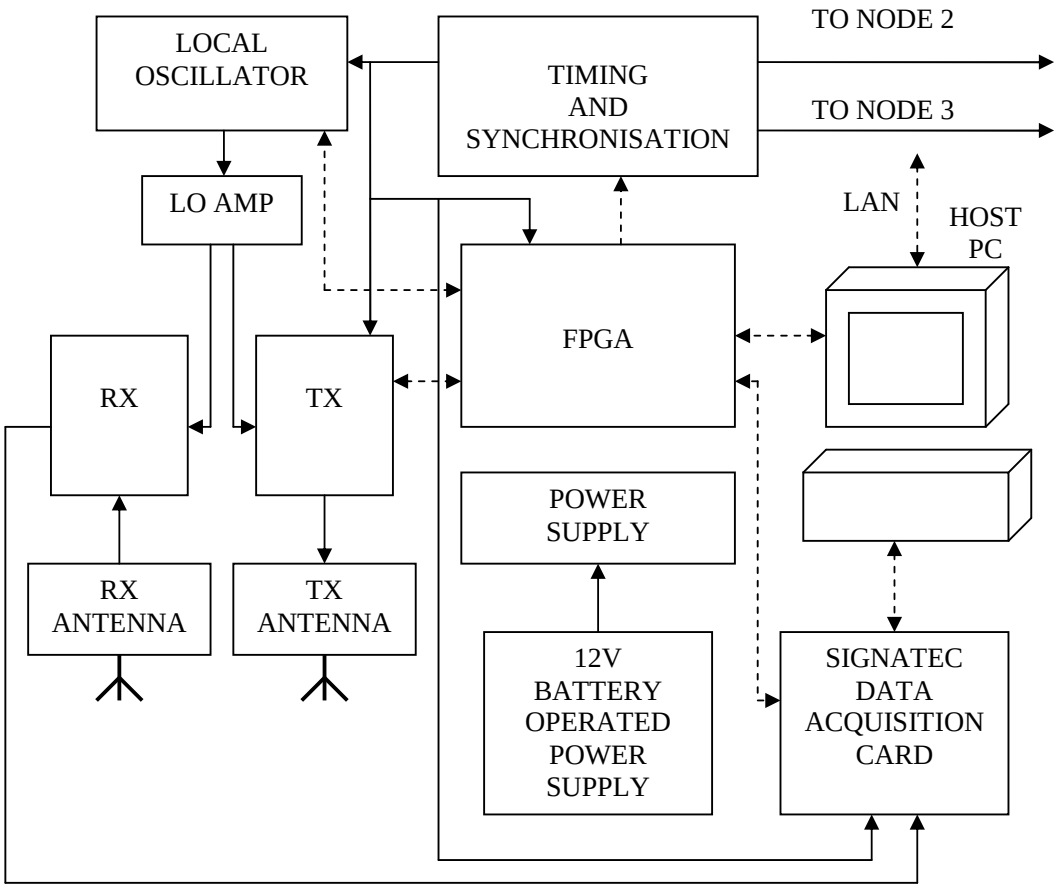

Figure A.1: System diagram - Node 1

time where it is unlikely to have mains power, it is necessary to provide mobile power supply for radar nodes. Therefore, a power supply is developed for each node. This provides the DC (Direct Current) supplies by using DC-DC converters powered by a 12 V 65 Ah battery. This will provide at least 10 hours of operation time. This will normally meet the need of one day trial. If multiple day trial is required, by using COTS car battery chargers it is easy to leave the batteries to charge overnight. By using battery power rather than generators the system does not require any fuel to be obtained and stored during trial. This obviously leads to safer system operation.

Figure A.3 and Figure A.4 show the interior hardware of the netted radar node which is placed inside the case, where mini PC, data capture board and power supply are shown in Figure A.3 and FPGA (Field-Programmable Gate Array) control, transmitter and receiver

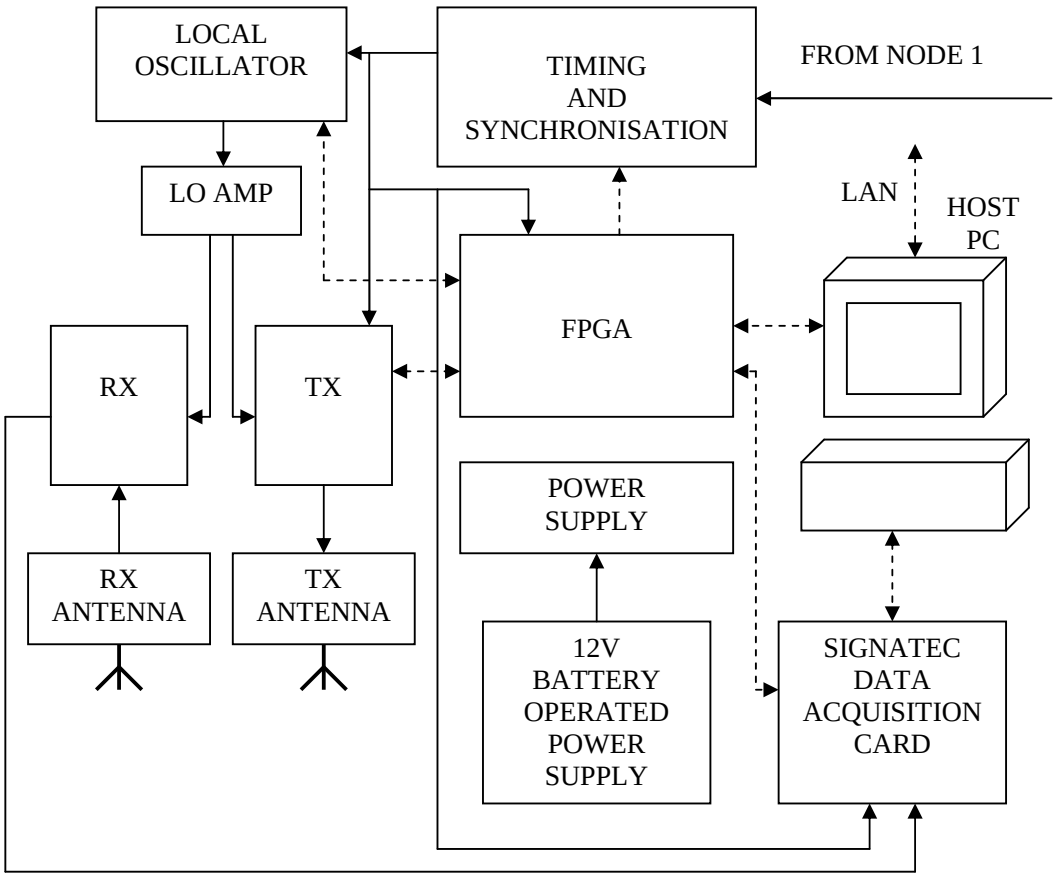

Figure A.2: System diagram - Node 2 and Node 3

chain are shown in Figure A.4.

A PC is included in each node. This enables fast dater transfer and easy storage of received data on the network between nodes. It also provide some other benefits. For example, the networking function can be realized by standard Windows based LAN (Local Area Network) networking over Ethernet links. This will transfer data faster than CAN (Controller Area Network) bus. This means that TCP/IP protocol can be used by software and the networking function can be handled by the operating system. In this way, further conventional COTS networking methods can be implemented as conveniently as in any other PC network. This also provides the opportunity to use wireless networking method. The general adaptability of a PC based system could also be seen. The PC motherboard mounted in a rack mount case could be connected to different other standard PC components, for example hard drive.

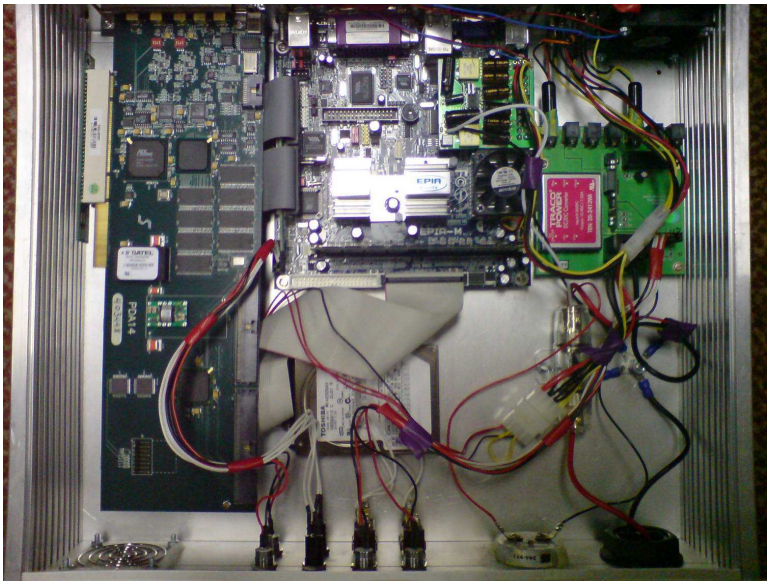

Figure A.3: Netted radar hardware A

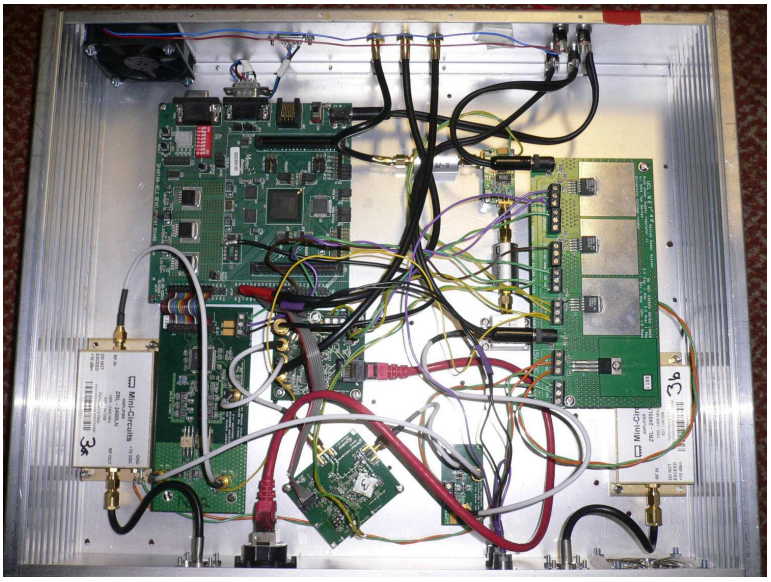

Figure A.4: Netted radar hardware B

Therefore the large capacity of hard drives will resolve the issue of storing large amount of data. Also, it is easy to transfer data to other computers either through Ethernet connection or a USB (Universal Serial Bus) storage device.

Two sets of antennas are available for current netted radar system to meet the needs of

different experiment requirements. They are both 2.4 GHz parabolic antennas considering the high availability for use in ISM band. One set is 8° beamwidth antenna and the other set is 30° beamwidth antenna. Pictures of these two kinds of antennas are shown in Figure A.5 and Figure A.6 respectively.

Figure A.5: 8° beamwidth antenna

Figure A.6: 30° beamwidth antenna

A comparison of main specifications of these two sets of antennas are listed in table A.1. It is seen that the 8° antenna provides higher gain than the 30° antenna. On the other hand it is bigger and heavier than the 30° antenna.

The antenna beam patterns for 8° and 30° antennas are shown in Figure A.7 and A.8 respectively. Since the on-site calibration of antennas is difficult due to the lack of large anechoic chamber. It is convenient to use the data provided in these figures for antenna gains.

In the field trial, the choice of antennas will depend on the specific experiment requirement. For example, if a wider angular coverage is required to detect target in a specific area,

	8° Antenna	30° Antenna
Gain (dBi)	24	15
Bandwidth (GHz)	2.4-2.485	2.4-2.485
3 dB beam pattern	8°×8°	30°×20°
Impedance (ohms)	50	50
Polarization	Vertical/Horizontal	Vertical/Horizontal
Length (cm)	91	45
Width (cm)	91	25
Weight (kg)	4.2	1.2

Table A.1: Antenna specifications

the 30° beamwidth antenna will be used. If a higher antenna gain is needed to capture weak target return signal, the 8° beamwidth antenna will be used.

The clock signal distribution and synchronisation is a key issue in any netted radar system design. In this UCL netted radar system, a single 100 MHz clock signal is distributed to each of the three nodes. The clock transmitter is hosted within node one. The same board is also transmitting the synchronisation pulse. Therefore, this board hosted within node one deals with distribution of timing and synchronisation while connecting to the other two nodes via cables. In the future, this board can be easily replaced if wireless solution is applicable. Heavy duty connectors are used at the front panel of each node, to avoid intermittent faults resulted from wear and tear on the connector which were found in the initial stage of system design and tests.

The communication between host PC and FPGA is realized by using the RS-232 serial port on the FPGA board. Only raw data are recorded. This is mainly the due to the following two aspects of consideration. First, it will ensure faster data capture and secondly, it will allow simpler application of a variety of offline DSP (Digital Signal Processing) methods such as applying different windowing functions on the matched filter. It should be noted that a pulse interleave mode is used in this netted radar system. This provides a way to distinguish which

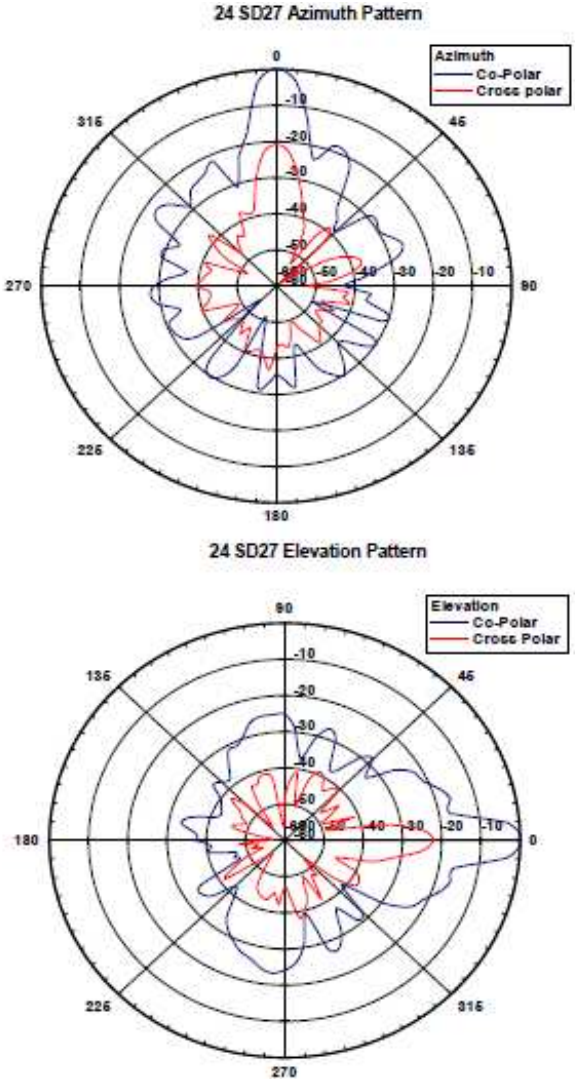

Figure A.7: 8° beamwidth antenna beam pattern

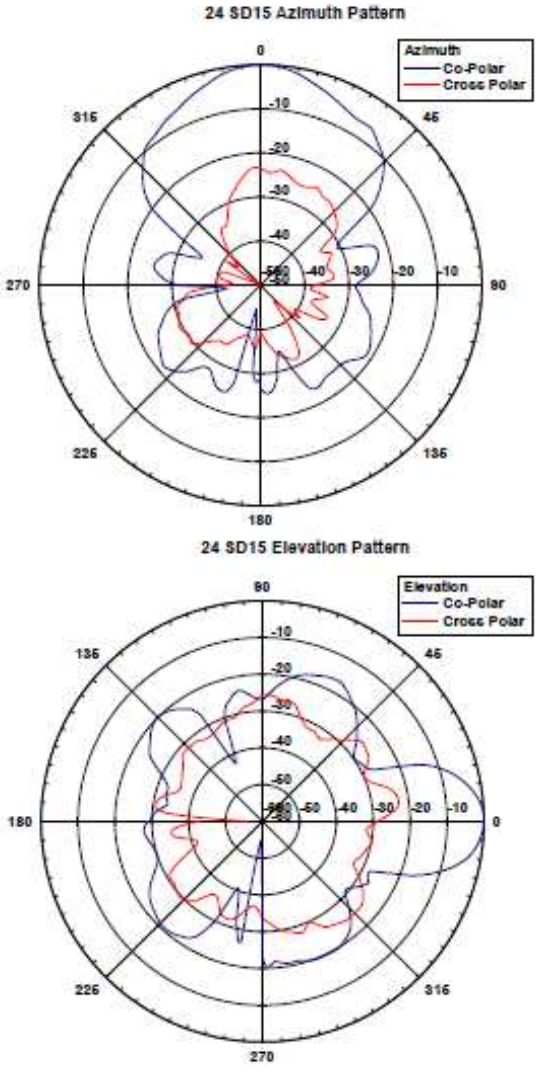

Figure A.8: 30° beamwidth antenna beam pattern

node is transmitting for each set of received data. In this mode, the receive PRF will be three times that of the transmit PRF if all nine transmitting-receiving channels in the system are used. The GUI (Graphical User Interface) which is operating the netted radar system is written in C#, an object-oriented programming language using .NET framework. The main functions of this GUI is first to handle the serial communication between the host PC and FPGA as well as further new functions of interfacing with the data capture board and secondly to handle the

TCP/IP networking between nodes. Additionally, the GUI also provides an implementation of the matched filtering which could be used as a quick confidence check during the field trial to roughly see that the targets are appearing as expected.

The main goal of the hardware development work is to make the experimental trials easy to set up and more reliable therefore to provide more reliable and higher quality field trial data. From the design of the current system, it can be seen that there are some aspects that can be improved. One apparent aspect is, the wired characteristic of current system will by nature present limitations in setting up the positions of radar nodes in trials. For example, the fixed length of 50 m of the cables linking between nodes will present difficulties when the required direct distance between two node exceeds 50 m in the trial. Also, if the trial field does not allow easy direct link between nodes, for example, if the nodes are required to be placed on top of different buildings for urban setting test, this will become a major problem and some alternative methods have to be developed. One possible COTS solution is to use GPS (Global Positioning System), which has the ability to provide position, synchronisation and a distributed reference. Sandenbergh and Inggs at the University of Cape Town [78] has developed a GPS time transfer system which is specifically used for multistatic radars. There is a plan to use this time transfer system to replace the wired timing board in current system. The integration of this GPS time transfer system will definitely need to be tested and system performance need to be verified.

There are some other development areas of interest. For example, to include a switch in the system to provide isolation for the receiver chain during transmission, because this was found as being a problem when full power was transmitted, and would become a major obstacle for higher power transmitter implementation. Another interesting development area is to transmit higher power in order to reach greater detection ranges, for example to detect airborne targets. However, the further development of the netted radar hardware would not limited to above-mentioned areas. New experimental measurements may very likely to present new requirement for the netted radar hardware design and development.

The main goal of this hardware development work is to make the experimental trials easy to set up and more reliable. In the current system the 50 m cables are used, and present little

problems. However, if the required distance between nodes is greater than 50 m or if obstacles, for example to situate on different buildings, is present, this will become a major problem and some alternative methods have to be developed. On possible COTS solution is the use of GPS, which has the ability to provide position, synchronisation and a distributed reference oscillator.

There are some other development areas of interest. Fore example, to include a switch in the system to provide suitable isolation for the receiver chain during transmission, because this was found as being a problem when full power was transmitted, and would become a major obstacle for higher power transmitter implementation. Another interesting development area is to transmit higher power in order to reach greater range, for example for airborne targets. However, the further development of the netted radar hardware would not limited to above-mentioned areas. New experimental measurements may very likely to present new requirement for the netted radar hardware development.

Bibliography

[1] V. S. Chernyak. *Fundamentals of Multisite Radar Systems*. Gordon and Breach Scientific Publishers, Amsterdam, The Netherlands, 1998.

[2] T. E. Derham. *The Design and Calibration of a Coherent Multistatic Radar System*. PhD thesis, University College London, April 2005.

[3] T. E. Derham, S. R. Doughty, K. Woodbridge, and C. J. Baker. Design and evaluation of a low-cost multistatic netted radar system. *IET Radar, Sonar and Navigation*, 1(5):362–368, Oct. 2007.

[4] S. Doughty, K. Woodbridge, and C. J. Baker. Characterisation of a multistatic radar system. In *Proceedings of the 3rd European Radar Conference*, pages 5–8, Sept. 2006.

[5] N. J. Willis. *Bistatic Radar*. Artech House, Garden City, NY, 1991.

[6] M. I. Skolnik. *Introduction to Radar Systems*. McGraw-Hill, New York, NY, third edition, 2001.

[7] A. Cameron. The jindalee operational radar network: its architecture and surveillance capability. In *Record of the IEEE 1995 International Radar Conference*, pages 692–697, May 1995.

[8] T. Johnsen, K. E. Olsen, and R. Gundersen. Hovering helicopter measured by bi/multistatic CW radar. In *Proceedings of the 2003 IEEE Radar Conference*, pages 165–170, May 2003.

[9] K. H. Bethke, B. Rode, M. Schneider, and A. Schroth. A novel noncooperative near-range radar network for traffic guidance and control on airport surfaces. *IEEE Transactions on Control Systems Technology*, 1(3):168–178, Sept 1993.

[10] G. Galati, M. Naldi, and M. Ferri. Airport surface surveillance with a network of mini-radars. *IEEE Transactions on Aerospace and Electronic Systems*, 35(1):331–338, Jan 1999.

[11] T. A. Seliga and F. J. Coyne. Multistatic radar as a means of dealing with the detection of multipath false targets by airport surface detection equipment radars. In *Proceedings of the 2003 IEEE Radar Conference*, pages 329–336, May 2003.

[12] H. Rohling, A. Hoss, U. Lubbert, and M. Schiementz. Multistatic radar principles for automotive RadarNet applications. In *German Radar Symposium 2002*, 2002.

[13] Applied Physics Laboratory. The cooperative engagement capability, 1995.

[14] Ministry of Defence UK. Network enabled capability JSP777, 2005.

[15] D. A. Lambert. Ubiquitous command and control. In *IDC 99. Proceedings-Information, Decision and Control*, pages 35–40, Feb 1999.

[16] M. Martin. Techsat 21 and revolutionizing space missions using microsatellites. In *Proceedings of the 15th AIAA/USU Conference on Small Satellites*, 2001.

[17] H. Steyskal, J. K. Schindler, P. Franchi, and R. J. Mailloux. Pattern synthesis for TechSat21-a distributed spacebased radar system. In *IEEE Proceedings, Aerospace Conference*, volume 2, pages 725–732, March 2001.

[18] H. Steyskal and J. K. Schindler. Separable space-time pattern synthesis for the techsat21 space-based radar system. In *Proceedings. 2003 IEEE Aerospace Conference*, volume 2, pages 955–960, March 2003.

[19] A. V. Mrstik. Multistatic-radar binomial detection. *IEEE Transactions on Aerospace and Electronic Systems*, AES-14(1):103–108, Jan 1978.

[20] D. Baumgarten. Optimum detection and receiver performance for multistatic radar configurations. In *Acoustics, Speech, and Signal Processing, IEEE International Conference on ICASSP '82*, volume 7, pages 359–362, May 1982.

[21] D. Bruyere and N. A. Goodman. Performance of multistatic space-time adaptive processing. In *2006 IEEE Conference on Radar*, pages 533–538, April 2006.

[22] D. Bruyere and N. A. Goodman. Optimum and decentralized detection for multistatic airborne radar. *IEEE Transactions on Aerospace and Electronic Systems*, 43(2):806–813, April 2007.

[23] R. Nilavalan, A. Gbedemah, I. J. Craddock, X. Li, and S. C. Hagness. Numerical investigation of breast tumour detection using. *Electronics Letters*, 39(25):1787–1789, Dec. 2003.

[24] B. Cheeseman and Y. Huang. Limited multi-static calibration technique without a phantom for the detection of breast cancer. In *2006. 3rd European Radar Conference*, pages 225–228, Sept. 2006.

[25] C. Yin, S. Xu, and D. Wang. Location accuracy of multistatic radars (TRn) based on ranging information. In *Proceedings, 1996 CIE International Conference of Radar*, pages 34–38, Oct 1996.

[26] C. Wei, S. Xu, and D. Wang. Target location based on range-difference information from a multistatic radar system. In *Proceedings, 1998. ICMMT '98. 1998 International Conference on Microwave and Millimeter Wave Technology*, pages 456–459, Aug. 1998.

[27] C. Wei, S. Xu, D. Wang, and W. Wang. Analysis and simulation for the location and length of thin cylindrical target with FMCW multistatic radar system. In *Proceedings, 1998. ICSP '98. 1998 Fourth International Conference on Signal Processing*, volume 2, pages 1501–1504, Oct. 1998.

[28] W. Yang and C. Wei. Target location and speed estimation by multistatic radar system us-

ing maximum likelihood approach. In *WCCC-ICSP 2000. 5th International Conference on Signal Processing Proceedings*, volume 3, pages 1964–1967, Aug 2000.

[29] L. Paradowski. Position estimation from netted radar systems with sensor position uncertainty. In *1996 Proceedings, CIE International Conference of Radar*, pages 609–613, Oct 1996.

[30] F. C. B. F. Muller, R. G. Farias, C. Ld. S. S. Sobrinho, and V. Dmitriev. Multistatic radar with ultra-wideband pulses: FDTD simulation. In *2005 SBMO/IEEE MTT-S International Conference on Microwave and Optoelectronics*, pages 574–577, Jul. 2005.

[31] L. He and Z. Sun. Location and tracking technique in a multistatic system established by multiple bistatic systems. In *Proceeding of the IEEE National Aeorspace and Electronics Conference*, volume 1, pages 437–441, May 1991.

[32] W. Que, Y. Peng, D. Lu, and X. Hou. An approach to radar netting. In *1996 Proceedings, CIE International Conference of Radar*, pages 573–577, Oct 1996.

[33] W. Que, Y. Peng, D. Lu, and X. Hou. A new approach to data fusion for stealth targets tracking. In *Radar 97 (Conf. Publ. No. 449)*, pages 657–661, Oct 1997.

[34] H. D. Griffiths, A. J. Garnett, C. J. Baker, and S. Keaveney. Bistatic radar using satellite-borne illuminators of opportunity. In *Radar 92. International Conference*, pages 276–279, Oct 1992.

[35] Y. Wu and D. C. Munson. Multistatic synthetic aperture imaging of aircraft using reflected television signals, Aug. 2001.

[36] Y. Wu and D. C. Munson. Multistatic passive radar imaging using the smoothed pseudo Wigner-Ville distribution. In *Proceedings. 2001 International Conference on Image Processing*, volume 3, pages 604–607, Oct 2001.

[37] V. Koch and R. Westphal. A new approach to a multistatic passive radar sensor for air defence. *IEEE Aerospace and Electronic Magazine*, 10(11):24–32, Nov. 1995.

[38] E. Fishler, A. Haimovich, R. Blum, L. Cimini, D. Chizhik, and R. Valenzuela. Performance of MIMO radar systems: advantages of angular diversity. In *2004. Conference Record of the Thirty-Eighth Asilomar Conference on Signals, Systems and Computers*, volume 1, pages 305–309, Nov. 2004.

[39] P. F. Sammartino, C.J C. J. Baker, and H. D. Griffiths. Target model effects on MIMO radar performance. In *2006. ICASSP 2006 Proceedings. 2006 IEEE International Conference on Acoustics, Speech and Signal Processing*, volume 5, pages 1129–1132, May 2006.

[40] K. W. Forsythe, D. W. Bliss, and G. S. Fawcett. Multiple-input multiple-output (MIMO) radar: performance issues. In *2004. Conference Record of the Thirty-Eighth Asilomar Conference on Signals, Systems and Computers*, volume 1, pages 310–315, Nov. 2004.

[41] G. S. Antonio and D. R. Fuhrmann. Beampattern synthesis for wideband MIMO radar systems. In *2005 1st IEEE International Workshop on Computational Advances in Multi-Sensor Adaptive Processing*, pages 105–108, Dec. 2005.

[42] D. R. Fuhrmann and G. S. Antonio. Transmit beamforming for MIMO radar systems using partial signal correlation. In *2004. Conference Record of the Thirty-Eighth Asilomar Conference on Signals, Systems and Computers*, volume 1, pages 295–299, Nov. 2004.

[43] F. C. Robey, S. Coutts, D. Weikle, J. C. McHarg, and K. Cuomo. MIMO radar theory and experimental results. In *2004. Conference Record of the Thirty-Eighth Asilomar Conference on Signals, Systems and Computers*, volume 1, pages 300–304, Nov. 2004.

[44] D. J. Rabideau and P. Parker. Ubiquitous MIMO multifunction digital array radar. In *2003. Conference Record of the Thirty-Seventh Asilomar Conference on Signals, Systems and Computers*, volume 1, pages 1057–1064, Nov. 2003.

[45] T. Aittomaki and V. Koivunen. Low-complexity method for transmit beamforming in MIMO radars. In *2007. ICASSP 2007. IEEE International Conference on Acoustics, Speech and Signal Processing*, volume 2, pages 305–308, April 2007.

[46] E. Fishler, A. Haimovich, R. Blum, D. Chizhik, L. Cimini, and R. Valenzuela. MIMO radar: an idea whose time has come. In *2004 IEEE Radar Conference*, pages 71–78, April 2004.

[47] E. Fishler, A. Haimovich, R. S. Blum, L. J. Cimini, D. Chizhik, and R.A. Valenzuela. Spatial diversity in radars-models and detection performance. *Signal Processing, IEEE Transactions on [see also Acoustics, Speech, and Signal Processing, IEEE Transactions on]*, 54(3):823–838, March 2006.

[48] A. D. Maio and M. Lops. Design principles of MIMO radar detectors. *IEEE Transactions on Aerospace and Electronic Systems*, 43(3):886–898, July 2007.

[49] P. F. Sammartino, C.J C. J. Baker, and H. D. Griffiths. MIMO radar performance in clutter environment. In *2006. CIE '06. International Conference on Radar*, pages 1–4, Oct. 2006.

[50] P. F. Sammartino, C.J C. J. Baker, and H. D. Griffiths. Adaptive MIMO radar system in clutter. In *2007 IEEE Radar Conference*, pages 276–281, April 2007.

[51] G. S. Antonio, D. R. Fuhrmann, and F. C. Robey. MIMO radar ambiguity functions. *Selected Topics in Signal Processing, IEEE Journal of*, 1(1):167–177, June 2007.

[52] C. Chen and P.P. Vaidyanathan. Properties of the MIMO radar ambiguity function. In *Acoustics, Speech and Signal Processing, 2008. ICASSP 2008. IEEE International Conference on*, pages 2309–2312, 2008.

[53] C. Chen and P.P. Vaidyanathan. MIMO radar ambiguity properties and optimization using frequency-hopping waveforms. *Signal Processing, IEEE Transactions on*, 56(12):5926–5936, December 2008.

[54] C. J. Baker and A. L. Hume. Netted radar sensing. *IEEE Aerospace and Electronic Systems Magazine*, 18(2):3–6, Feb 2003.

[55] T. Tsao, M. Slamani, P. Varshney, D. Weiner, H. Schwarzlander, and S. Borek. Ambiguity function for a bistatic radar. *IEEE Transactions on Aerospace and Electronic Systems*, 33(3):1041–1051, July 1997.

[56] E. F. Knott, J. F. Shaeffer, and M. T. Tuley. *Radar Cross Section*. SciTech Publishing Inc., Raleigh, second edition, 2004.

[57] S. Kingsley and S. Quegan. *Understanding Radar Systems*. McGraw-Hill Book Company Europe, Amsterdam, The Netherlands, 1992.

[58] G. W. Stimson. *Introduction to Aireborne Radar*. SciTech Publishing Inc., second edition, 1998.

[59] H. D. Griffiths. From a different perspective: principles, practice and potential of bistatic radar. In *Proceedings of the International Radar Conference*, pages 1–7, Sept. 2003.

[60] B. Wang. The nature of bistatic and multistatic radar. In *Proceedings, 2001 CIE International Conference on Radar*, pages 882–884, Oct. 2001.

[61] K. Liu. An analysis of some problems of bistatic and multistatic radars. In *Proceedings of the International Radar Conference*, pages 429–432, Sept. 2003.

[62] W. G. Bath. Tradeoffs in radar networking. In *RADAR 2002*, pages 26–30, Oct. 2002.

[63] F. Lombardini and L. Verrazzani. Communication-constrained distributed radar detection in spiky clutter. In *Proceedings of the 1996 IEEE National Radar Conference*, pages 285–290, May 1996.

[64] H. Deng. Discrete frequency-coding waveform design for netted radar systems. *IEEE Signal Processing Letters*, 11(2):179–182, Feb. 2004.

[65] Y. Chen, X. Lu, H. Qing, and X. Jing. On study of the application of ATM switches in netted-radar systems. In *NAECON 1997, Proceedings of the IEEE 1997 National Aerospace and Electronics Conference*, volume 2, pages 970–974, July 1997.

[66] M. Vespe. *Multi-Perspective Radar Target Classification*. PhD thesis, University College London, March 2007.

[67] M. Vespe, C. J. Baker, and H. D. Griffiths. Node location for netted radar target classification. In *Proceedings of the 2006 International Waveform Diversity and Design Conference*, pages 256–260, Jan. 2006.

[68] M. Vespe, C. J. Baker, and H. D. Griffiths. Aspect dependent drivers for multi-perspective target classification. In *Proceedings of the 2006 IEEE Radar Conference*, pages 256–260, Apr. 2006.

[69] M. Vespe, C. J. Baker, and H. D. Griffiths. Multi-perspective target classification. In *Proceedings of the 2005 Int. IEEE Radar Conference*, pages 877–882, May 2005.

[70] T. Johnsen. Time and frequency synchronization in multistatic radar. consequences to usage of GPS disciplined references with and without GPS signals. In *Proceedings of the IEEE Radar Conference*, pages 141–147, April 2002.

[71] M. Weiss. Synchronisation of bistatic radar systems. In *Proceedings. 2004 IEEE International Geoscience and Remote Sensing Symposium, IGARSS '04.*, volume 3, pages 1750–1753, Sept. 2004.

[72] G. W. Stimson. *Introduction to Airborne Radar*. SciTech Publishing, 2 edition, 1998.

[73] M. I. Skolnik. *Radar Handbook (2nd Edition)*. McGraw-Hill, 1990.

[74] P. M. Woodward. *Probability and Information Theory, with Applications to Radar*. Pergamon Press, Ltd., London, England, 1953.

[75] N. Levanon and E. Mozeson. *Radar Signals*. John Wiley & Sons, Inc., Hoboken, New Jersey, 2004.

[76] N. Levanon. *Radar Principles*. John Wiley & Sons, Inc., the US, 1988.

[77] P. Beckmann and A. Spizzichino. *The Scattering of Electromagnetic Waves from Rough Surfaces*. Artech House Inc., 685 Canton Street, Norwood, MA02062, 1987.

[78] J. S. Sandenbergh and M. R. Inggs. A common view GPSDO to synchronise netted radar. In *Proceedings of the IET International Conference on Radar Systems*, pages 1–5, October 2007.